Approved for public release; distribution is unlimited.

An Observational Study of Long Waves in the Equatorial Pacific Ocean During the 1991-1993 El Niño

by

Todd W. Sitler
Lieutenant, United States Navy
B.S., Pennsylvania State University, 1984

Submitted in partial fulfillment
of the requirements for the degree of

MASTER OF SCIENCE IN METEOROLOGY, and
MASTER OF SCIENCE IN PHYSICAL OCEANOGRAPHY

from the

NAVAL POSTGRADUATE SCHOOL
June 1994

REPORT DOCUMENTATION PAGE

Form Approved OMB No. 0704

1. AGENCY USE ONLY *(Leave blank)*	2. REPORT DATE 16 JUNE 1994	3. REPORT TYPE AND DATES COVERED Master's Thesis

4. TITLE AND SUBTITLE AN OBSERVATIONAL STUDY OF LONG WAVES IN THE EQUATORIAL PACIFIC OCEAN DURING THE 1991-1993 EL NIÑO

5. FUNDING NUMBERS

6. AUTHOR(S) TODD WILLIAM SITLER

7. PERFORMING ORGANIZATION NAME(S) AND ADDRESS(ES)
Naval Postgraduate School
Monterey CA 93943-5000

8. PERFORMING ORGANIZATION REPORT NUMBER

9. SPONSORING/MONITORING AGENCY NAME(S) AND ADDRESS(ES)

10. SPONSORING/MONITORING AGENCY REPORT NUMBER

11. SUPPLEMENTARY NOTES The views expressed in this thesis are those of the author and do not reflect the official policy or position of the Department of Defense or the U.S. Government.

12a. DISTRIBUTION/AVAILABILITY STATEMENT
Approved for public release; distribution is unlimited.

12b. DISTRIBUTION CODE
A

13. ABSTRACT *(maximum 200 words)*

Long waves in the equatorial Pacific Ocean during the 1991-1993 El Niño event were examined using temperature, current, and wind time series from the Tropical Oceans-Global Atmosphere Tropical Atmosphere-Ocean (TOGA-TAO) moored buoy array. Numerous episodes of long wave activity were detected. The most prominent episodes were associated with eastward propagating equatorial Kelvin waves and with westward propagating tropical instability waves and mixed Rossby-gravity waves.

Equatorial Kelvin waves, which were generated by westerly wind events in the western and central Pacific, were evident in the data between 2°N to 5°S and from 170°W to 110°W. These Kelvin waves, which were most pronounced from 75 to 300 m, had periods of 40 to 70 days, eastward phase speeds of 1.9 to 6.5 m/s, and zonal wavelengths on the order of 10,000 km. These waves were most evident in the northern hemisphere fall and winter. The period of greatest Kelvin wave activity was August 1991-May 1992, during the peak phase of the 1991-1993 El Niño event.

Tropical instability waves were most evident in the data between 8°N to 5°S and from 170°W to 110°W. These waves occurred during the northern hemisphere summer and fall and were confined to the upper 75 m. There was evidence of possible mixed Rossby-gravity waves in association with the tropical instability waves. These waves occurred between 8°N and 2°N and from approximately 100 m to 250 m. Both the tropical instability waves and the apparent mixed Rossby-gravity waves had similar westward phase speeds, 0.5 to 1.5 m/s, and zonal wavelengths, 1500 to 3000 km. The tropical instability waves and mixed Rossby-gravity waves had slightly different periods, 15 to 30 days and 25 to 30 days, respectively. There were strong negative correlations between the temperature time series associated with the tropical instability waves and that associated with the mixed Rossby-gravity waves.

14. SUBJECT TERMS El Niño/Southern Oscillation, ocean climate, equatorial Pacific Ocean, equatorial long waves, Kelvin waves, mixed Rossby-gravity waves, tropical instability waves, TOGA

15. NUMBER OF PAGES 159

16. PRICE CODE

17. SECURITY CLASSIFICATION OF REPORT	18. SECURITY CLASSIFICATION OF THIS PAGE	19. SECURITY CLASSIFICATION OF ABSTRACT	20. LIMITATION OF ABSTRACT
Unclassified	Unclassified	Unclassified	UL

NSN 7540-01-280-5500

Standard Form 298 (Rev. 2-89)
Prescribed by ANSI Std. 239-18

ABSTRACT

Long waves in the equatorial Pacific Ocean during the 1991-1993 El Niño event were examined using temperature, current, and wind time series from the Tropical Oceans-Global Atmosphere Tropical Atmosphere-Ocean (TOGA-TAO) moored buoy array. Numerous episodes of long wave activity were detected. The most prominent episodes were associated with eastward propagating equatorial Kelvin waves and with westward propagating tropical instability waves and mixed Rossby-gravity waves.

Equatorial Kelvin waves, which were generated by westerly wind events in the western and central Pacific, were evident in the data between 2°N to 5°S and from 170°W to 110°W. These Kelvin waves, which were most pronounced from 75 to 300 m, had periods of 40 to 70 days, eastward phase speeds of 1.9 to 6.5 m/s, and zonal wavelengths on the order of 10,000 km. These waves were most evident in the northern hemisphere fall and winter. The period of greatest Kelvin wave activity was August 1991-May 1992, during the peak phase of the 1991-1993 El Niño event.

Tropical instability waves were most evident in the data between 8°N to 5°S and from 170°W to 110°W. These waves occurred during the northern hemisphere summer and fall and were confined to the upper 75 m. There was evidence of

possible mixed Rossby-gravity waves in association with the tropical instability waves. These waves occurred between 8°N and 2°N and from approximately 100 m to 250 m. Both the tropical instability waves and the apparent mixed Rossby-gravity waves had similar westward phase speeds, 0.5 to 1.5 m/s, and zonal wavelengths, 1500 to 3000 km. The tropical instability waves and mixed Rossby-gravity waves had slightly different periods, 15 to 30 days and 25 to 30 days, respectively. There were strong negative correlations between the temperature time series associated with the tropical instability waves and that associated with the mixed Rossby-gravity waves.

TABLE OF CONTENTS

ACKNOWLEDGMENTS

There are a number of individuals who have provided moral and scientific support during my thesis research and I would like to offer my thanks and appreciation to them at this time. I would first like to thank my thesis advisors Professors Murphree and Garwood for their guidance and wisdom. The technical assistance from Mike Cook in creating MATLAB programs and from Mike McCann in generating the computer animation has been invaluable.

Most importantly, I would like to thank my wife, Cheryl, for her love, understanding and support throughout this demanding endeavor. I would like to say a special thanks to my parents, Barb and Bill, for their love and encouragement throughout my life.

I. INTRODUCTION

A major feature of the equatorial ocean is the large scale variability at intraseasonal, interseasonal, and interannual time scales. Free propagating long waves are a major cause of this variability. These waves are directly responsible for transporting heat in the equatorial ocean. This has a major impact on the transfer of heat between the ocean and atmosphere which strongly affects the development of tropical weather systems and the global atmospheric circulation.

The dominant long waves in the equatorial oceans are Kelvin waves, Rossby waves, mixed Rossby-gravity waves, and tropical instability waves. These waves can change the heat content and sea surface temperature, possibly setting up a positive feedback mechanism by changing the equatorial wind field which can then generate more long waves. One of the dominant feedback loops that occurs in the equatorial oceans is El Niño/Southern Oscillation (ENSO). This study has attempted to detect and determine the properties and possible forcing mechanisms of these four wave types during the 1991-1993 El Niño in the equatorial Pacific Ocean. This has been done by using ocean temperature, current, and wind time series from the Tropical Ocean-Global Atmosphere Tropical Atmosphere-Ocean (TOGA-TAO) array of moored buoys. These time series have been analyzed using time series analysis techniques and

computer animation.

A. EQUATORIAL LONG WAVES

For this study, equatorial long waves are defined as waves with periods greater than 10 days and wavelengths greater than 1000 km. The four types of long waves that were investigated in this study are described below. These waves can be described as barotropic or baroclinic waves depending on their vertical structure. Figure 1 shows schematically the vertical structure of the barotropic and baroclinic modes for a propagating wave.

The velocity and pressure distribution in the horizontal can be used to determine the type of wave detected. Figure 2 shows examples of the horizontal velocity and pressure structure of propagating equatorial Kelvin waves, Rossby waves, and mixed Rossby-gravity waves. Subsurface temperature and current records can be used to determine the vertical structure of detected waves.

1. EQUATORIAL KELVIN WAVES

Equatorial Kelvin waves only propagate eastward and are confined to the equatorial wave guide. The equatorial wave guide's latitudinal extent is dictated by the equatorial Rossby radius of deformation which for baroclinic waves is approximately 100-250 km or 3° of latitude (Gill 1982). They can have zonal scales along the equator on the order of 10,000 km but meridional scales of only 200 km (Miller et al. 1988).

These waves can have periods from 10 to 60 days (Lukas et al. 1984, Cooper 1992). The period is determined in part by the time scale of the forcing that generates the wave.

First baroclinic equatorial Kelvin waves have been observed to propagate with phase speeds of approximately 3 m/s in the central Pacific and 2.5 m/s in the eastern Pacific (Knox and Halpern 1982, Miller et al. 1988, McPhaden et al. 1988, Hayes et al. 1991, Delcroix et al. 1991, Cooper 1992, Johnson and McPhaden 1993). These phase speeds are greater than those predicted by linear theory. Linear theory predicts that the phase speeds in the eastern Pacific should be about 2 m/s for the first baroclinic mode and 1.2 m/s for the second baroclinic mode (Giese and Harrison 1990). This increase in observed phase speed over predicted may be due to Doppler shifting of the wave by eastward flowing equatorial currents (Knox and Halpern 1982, Eriksen et al. 1983, McPhaden et al. 1987, McPhaden et al. 1988) or by nonlinear self-advection (Giese and Harrison 1990).

Currents also effect the vertical structure of the individual baroclinic modes. Modeling studies by Giese and Harrison (1990) show that the first baroclinic mode is dominant in the western Pacific while the second baroclinic mode is dominant in the eastern Pacific. Figure 3 shows the vertical zonal velocity structure of the first four baroclinic modes for the eastern and western Pacific (Giese and Harrison 1990). Figure 4 shows schematically the vertical structure of

a first baroclinic equatorial Kelvin wave. The dominant mode detected in observations of the eastern Pacific has been the first baroclinic mode (Knox and Halpern 1982, Eriksen et al. 1983, Lukas et al. 1984, Miller et al. 1988, Hayes et al. 1991, Delcroix et al. 1991, Cooper 1992, Johnson and McPhaden 1993). The only reported detection of a second baroclinic mode Kelvin wave was by Lukas et al. (1984) during the 1982-1983 El Niño. McPhaden et al. (1986) studied the effects of zonal currents on equatorial Kelvin waves. They found that the lowest baroclinic modes are modified the least by the currents and are not appreciably Doppler shifted, as are the higher baroclinic modes. This equatorial Kelvin wave-mean current interaction may help explain why detection of equatorial Kelvin waves is primarily confined to the first baroclinic mode.

Equatorial Kelvin waves can be generated in a number of ways. The most common are: (a) the relaxation or reversal in direction of the trade winds (Philander 1981, Lukas et al. 1984); and (b) the formation of westerly wind bursts in the equatorial western and central Pacific (Knox and Halpern 1982, McPhaden et al. 1988, Cooper 1992, McPhaden 1993). According to Wyrtki (1975), an El Niño may be initiated when the trade winds relax or shift in direction. This means that the westward sea level gradient along the equator, caused by the wind accumulation of water in the western Pacific, cannot be maintained. Thus, water starts to flow to the east in the form

of an equatorial Kelvin wave.

An expanded theory of El Niño was put forward by Graham and White (1988) to help explain its quasi-periodicity. They concluded that warm eastern and central Pacific equatorial sea surface temperature (SST) anomalies cause westerly zonal wind stress anomalies to the west of the SST anomalies. These wind stress anomalies generate downwelling equatorial Kelvin waves. These waves propagate into the central and eastern Pacific and reinforce the warm SST anomalies. The net wind stress anomaly field generates a wind stress curl field outside the equatorial wave guide that produces positive Ekman pumping. This generates upwelling baroclinic Rossby waves which propagate westward. The Rossby waves take approximately 9 months to cross the Pacific near the equator and 4 years to cross at 12°N/S. Upon reaching the western boundary, they reflect into the equatorial wave guide as upwelling equatorial Kelvin waves. These upwelling equatorial Kelvin waves reverse the sign of the SST anomalies in the central and eastern Pacific. This produces easterly winds, thus ending the warm phase of the El Niño. The cycle then reverses, producing a cool event, or an anti-El Niño. Graham and White (1988) proposed this mechanism could be responsible for the observed 3 to 5 year time scale of the El Niño cycle.

Equatorial Kelvin waves may therefore be generated by off-equatorial Rossby waves reflecting off the western

boundary of the Pacific Ocean. This reflection process has been observed in subsurface temperature records by Kessler (1990) and in Geosat altimetric sea level observations (White and Tai 1992).

As the downwelling equatorial Kelvin waves propagate into the central and eastern Pacific, SST increases. This increase in SST can be caused by anomalous advection of warm western Pacific water by the equatorial Kelvin wave fronts (Harrison and Schopf 1984) and by the downwelling associated with the waves, which deepens the thermocline and inhibits the entrainment of deep, cold water into the mixed layer (McPhaden et al. 1988).

Kent (1993) has hypothesized an interesting feedback mechanism between tropical cyclones and equatorial Kelvin waves. He noted that tropical cyclones in the western Pacific may generate equatorial Kelvin waves that propagate eastward and thicken the mixed layer. This thickened, warm mixed layer leads to the generation in the central Pacific of equatorial westerly winds with cyclonic vorticity just north and south of the equator. The thickened, warm mixed layer and the cyclonic winds then contribute to the formation of central Pacific tropical cyclones that propagate westward.

Numerous observational methods have been used to detect equatorial Kelvin waves during the last few El Niños. Lukas et al. (1984) detected equatorial Kelvin waves prior to and during the 1982-1983 El Niño using sea level and

subsurface pressure measurements recorded at Pacific islands near the equator. Remote sensing satellites have been used recently to detect equatorial Kelvin waves. Miller et al. (1988) and Delcroix et al. (1991) detected equatorial Kelvin waves during the 1986-1987 El Niño by using altimetric measurements from Geosat. With the deployment of moored current meters and thermistor chains in the equatorial wave guide, the detection and analysis of Kelvin waves and their effects was made easier. A few of these moorings were deployed prior to the 1986-1987 El Niño. Johnson and McPhaden (1993) used the measurements from moored current meters and thermistor chains in the equatorial eastern Pacific to isolate an equatorial Kelvin wave signal and to determine its vertical and meridional structure and its interaction with the zonal mean flow of the Equatorial Undercurrent (EUC)/South Equatorial Current (SEC) system. These moorings, along with ones in the western Pacific and sea level stations, were also used by McPhaden et al. (1988) to study the response of the equatorial Pacific Ocean to a westerly wind burst during the 1986-1987 El Niño. Cooper (1992) examined surface and subsurface temperature records from thermistor chain moorings during the 1991-1992 El Niño. These moorings were part of the Tropical Ocean-Global Atmosphere (TOGA) Tropical Atmosphere-Ocean (TAO) Array. He examined data from October 1991 to April 1992. Large subsurface temperature fluctuations during this period were associated with the passage of first

baroclinic equatorial Kelvin waves.

In this study, we analyzed the evidence for equatorial Kelvin waves found in the TOGA-TAO sea surface and subsurface temperature records and the Equatorial Pacific Ocean Climate Studies (EPOCS) current records from 01 January 1991 through 31 December 1993. This period covers the 1991-1993 El Niño event.

2. ROSSBY WAVES

Equatorial Kelvin wave energy incident on the west coast of South America may excite coastally trapped Kelvin waves that propagate poleward along the coast of the Americas and partially reflect into westward propagating equatorial Rossby waves. Figure 5, from a model simulation, shows the reflection of equatorial Rossby waves from a first and second baroclinic mode equatorial Kelvin wave at the eastern model boundary (Giese and Harrison 1990). Westward propagating equatorial Rossby waves can also be generated by wind stress fluctuations in the equatorial wave guide and wind stress curl fluctuations in the off-equatorial region. Equatorial Rossby waves may be generated by the same equatorial wind forcing that generates the equatorial Kelvin waves. Off-equatorial Rossby waves may be generated by the wind stress curl away from the equator (Philander 1981). For this study, off-equatorial Rossby waves will be grouped with equatorial Rossby waves because the latitudinal domain, 8°N to 8°S, includes

areas of interest for both types of waves.

The zonal phase speeds and zonal wavelengths of Rossby waves are latitude dependent, becoming larger toward the equator, increasing by the square of the Rossby radius of deformation (White 1977). Near the equator, the predicted phase speed of a first baroclinic mode equatorial Rossby wave is approximately 0.9 m/s (Gill 1982). Zonal phase speeds of 1 m/s have been observed near the equator (Lukas et al. 1984, Delcroix et al. 1991). White (1977) observed phase speeds of 0.5 m/s, zonal wavelengths of 15,000 km, and periods of about one year for a first baroclinic mode Rossby wave at about 10°N.

There have been very few reported detections of equatorial Rossby waves. Delcroix et al. (1991) used sea level anomalies and surface geostrophic zonal current anomalies generated from Geosat altimetric measurements to detect a first meridional first baroclinic mode equatorial Rossby wave during the 1986-1987 El Niño. This wave was probably caused by the reflection of an upwelling equatorial Kelvin wave that was also detected. The Rossby wave propagated over most of the equatorial Pacific Ocean. Rossby waves in the equatorial and off-equatorial regions were also detected by White and Tai (1992) using Geosat data from November 1986 to August 1989. Lukas et al. (1984) detected a first baroclinic mode equatorial Rossby wave during the 1982-1983 El Niño using sea level measurements. Off-equatorial

Rossby waves were also detected by Kessler (1990) using bathythermograph profiles collected throughout the Pacific Ocean from 1970 to 1987. He detected a Rossby wave at 5°N. Apparently, no one has yet detected equatorial or off-equatorial Rossby waves using moored current meters or thermistor chains.

In this study, we have looked for evidence of Rossby waves in records of equatorial temperatures and currents. However, as shown in chapters II and III, these records covered only three years, had long data gaps, were dominated by high-frequency fluctuations, and spanned a relatively limited latitudinal extent. Thus, the detection of Rossby waves with relatively long periods and slow phase speeds was problematic.

3. MIXED ROSSBY-GRAVITY WAVES

Mixed Rossby-gravity waves were detected by Weisberg et al. (1979) along the equator in the Gulf of Guinea. They had a period of 31 days, westward phase speed of 0.45 m/s, upward phase speed of 0.037 cm/s, eastward group velocity of 0.16 m/s, downward group velocity of 0.014 cm/s, zonal wavelength of 1220 km, and vertical wavelength of 990 m. Using satellite infrared imagery, Legeckis (1977) detected tropical instability waves at the sharp SST boundary between the South Equatorial Current (SEC) and the North Equatorial Countercurrent (NECC) in the eastern equatorial. These waves

had periods of 20 to 30 days, westward phase speeds of 0.46 m/s, and zonal wavelengths of 800-1200 km. Tropical instability waves have similar features to equatorially trapped mixed Rossby-gravity waves, such as westward and upward phase propagation and eastward and downward propagation of energy (Halpern et al. 1988).

Tropical instability waves are primarily generated by barotropic instability between the SEC and the NECC (Figure 6) (Legeckis 1977, Cox 1980, Hansen and Paul 1984). There is also significant conversion of mean potential energy to eddy kinetic energy; thus, baroclinic instability is considered a secondary mechanism (Hansen and Paul 1984).

Seigel (1985) found that near the equator the period of tropical instability waves varied from 20 to 30 days. The shorter period waves tended to occur nearer the equator because the period of the waves was inversely related to the strength of the SEC. Philander et al. (1985) found that the period of the most energetic fluctuations varied from 30 days at 4.5°N to 70 days at 10°N. Périgaud (1990) detected instability waves between 3°N and 8°N with periods between 28 and 40 days. The maximum wave energy was along 6°N with a period of 33 days in the eastern Pacific and 40 days in the western Pacific. Périgaud (1990) speculated that this increase in period from east to west may be explained by wave dispersion.

Tropical instability wave westward phase speeds range

from 0.4 m/s (Périgaud 1990) to 0.93 m/s (Halpern et al. 1988). The zonal wavelengths range from 400 km (Legeckis et al. 1983) to 2200 km (Périgaud 1990), while meridional amplitudes are 200 km to 400 km (Legeckis et al. 1983). These waves occur mainly between 90°W and 160°W and between 3°S and 5°N (Legeckis 1984), which are the regions of maximum horizontal shear (Philander et al. 1986).

Since the unstable mean currents are confined to about the upper 100 m, tropical instability waves tend to be confined to this region (Philander et al. 1985). The vertical extent of this layer depends on the depth of the thermocline which varies significantly with longitude (Philander et al. 1986). In a survey of the data record from 1979 to 1985, Halpern et al. (1988) found that the depth of penetration of tropical instability waves was greatest at 110°W and least at 140°W. Cox (1980) used a model simulation and detected waves with a 20 day period trapped near the surface and waves with a 30 day period penetrating to deeper depths. He believed these to be two different types of waves. Philander (1978) determined that tropical instability waves in the upper layer of the ocean may excite vertically propagating equatorially trapped mixed Rossby-gravity waves that propagate into the deep ocean. These vertically propagating mixed Rossby-gravity waves have their maximum amplitude within a few degrees latitude of the equator, while fluctuations observed poleward of 4°N and 4°S are from the higher latitudinal modes of the

deep ocean (Philander et al. 1985).

Tropical instability waves are mainly generated during the northern hemisphere summer and fall between the equator and 5°N, and to a lesser extent during the northern winter just south of the equator (Cox 1980). Tropical instability waves are most prominent in the northern summer and fall when the southeast trade winds are at their peak, causing the SEC and NECC to become highly unstable (Philander et al. 1985, Gordon 1992).

The westward flow of the SEC is cold because of equatorial upwelling and advection of upwelled cold water from the coast of South America. The eastward flowing NECC is advecting warm water from the western Pacific. The eddies associated with the tropical instability waves transport heat equatorward in opposition to the poleward transport due to Ekman divergence (Cox 1980). This equatorial transport of heat is of potential importance for the heat balance and SST in the equatorial region.

Most studies of tropical instability waves have used satellite infrared (IR) measurements. Topical instability waves have not been detected in this way during El Niño periods because the warming of the central and eastern Pacific limits the magnitude of the SST gradients (Legeckis et al. 1983, Legeckis 1984). Périgaud (1990) did detect tropical instability waves during the 1986-1987 El Niño using the Geosat altimeter. The amplitudes of the tropical instability

waves were relatively weak during this period, presumably because of the reduced current shear caused by the decrease in the intensity of the trade winds. Very few studies of tropical instability waves using moored current meters and thermistor chains have been conducted. Halpern et al. (1988) used moored current and temperature measurements along the equator and at near-equatorial sites north and south of the equator. They detected tropical instability waves from 1979 to 1985. The tropical instability waves were absent during the onset of the 1982-1983 El Niño. Weddle (1993) simulated the 1991-1993 El Niño using a general ocean circulation model with embedded mixed layer physics and realistic daily varying wind stresses covering the period 1991 and 1992. The model developed tropical instability waves in the eastern Pacific.

Based on the Geosat observation of tropical instability waves during the 1986-1987 El Niño and their generation in the 1991-1993 El Niño model simulation, this study should be able to detect tropical instability waves during the 1991-1993 El Niño using moored thermistor chain and current measurements. This study should also be able to determine the vertical, latitudinal, and longitudinal extent of the waves at and near the equator because of the extended areal coverage the TOGA-TAO Array now offers.

B. 1991-1993 EL NIÑO

In this study, we investigated the 1991-1993 El Niño event. This was an unusually long event with two distinct episodes of equatorial westerly wind anomalies in the western and central Pacific and positive equatorial SST anomalies in the central and eastern Pacific. There were also a number of propagating equatorial Kelvin waves present during this period (Cooper 1992, Kent 1993). The following chronology of the 1991-1993 El Niño is a summary of the information presented by Kousky (1991, 1992, 1993) unless otherwise stated.

In February 1991, the depth of the thermocline decreased (increased) in the western (eastern) equatorial Pacific. These changes in the thermocline appear to have been caused by the eastward propagation of equatorial Kelvin waves. These waves were probably initiated by westerly winds that occurred in the western and central equatorial Pacific during November and December 1990.

Positive SST anomalies decreased in the equatorial Pacific during March 1991 and the thermocline depth was near normal. In the western Pacific, low level westerly wind anomalies were observed. During April 1991, positive SST anomalies, the depth of the thermocline, and sea level increased in the central equatorial Pacific. During May 1991, positive SST anomalies increased as low level westerly wind anomalies formed throughout the equatorial Pacific. In June 1991 it was determined that an El Niño, or warm episode, was in progress

because there were low level westerly wind anomalies, the SST anomaly increased eastward, the thermocline had deepened east of 160°W and shoaled in the west, and there was an increase in the upper ocean heat storage in the eastern Pacific. These conditions continued through July, August, and September 1991. A westerly wind burst of several weeks duration, west of the dateline, abruptly increased SST in September 1991, which interrupted the normal seasonal evolution of the equatorial cold tongue (McPhaden 1993).

This westerly wind burst generated an equatorial Kelvin wave that increased the thermocline depth between 170°W and 90°W and decreased it west of the dateline. The equatorial Kelvin wave also intensified eastward, propagating positive subsurface temperature anomalies near the depth of the thermocline (Figure 7). The equatorial Kelvin wave reached the coast of South America at the end of October 1991 and abruptly increased the SST along the coast of Peru. The equatorial Kelvin wave caused fluctuations of the upper thermocline from 25 to 50 m in the central and eastern Pacific (McPhaden 1993).

The warm episode continued to intensify in November 1991 and December 1991. Low level westerly wind anomalies shifted further eastward in December 1991. In January 1992, SST anomalies continued to increase, the thermocline along the South American coast deepened considerably, and the SST along the Peruvian coast increased sharply. This was an indication

that the warm episode had moved into the mature phase. The warmest equatorial water shifted east of the dateline to 160°W in February 1992. This was associated with a reversal of the SEC across the equatorial Pacific associated with the passage of the equatorial Kelvin wave (McPhaden 1993). Along the South American coast, the SST anomalies increased substantially in March 1992. The mature phase of the warm episode was associated with deep (shallow) thermocline anomalies in the eastern (western) Pacific and positive (negative) sea level anomalies in the eastern (western) Pacific (Figure 8). The mature phase continued through April 1992.

The warm episode weakened from May to July 1992. The SST anomalies in the central Pacific decreased, the thermocline shoaled in the eastern Pacific and low level easterly winds strengthened in the eastern and central equatorial Pacific. By August 1992, equatorial eastern Pacific conditions were near or below normal. In particular, the easterly trade winds were normal, there was a negative SST anomaly, and the thermocline had shoaled.

These conditions continued until November 1992 when low level easterly winds weakened throughout the Pacific. During December 1992, SST anomalies increased in the central Pacific. The weakening of the easterlies and the increase in SST anomalies signaled the return of mature warm episode conditions. The thermocline deepened (shoaled) in the eastern

(western) Pacific in January 1993. These conditions were similar but weaker than those observed during the mature phase of the previous warm episode. These conditions continued into March 1993. The conditions in March had characteristics of the mature phase. The mature phase of the warm episode continued until June 1993. In June, the SST anomalies decreased in the eastern Pacific and the thermocline shoaled in the central Pacific. This indicated a weakening of the warm episode. The warm episode continued to weaken through July 1993, when the equatorial easterly winds strengthened. In August 1993, SST was almost normal, but the easterly winds were weaker than normal.

The SST anomalies increased across the Pacific during September 1993, and the thermocline in the central Pacific deepened. Positive depth anomalies of approximately 20 m propagated eastward from 140°W to 120°W (Figure 9). This was probably caused by the passage of an equatorial Kelvin wave that was generated in August by the weakening of the easterlies. The propagating equatorial Kelvin wave increased thermocline depths and subsurface temperature anomalies in the eastern Pacific. In the wake of the equatorial Kelvin wave, the thermocline depth and subsurface temperatures returned to near normal between 140°W and 160°W. The equatorial Kelvin wave reached the South American coast in late October and increased the SST. A weaker equatorial Kelvin wave was generated in late October, and it reached 130°W in mid-

November 1993.

The warm episode showed signs of weakening in December 1993. The easterly winds increased to near normal intensity, there was a downward trend in SST anomalies, and subsurface temperature and thermocline depths were near normal throughout the equatorial Pacific.

The 1991-1993 El Niño contained three periods of strong equatorial Kelvin wave activity. This study will attempt to detect these equatorial Kelvin waves and any other equatorial long waves present during this period by using surface and subsurface temperature and current velocity measurements. The wind fields will also be used to determine the forcing mechanisms that generated the waves.

C. PURPOSE OF STUDY

In this study, the TOGA-TAO moored buoy array records of surface and subsurface ocean temperature and surface wind, along with the EPOCS current records, during the 1991-1993 El Niño were analyzed. These analyses were performed to identify propagating long waves in the equatorial Pacific ocean.

The temperature, current, and wind records were analyzed using time series methods to determine the presence of waves, their characteristics, and their possible forcing mechanisms. The temperature records were also analyzed using a four dimensional visualization program called VIS 5D (Hibbard et al. 1993). This visualization was performed to enhance the

detection and characterization of propagating long waves.

Four main questions were addressed in this study:

(1) What equatorial waves occurred and what were their periods, phase speeds, spatial extent, and seasonal and interannual fluctuations?

(2) Can tropical instability waves be detected during the 1991-1993 El Niño using surface and subsurface temperature and current records?

(3) What were the relationships of the detected wave types to each other, to the wind and other forcings, and to the evolution of the 1991-93 El Niño?

(4) Can propagating long waves in the equatorial region be detected using computer animation of the moored buoy array data?

Chapter II describes the observational data sources, data processing, time series methods, and the computer animation procedure. Results are presented in Chapter III and conclusions in Chapter IV.

II. DATA AND METHODS

A. DATA

The sea surface and subsurface temperature time series used in this study were recorded by the Tropical Ocean-Global Atmosphere Tropical Atmosphere-Ocean (TOGA-TAO) moored buoy array and the Equatorial Pacific Ocean Climate Studies (EPOCS) moored buoys. Current time series were also recorded by the EPOCS buoys.

The TOGA-TAO Array consists of Autonomous Temperature Line Acquisition System (ATLAS) moorings. The ATLAS moorings measure air temperature, surface wind speed and direction, relative humidity, SST, and subsurface temperatures to 500 m. The temperature measurements are taken with thermistor chains. The EPOCS moorings consist of thermistor chains and current meters. They measure current speed and direction, surface wind speed and direction, and sea surface and subsurface temperatures.

The buoys are located across the equatorial Pacific ocean from 95°W to 136°E and from 8°N (9°N at 140°W) to 8°S (Figure 10). This study used wind and surface and subsurface temperature measurements from buoys located at 8°N, 5°N, 2°N, 0°, 2°S, 5°S, and 8°S at longitudes 110°W, 125°W, 155°W, 170°W, and 165°E; at 9°N, 5°N, 2°N, 0°, 2°S, and 5°S at

longitude 140°W, and at 5°N, 2°N, 0°, 2°S, and 5°S at longitude 156°E. The EPOCS moorings used to obtain temperature data were located on the equator at 110°W, 140°W, 169°W, and 165°E. The current measurements were from EPOCS buoys, also located on the equator, at 110°W, 140°W, 165°E, and 156°E.

The SST is measured 1 m below the sea surface while the winds are measured 4 m above. The subsurface temperatures are measured at different depths in the eastern Pacific than in the western Pacific because of the differences in stratification (Figure 11) (Hayes et al. 1991). The currents are also measured at different depths for different locations.

The winds are vector averaged over 6 hours and the temperatures are averaged over 24 hours. These averaged measurements are telemetered to shore via Service ARGOS. The National Oceanic Atmospheric Administration (NOAA) Pacific Marine Environmental Laboratory (PMEL) in Seattle, WA receives the data and then makes it available to outside users via Internet anonymous file transfer protocol (ftp) procedures.

The resolutions of the wind measurements are +/- 0.1 m/s for speed and +/- 10° for direction; the SST and subsurface resolutions are +/- 0.01°C (Kent 1993). The current resolutions are +/- 1 cm/s for speed and +/- 10° for direction.

This study used data from 01 January 1991 to 31 December 1993. This time frame encompasses the complete 1991-1993 El

Niño.

B. MISSING DATA

There were numerous data gaps in the temperature (Figure 11), current, and wind time series for 1991-1993. These were the result of equipment failures, losses in data transmission, and deployment of buoys after the beginning of the study period. Some of these data gaps were filled so that time series analysis techniques and computer animation could be performed.

To fill in the temperature data gaps, MATLAB linear interpolation and averaging procedures were used (Anonymous 1992, Little and Shure 1992). The current and wind data gaps were filled with zeroes. These data gaps were not filled by linear interpolation or averaging, because the current meters were located a considerable distance from each other and at only one latitude. Also, the winds tended to change considerably over short distances.

The time series were linearly interpolated between depths to common depths. This was required for computer animation and to facilitate time series comparisons. The common depths used in this study were 1, 25, 50, 100, 125, 150, 200, 250, 300, and 500 m.

For data gaps of 30 days or less, the data was linearly interpolated between the last data point before the gap and the first data point after the gap. For gaps greater than 30

days, TOGA-TAO and EPOCS temperature data were combined or averaging procedures were used.

To fill gaps at the equator, data at 2°N and 2°S were averaged, as was done by Cooper (1992). Data gaps at 2°N/S, 5°N/S, and 8°N/S were filled by averaging data at adjacent locations to the east and west. The buoy at 9°N 140°W was assumed to approximate the missing data at 8°N 140°W.

To computer animate the TOGA-TAO fields using VIS 5D software, the data had to be located on a rectangular array in the x, y, and z directions. Since there were no observations at 8°S 140°W, 8°N 156°E, and 8°S 156°E, data there had to be generated. The data at 8°S 110°W and 8°S 155°W were averaged to give values at 8°S 140°W. Since there were no observations to the north of 5°N 156°E and south of 5°S 156°E, values for 8°N 156°E and 8°S 156°E were set equal to zero. The VIS 5D software was then able to determine that these two locations did not contain useable data. Since there was a large longitudinal gap between 165°E and 170°W, time series were created for 177.5°E by averaging data for the two longitudes.

This procedure for filling data gaps may have produced some unrealistic features in the computer animation and time series analyses. Therefore, caution was taken in the analyses. The filled time series were used in the computer animation, as well as in time series analyses that required continuous data, such as cross-correlations and spectral analysis. However, to minimize problems with the artificially

generated data, most of the analyses were limited to time series that contained very little or no missing data.

C. ANALYSIS METHODS

Time series analysis methods were used to find wave-like features of interest in the buoy data. Prior to analysis, time series of the daily averages of all the fields were calculated. These time series were then linearly detrended. Time-longitude plots of the unfilled data were examined for evidence of propagating waves. Where waves were detected, cross-correlations were calculated for the filled data to determine time lags between longitudes. These lags were then used to determine phase speeds. Note that in cases where phase speed and group velocity were not identical, it is possible that the calculated propagation speeds may represent group velocities. Cross-correlations were also used to determine relationships between the waves and the winds. Spectral analysis were used to determine temporal characteristics of the waves, to identify wave types, and to infer relationships between different wave types. The linear detrending and time series analyses were done with MATLAB programs (Anonymous 1992, Little and Shure 1992).

The 95% significance levels for the cross-correlations were not calculated in this study. Kent (1993) used a six month subset of the data set used in this study and calculated 95% significant levels at correlations as low as +/- 0.1. In

this study, any correlations with values above +/- 0.2 were assumed to be significant.

The temperature data were animated using a visualization program called VIS 5D. VIS 5D is a graphics visualization software package developed at the University of Wisconsin - Madison (Hibbard et al. 1993). This software was run on a Silicon Graphics workstation attached to a SGI 4D/380 VGX system, with 256 MB of RAM and 8 processors and graphics capable of displaying 10^6 shaded polygons/sec (Weddle, 1993). This portion of the study was conducted to determine if this software can be used to conveniently and accurately detect and characterize propagating long waves.

III. RESULTS

A. DETECTED LONG WAVES

In this study, ocean temperature and current time series were analyzed to identify propagating long waves. Wind time series were also analyzed to determine possible forcing mechanisms for the detected waves. The time period of this study was from 01 January 1991 to 31 December 1993, which included a strong and persistent El Niño event.

Due to the extensive amount of data used in this study, we use in this chapter the time series at 5°N 140°W, 0° 140°W, and 5°S 140°W, and the analyses based on these time series, as representative examples. These time series are representative of the other locations where long wave activity was detected.

1. TEMPERATURE TIME SERIES

The temperature time series were the primary data examined for evidence of propagating long waves, because they had long records at multiple depths and were available at all the buoys, which made it easier to detect and analyze wave activity. The data domain extended from 8°N to 8°S and from 156°E to 110°W. This made latitudinal and longitudinal comparisons possible.

a. 5°N 140°W

Figure 12 shows the temperature time series at 5°N 140°W. A seasonal cycle can be seen in the surface temperature signal with a maximum between June and September 1991 (Figure 12a) and from May to June 1992 (Figure 12b). In 1993, the seasonal maximum signal was not seen because of a data gap (Figure 12c).

The largest temperature variability occurred during four time intervals. The upper layer temperatures from the surface to 75 m showed weak long wave activity from the beginning of the record at 01 January 1991 to March 1991 and from June to September 1991 (Figure 12a). There was strong activity from July 1992 to March 1993 and from October 1993 to the end of the record at 31 December 1993 (Figure 12b,c). The period of these waves was approximately 30 days. Below 75 m, there was also wave activity at the same times. The largest amplitudes were from 100 m to 250 m and had approximately the same period as the waves in the upper layer, as can be seen in Figure 12b from July 1992 to February 1993 and in Figure 12c from October to 31 December 1993. The upper layer (surface to 75 m) temperatures tended to be low when the deeper temperatures were high, and vice versa. Figure 12b shows this relationship from September to November 1992. This relationship is discussed in section C4. Similar difference in near-surface and deeper wave activity were also present at 8°N and 2°N, and from 110°W to 170°W (not shown).

b. 0° 140°W

The temperature time series at 0° 140°W (Figure 13) had a stronger upper layer seasonal signal than that at 5°N 140°W. The maximum temperatures occurred from May to June 1991 (Figure 13a), March to April 1992 (Figure 13b), and from April to June 1993 (Figure 13c). The difference in the time period of the maximum upper layer temperature in 1992 compared to 1991 and 1993 will be discussed in section B8.

The temperatures below 50 m showed strong variability while those at and near the surface have smaller variations. This can be seen in Figure 13b from January to March 1992. There was weak long wave activity in the upper layer at approximately the same time and with the same characteristics as at 5°N 140°W (e.g., July to December 1992, Figure 13b). There was, however, no deep wave activity of the type seen at 5°N 140°W during 1992 and 1993 (Figure 13b,c). The strong deep wave activity at 0° 140°W occurred from November 1991 to April 1992 (Figure 13b,c). These waves had a period of approximately 60 days. The deeper temperatures and the upper layer temperatures tended to vary in phase (e.g., January to February 1992, Figure 13b). Note that the time of the seasonal maximum temperature in 1992, March, (Figure 13b) was early compared to that for 1991, June, (Figure 13a) and 1993, May (Figure 13c). This will be discussed in more detail in a section B4. Upper layer wave activity was present from 8°N to 5°S and from 110°W to 170°W

(not shown). Deep wave activity was also present from 2°N to 5°S and from 110°W to 170°W (not shown).

c. 5°S 140°S

There was much less variability in the temperature time series at 5°S 140°W (Figure 14). However, the upper layer wave activity seen at 5°N and 0° was evident. Figure 14b shows this activity from August to December 1992. The deep wave activity seen at 0° was also evident but weaker (e.g., January to February 1992, Figure 14b). The wave activity and seasonal temperature variations were similar in their timing and in their latitudinal and longitudinal extent to those at 0° 140°W.

2. CURRENT TIME SERIES

The only current meter data available for this study were from four equatorial buoys (see Chapter II). Thus, wave activity in the currents could be analyzed only on the equator. Time series of the currents are very useful complements to the temperature records in detecting and characterizing propagating waves.

The current meter record at 0° 140°W (Figure 15) is representative of the current records in our data set. The mean zonal current from the surface to 25 m was approximately zero (Figure 15a,b,c). There was strong variability in the direction of this near-surface flow from October 1991 to February 1992 (Figure 15a,b). This time frame corresponded to

the time of deep wave activity present in the temperature record (Figure 13a,b). Below 25 m, the dominant mean flow was eastward, corresponding to the Equatorial Undercurrent (EUC). Flow variations similar to those seen from the surface to 25 m during October 1991-February 1992 were also present down to 200 m (Figure 15a,b). There were shifts in the current direction from 45 m to 80 m. Below 80 m, the current flowed to the west, but the speed varied. The period of these variations was approximately 60 days, which is the approximate period of the temperature fluctuations (Figure 13a,b) discussed in section A1b.

The mean flow of the meridional current was approximately zero (Figure 15d,e,f). There were large fluctuations in meridional direction and speed from August to September 1991 at 3 and 25 m (Figure 15d); from July to September 1992 at 3, 25, and 45 m (Figure 15e); and from December 1992 to March 1993 at 25 m (Figure 15e,f). These correspond to the upper layer wave episodes discussed in section A1b. The period of these current fluctuations was approximately 20-30 days which was the approximate period of the temperature fluctuations (Figure 13a,b,c) discussed in section A1b. These meridional fluctuations and the ones in the zonal current were also present at 0° 110°W (not shown).

Figure 15 also shows other periods of strong current fluctuations. However, these fluctuations were not examined in this study because there were no corresponding large

temperature fluctuations associated with these current fluctuations.

3. WIND TIME SERIES

The wind time series were used to determine if any of the detected long wave activity appeared to be forced by the local wind. The wind records are from the same locations as the temperature data. Extensive analyses of the October 1991-March 1992 equatorial wind data were conducted by Cooper (1992) and Kent (1993). In this study, relationships between the wind and the temperature and current data were determined for the entire 1991-1993 period and for equatorial and off-equatorial locations.

a. 5°N 140°W

The mean direction of the zonal wind (Figure 16) was to the west, corresponding to the trade winds. Weakenings or reversals in the trade winds are called westerly wind events. There were numerous westerly wind events during the last half of 1991 (Figure 16a) and during much of 1992 (Figure 16b).

The meridional wind had a seasonal alternation between northerly and southerly flow (Figure 16a,b,c). The northerly flow tended to occur during the northern hemisphere winter and spring while southerly flow tended to occur during the northern summer and fall. This cycle was also present at 8°N and to a weaker extent at 2°N (not shown). This

seasonality in the meridional wind represents the seasonal shift in the intertropical convergence zone.

b. 0° 140°W

There were strong westerly wind events during January and March 1992 (Figure 17b). These wind events were more pronounced at 155°W, 170°W, and 165°E (not shown). There were other strong westerly wind events from November to December 1991 at 155°W, 170°W, and 165°E (not shown). These events also extended from 2°N to 5°S (not shown). Cooper (1992) and Kent (1993) extensively examined these wind events and determined they were associated with tropical cyclones.

The wind events from November 1991 to March 1992 occurred just before or during the strong wave activity in the deep temperature record (Figure 13a,b) and the upper layer zonal current record (Figure 15a,b).

The variations of the meridional wind were weaker and shorter in duration than those for the zonal wind (Figure 17). The meridional wind did not show the strong seasonal oscillations present at 5°N (Figure 16). The mean flow was approximately zero from 0° to 5°S (not shown).

c. 5°S 140°W

The wind showed the same type of variability found at 0°N (Figure 18). There are strong westerly wind events during December 1991 (Figure 18a), and from January to February 1992 (Figure 18b). These events also occurred before

or during the period of deep wave activity in the temperature record (Figure 14a,b).

The time series of temperatures, currents, and winds contained extensive data gaps that made analyses of the entire three year study period difficult. Also, seasonal variations in the activity of different wave types made the analysis of the entire period problematic, especially for understanding wave physics. Therefore, for this study, most of our analyses focused on periods within the three year record when data gaps were minimal and when intense wave activity was present.

B. EQUATORIAL KELVIN WAVES

This section focuses on analyses of the 125 m temperature data and zonal surface current data at the equator, during 31 August 1991-31 May 1992. These were locations and times when wave activity in the temperature record was strong and current data was available (Figures 19 and 20a). The waves at these locations and times are referred to, for convenience, as the 91-92 EQ waves. A subset of this data (10 October 1991-31 March 1992) was previously analyzed by Cooper (1992) and Kent (1993) in studies of the oceanic response to anomalous westerly wind forcing. The passage of equatorial Kelvin waves during this time frame was detected by Kousky (1991, 1992) and Cooper (1992). In this study, we used a longer record and concentrated on a more detailed analysis of the wave activity.

1. SPATIAL EXTENT

Wave activity similar to that at 0° 140°W during September 1991-April 1992, October 1992-February 1993, and August-October 1993 (Figure 13) was also present at 2°N to 5°S during these times (not shown). Similar wave activity was also present several days to weeks earlier at 155°W and 170°W, and several days to weeks later at 125°W and 110°W (Figure 19). It was also present in the zonal current at 0° 140°W (Figure 20a) and 0° 110°W (not shown). This wave activity was strongest from 2°N to 2°S and very weak at 5°S (not shown). Thus, this wave activity was strongest in the equatorial wave guide. There was no evidence of this wave activity in the western Pacific. This may have been due to large data gaps in the temperature and current data, poor horizontal resolution, and weak vertical temperature gradients in the western Pacific.

2. TIME PERIODS

Strong individual wave events occurred in the central Pacific 125 m temperature field from September 1991 to April 1992 (Figures 12-14, 19). Weaker events occurred from November 1992 to February 1993, and August 1993 to October 1993 (Figures 12-14, 19).

The zonal current at 45 m and above showed several reversals of the SEC and strong fluctuations in the EUC from September 1991 to the end of February 1992 (Figure 20a). This

is the same period during which strong wave activity was seen in the temperature record (Figures 12-14, 19). The meridional current did not show any strong oscillations at these times (Figure 20b).

3. WAVE PERIODS

Wave periods were estimated using frequency spectra based on the 0° 140°W 125 m temperature and the near-surface current time series. For the activity during August 1991-May 1992, September 1992-February 1993, and August 1993-October 1993 (Figures 19 and 20a), these spectra show periods of 40 to 70 days (not shown). The 91-92 EQ waves had a pronounced peak in the temperature and zonal current spectra from approximately 48 to 52 days (Figure 21a,b). There was a minimum at this period in the spectral energy of the meridional current (Figure 21c). Similar spectral analyses were done for the temperature and current time series at other times, depths, latitudes, and longitudes, where similar wave activity was present. These analyses also showed periods of 40 to 70 days (not shown). These wave periods are similar to the 10 to 60 day periods observed for equatorial Kelvin waves detected in other studies (Lukas et al. 1984, Cooper 1992).

4. DEPTH EXTENT

In the temperature record at 110°W, the waves occurred at depths from 75 m to 200 m, with the strongest amplitude at 100 m (not shown). From 125°W to 170°W they occurred from

100 m to 300 m and had their strongest amplitudes at 125 m (e.g., Figure 13). This difference between the eastern and central Pacific was related to the slope in the thermocline, which was deeper in the west and shallower in the east. The zonal current data showed wave activity from 3 m to 80 m at 140°W (e.g., Figure 20a) and at 110°W (not shown). The 3 m zonal current data was used in many current analyses because it contained the longest continuous record and strongest wave signal. The daily averaging of the data (Chapter II) eliminated most of the surface gravity wave current signal.

Correlations of temperature data at 2°N, 2°S, and 5°S, between different depths, showed no lags at and below 100 m (75 m at 110°W) (not shown). However, at 0° the temperature at 125 m led the shallower temperatures (e.g., surface temperature by 4 days and the 75 m temperature by 6 days (Figure 22a-d)). Temperatures deeper than 150 m lagged the temperature at 125 m by approximately 2 days at 200 m to 10 days at 500 m (Figure 22g-j). This difference between depths was probably caused by variations in the background flow with depth. The current direction from 3 m to 25 m was primarily to the west due to the SEC, while from 80 m to 200 m it was to the east, due to the EUC (Figure 20a). The SEC likely slowed the eastward propagating signals while the EUC sped up these signals. The lags at depths below 200 m cannot be explained in this way because no current data is available. This type of zonal current effect on equatorial Kelvin waves was also

noted by McPhaden et al. (1986).

5. PHASE SPEEDS

Time-longitude plots of temperature show the 91-92 EQ waves propagating from west to east (Figure 19). The phase speeds for these waves were estimated from cross correlations of the equatorial 125 m temperatures at different longitudes (Figure 23a-d). These correlations show that the 125 m temperature at a given buoy lagged that at buoys to the west and led that at buoys to the east. The phase speed was calculated by dividing the zonal distance between the buoys by the lead/lag time. The lengths of these lags and leads (Figure 23a-d) imply phase speeds of 1.9 m/s to 6.5 m/s. Similar correlations were applied to the zonal surface current (Figure 23e). The phase speeds computed using the temperature and zonal current data were in the same range. The phase speed calculated from the correlation between 170°W and 140°W was 4.3 m/s; between 155°W and 140°W, 6.5 m/s; between 140°W and 125°W; 1.9 m/s, and between 140°W and 110°W, 2.4 m/s. The phase speed computed using the zonal surface current was 1.9 m/s between 140°W and 110°W. These differences in computed phase speeds could be caused by interaction with the background currents, differences in the background stratification, or local disturbances of the wave signal at the different buoy longitudes. This study did not investigate the causes of these differences. These eastward phase speeds

are generally consistent with the 2.5 to 3 m/s phase speeds observed for first baroclinic equatorial Kelvin waves in other studies (Knox and Halpern 1982, Miller et al. 1988, McPhaden et al. 1988, Hayes et al. 1991, Delcroix et al. 1991, Cooper 1992, Johnson and McPhaden 1993).

6. WAVELENGTH

The cross-correlations in the previous subsection were also used to determine wave lengths. This was done by multiplying the phase speed by the number of days of lag between positive correlation peaks. This calculation gave wavelengths of 10,000 to 33,000 km, comparable to what Cooper (1992) found.

7. TEMPERATURE AND CURRENT CORRELATIONS

There was a strong positive correlation between the 91-92 EQ wave activity in the temperature record and the zonal current at 3 m (Figure 24). Thus, when the temperature was high, the current direction tended to be eastward; and when the temperature was low, the current direction tended to be westward. There was very little or no correlation between the temperature and the meridional surface current (not shown). This is consistent with the vertical structure of a propagating first baroclinic mode equatorial Kelvin wave (cf. Figures 2a,3,4). Modeling (Giese and Harrison 1990) and observational studies (Knox and Halpern 1982, McPhaden et al. 1988, Johnson and McPhaden 1993) of propagating equatorial

Kelvin waves also showed this relationship between temperature and zonal current.

8. EVIDENCE FOR EQUATORIAL KELVIN WAVES

Much of the deep wave activity at 0° 140°W (Figure 13, 15a,b,c) was apparently due to the propagation of equatorial Kelvin waves. The previous subsections have presented evidence that the deep wave activity in the temperature (Figure 13) and zonal current records (Figure 20a) were propagating first baroclinic mode equatorial Kelvin waves. The waves were mostly confined to the equatorial wave guide. They propagated to the east at phase speeds consistent with those for equatorial Kelvin waves. The periods of the waves and their wavelengths were in the range of equatorial Kelvin waves detected by previous investigators (Miller et al. 1988, Cooper 1992). There were strong variations in the speed and direction of the zonal near-surface current while variations in the meridional near-surface current were much weaker. There was a strong positive correlation between the subsurface temperature data and the zonal near-surface current. There was also a strong positive correlation between subsurface temperature and surface temperature at the equator (Figure 22a). When the downwelling (upwelling) phase of the equatorial Kelvin waves passed, they apparently raised (lowered) the sea surface temperature by warm water advection from the west and downwelling. All these features are

consistent with what has been observed during previous years of equatorial Kelvin wave activity (Knox and Halpern 1982, Erickson et al. 1983, Lukas et al. 1984, Miller et al. 1988, McPhaden et al. 1988, Hays et al. 1991, Delcroix et al. 1991, Cooper 1992, Johnson and McPhaden 1993).

9. TEMPERATURE ANIMATIONS

Temperature and temperature anomaly fields for the 91-92 EQ waves were animated using VIS 5D. The temperature anomaly fields were computed by subtracting the 1991-1993 mean temperature field from the total temperature fields. The discussion in this section is based on animations of temperature cross sections along 140°W and the equator on 17 January, 01 February, and 14 March 1992 (not shown). These times corresponded to a minimum, maximum, and minimum in the temperature signal at 125 m (Figure 13b).

The mean temperature cross section along 140°W showed the thermocline sloping from approximately 80 m at 8°N to 125 m at 5°S. The thermocline bulged upward at the equator and cooler temperatures were present in the upper layer compared to the regions to the north and south. This indicated upwelling had occurred at the equator. The cross section along the equator showed that the thermocline sloped from approximately 125 m at 156°E to 60 m at 110°W.

On 17 January 1992 the thermocline sloped downward from approximately 100 m at 8°N to 130 m at 2°N and then

bulged upward at the equator before continuing downward to 150 m at 5°S. The upper layer was coolest at the equator. On 01 February 1992 the thermocline deepened between 2°N and 5°S from approximately 150 m to 175 m and the upper layer warmed from 27.5°C to greater than 28°C. The temperature field on 14 March 1992 returned to approximately the same conditions as were present on 17 January 1992, except the thermocline was deeper north of 5°N and shallower from 2°N to 5°S. The upward bulge in the thermocline was still evident at the equator.

There were positive temperature anomalies between 5°N and 5°S and from the surface to 200 m on 17 January 1992. The maximum positive anomaly was at 125 m between the equator and 5°S. On 01 February 1992 the positive temperature anomalies increased in intensity throughout the water column. The location of the maximum positive anomaly deepened to 150 m between the equator and 2°S. The temperature anomaly field on 14 March 1992 was considerably different than the one on 17 January 1992. Negative temperature anomalies spanned the entire water column from approximately 100 m to 250 m. The maximum negative anomaly was located at 125 m between 2°N and the equator.

The cooler temperatures, weak positive anomalies in the upper layer, and the upward bulge in the thermocline, at the equator, on 17 January 1992 and 14 March 1991 indicated upwelling had occurred. The deepening of the thermocline, the increase in upper layer temperature, and the presence of

strong positive anomalies throughout the water column between 2°N and 5°S on 01 February 1992 indicated downwelling occurred.

The presence of upwelling, followed by downwelling, followed by upwelling between 2°N and 5°S indicated that a wave propagated through this area. The animation gives a good representation of the passage of the upwelling and downwelling phases of propagating equatorial Kelvin waves.

A longitudinal cross section of temperature along the equator on 17 January 1992 showed the thermocline in the western Pacific at 100 m. The thermocline deepened between 170°W and 155°W to about 150 m, then shoaled to 125 m at 140°W, and 100 m at 110°W. The maximum temperature is located at about 50-70 m between 156°E and 170°W. On 01 February 1992, the deepest thermocline was at approximately 165°W and the maximum upper layer temperature was at about 90 m at 160°W. By 14 March 1992, the thermocline had shoaled to approximately 75 m and the upper layer temperature had cooled throughout the Pacific.

On 17 January 1992, between 100 and 150 m there were negative temperature anomalies in the western Pacific, strong positive anomalies between 170°W and 155°W, and weaker positive anomalies between 140°W and 110°W. By 01 February 1992, the strongest positive temperature anomalies had moved to the east, from between 170°W and 155°W to between 140°W and 125°W while the negative anomalies in the western Pacific

moved to the central Pacific. By 14 March 1992, the negative temperature anomalies at 125 m had propagated to the east and the deep layer positive temperature anomalies were only present in the eastern Pacific.

The eastward propagation of the depressed thermocline, the upper layer temperature maximum, and the strong positive temperature anomalies followed by the negative anomalies indicated that subsurface waves had propagated from the western to eastern Pacific as shown in Figure 19. The phase speed of these propagating features was approximately 2.4 m/s. These waves are the equatorial Kelvin waves described in section B8.

10. FORCING MECHANISMS

There were numerous strong westerly wind events during 31 August 1991-31 May 1992 (Figures 17a,b and 25). Similar wind events also occurred at 2°N, 2°S and 5°S (not shown). Cooper (1992) determined that these wind events probably caused the formation of the equatorial Kelvin waves during this period. There were strong positive correlations between the subsurface temperature data and the zonal wind located to the west (Figure 26). There was also a strong positive correlation between the zonal surface current and the zonal wind located to the west (Figure 27). No relationships were evident between the temperature or current data with the winds located to the east.

The cross-correlations also showed that, moving eastward away from the location of the westerly wind events, the lead time between the western Pacific zonal wind and both the subsurface temperature and zonal surface current increased (Figures 26 and 27). This was also detected by Cooper (1992).

The strong positive correlation and the increase in lead time from west to east provide strong evidence that the westerly wind events in the western and central Pacific generated the equatorial Kelvin waves during 13 August 1991-31 May 1992. Cooper (1992) came to the same conclusion using a shorter record.

C. TROPICAL INSTABILITY WAVES

The wave activity in the upper layer from 8°N to 5°S, and at deeper depths from 8°N to 2°N, (Figures 12-14) occurred at different times than those of the equatorial Kelvin waves (Figure 13). The focus in this section is on the analyses of temperature at 5°N 140°W (Figure 12) and of current data at 0° 140°W (Figure 15). These analyses are representative of those based on data from other locations. Particular emphasis is placed in this section on the wave activity during 31 May 1992-30 April 1993 (Figures 12b,c, 13b,c, and 14b,c). During this period, there were few data gaps and the wave activity was especially strong. The waves during this period are, for convenience, referred to as the 92-93 5N waves.

1. SPATIAL EXTENT

The strongest off-equatorial wave activity was at 5°N (Figure 12) and 2°N (not shown) and from 110°W to 155°W. Wave activity was present from 8°N to 5°S and from 110°W to 170°W (not shown). The waves were mainly confined to regions poleward of the equatorial wave guide. This spatial extent was observed by Legeckis (1977), Legeckis et al. (1983), Legeckis (1984), Hansen and Paul (1984), Pullen et al. (1987), Malardé et al. (1987), Halpern et al. (1988), Périgaud (1990), and Hays et al. (1991) for tropical instability waves.

2. TIME PERIODS

There were three main episodes of distinct wave activity at 8°N (not shown), 5°N (Figure 28), 2°N (not shown), 0° (Figure 13), 2°S (not shown), and 5°S (Figure 14). Propagating waves occurred from July 1991 to January 1992 at 5°N (Figure 28) and 2°N (not shown). These waves were not detected at other latitudes either because they were too weak or because data were missing. The waves present from June 1992 to March 1993 were very strong and occurred from 8°N to 5°S (e.g., 5°N, Figure 28; 0°, Figure 13b,c; 5°S, Figure 14b,c). They were very weak at the equator (Figure 13b,c). This was also the case for the waves from June 1993 to the end of the data record at 31 December 1993. The first two episodes of wave activity can also be seen in fluctuations of the meridional current at 0° 140°W (Figure 29b) and to a

lesser extent in the zonal current (Figure 29a). Notice that these waves are only present in the northern hemisphere summer and fall. This is the time of year other investigators have observed tropical instability waves (Legeckis 1977, Legeckis et al. 1983, Legeckis 1984, Hansen and Paul 1984, Pullen et al. 1987, Malardé et al. 1987, Halpern et al. 1988, Périgaud 1990, Hays et al. 1991)

3. WAVE PERIODS

The wave periods were also estimated using frequency spectra as discussed in section B3. The spectra were based on the 25 m temperature (Figure 28a) and current (Figure 29) data, the 125 m temperature data (Figure 28c), and the 120 m current data (Figure 29). For the 92-93 5N waves, these spectra show periods of 15 to 30 days at 25 m (Figure 30a-c) and 25 to 30 days for temperature at 125 m (Figure 28d) and currents at 120 m (Figure 28e,f). This difference with depth is discussed in section C4, below. Similar spectral analyses were done for the temperature at other latitudes, longitudes, depths, and times at which similar wave activity was present. These analyses also showed wave periods of 15 to 30 days. These periods are similar to the 20-30 day tropical instability wave periods observed by other investigators (Legeckis 1977, Legeckis et al. 1983, Legeckis 1984, Hansen and Paul 1984, Pullen et al. 1987, Malardé et al. 1987, Halpern et al. 1988, Périgaud 1990, Hays et al. 1991).

4. DEPTH EXTENT

At 8°N, 5°N, and 2°N waves were present from the surface to at least 250 m (e.g., 5°N, Figure 12). The depth of maximum wave amplitude at 110°W was 100 m (not shown) while from 125°W to 170°W it was 125 m (Figure 28c). This depth variation was likely due to the slope in the thermocline, as described in the equatorial Kelvin wave section, B4. The wave activity from 0° (Figure 13) to 5°S (Figure 14) was only detectable from the surface to approximately 75 m in the temperature record. This was probably due to a weak signal, caused possibly by the current shear south of the equator being weaker than to the north of it. The South Equatorial Countercurrent (SECC) is generally weaker than the NECC. However, wave activity at the equator was seen in the current record from the surface to 120 m (Figure 29).

The waves in the upper layer (above 75 m) were apparently different from those in the deep layer (below 75 m). There was no clear continuity between the waves in the upper layer and those in the deep layer (Figure 28). Waves were detectable at 25 m (Figure 28a) and 125 m (Figure 28c) but they were difficult to detect at 75 m (Figure 28b). As discussed in the previous section, C3, the period of the waves in the upper layer was slightly less than those in the deep layer. There was also a strong negative correlation at zero lag between the upper layer temperature and the deep layer temperature (e.g., Figure 31a). In the deep layer, the

temperatures were strongly positively correlated (e.g., Figure 31b).

One possible explanation for these differences is that the waves in the upper and deep layer are of different types. The results of numerical modeling studies of tropical instability waves by Philander (1978); Cox (1980), Philander et al. (1985), and Philander et al. (1986) indicate that tropical instability waves tend to be confined to the upper layer and may excite mixed Rossby-gravity waves that propagate downward into deeper layers. Thus, the waves at 125 m (Figure 28c) may have been mixed Rossby-gravity waves which were overlain by tropical instability waves (Figure 28a).

5. PHASE SPEEDS

The time-longitude plots of 25 and 125 m temperatures at 5°N show that the 92-93 5N waves propagated to the west (Figure 28a,b). The phase speeds were estimated from cross-correlations of temperatures at 25 and 125 m at different longitudes (Figure 32a,b). These correlations show that the 25 m and 125 m temperatures at 155°W lag the temperatures at 140°W by approximately 35 days (Figure 32a) and 33 days (Figure 32b), respectively. This implies a westward phase speed of 0.6 m/s. The range of westward phase speeds calculated for the wave activity at all locations and time periods was 0.5 to 1.5 m/s. There was no apparent dependence of phase speed on depth, latitude, and longitude. The phase

speeds found in this study are similar to the 0.4 to 0.93 m/s tropical instability wave speeds observed by Legeckis (1977, Pullen et al. (1987), Malardé et al. (1987), Halpern et al. (1988), and Périgaud (1990), and modeled by Cox (1980) and Gordon (1992). Observed (Wiesberg et al. 1979) and modeled (Cox 1980) mixed Rossby-gravity waves also had similar phase speeds of 0.35 to 0.45 m/s.

6. WAVELENGTH

The zonal wavelength of the 92-93 5N waves was calculated using the method described in section B6. This calculation gave wavelengths of 1500 to 3500 km. These are on the order of the 400 to 2200 km tropical instability wavelengths observed by other investigators (e.g., Legeckis et al. 1983, Périgaud 1990).

7. TEMPERATURE AND CURRENT CORRELATIONS

The 25 m temperature at 0° 140°W from 31 May 1992 to 30 April 1993 (Figure 13b,c) had a weak positive correlation at zero lag with the co-located zonal current and a very weak correlation with the meridional current (Figure 33). Thus, warm water in these waves was associated with relatively eastward flow and cool water was associated with relatively stronger westward flow. Since these correlations are based on equatorial data, these current variations presumably represent the weakening and strengthening of the SEC. These relationships are consistent with previously reported

temperature-current relationships associated with tropical instability waves (e.g., Legeckis et. al. 1983).

8. EVIDENCE FOR TROPICAL INSTABILITY WAVES

Based on their location, propagation direction, phase speed, and time period, the 92-93 5N and similar waves appear to be tropical instability waves. There is strong evidence for propagating tropical instability waves and suggestive evidence for mixed Rossby-gravity waves. The location of the waves, mainly to the north of the equator, and their occurrence during the northern hemisphere summer and fall are consistent with the tropical instability wave results from other researchers (e.g., Legeckis et al. 1983, Legeckis 1984). Also, the waves' period, phase speed, wavelength, and correlation with currents are consistent with those previously determined for tropical instability waves (e.g., Legeckis et al. 1983, Pullen et al. 1987).

The major difference between this study and others is that the instability waves were detected during an El Niño event using temperature and current data. This study also provides the first observational support for the numerical modeling results of Philander (1978) and Cox (1980) that associated tropical instability waves with subsurface mixed Rossby-gravity waves.

9. TEMPERATURE ANIMATIONS

VIS 5D was used to animate temperature and temperature anomaly fields of the 92-93 5N waves. The temperature anomaly fields were computed by the same method described in section B9. The discussion in this section is based on animations of temperature cross sections on 22 August, 03 September, and 18 September 1992 along 140°W and 5°N (not shown). These times correspond to periods of intense wave activity between 8°N and 2°N with a temperature maximum in the upper layer and minimum in the deep layer, followed by a minimum in the upper layer and maximum in the deep layer, followed by another maximum in the upper layer and minimum in the deep layer (Figure 12b).

The mean temperature cross sections along 140°W and the equator were described in section B9. The mean temperature cross section along 5°N showed that the thermocline was at approximately 125 m from 156°E to 140°W. It then sloped upward to approximately 75 m from 140°W to 110°W. The warmest upper layer water was between 156°E to 155°W.

The temperature cross section along 140°W for 22 August 1992 showed that the thermocline sloped from about 80 m at 8°N to 120 m at 5°N, then sloped upward to about 50 m at the equator and then back down to 100 m at 5°S. Cool water was concentrated in the upper layer between 2°N and 2°S. By 03 September 1992 the thermocline had deepened to 125 m at 8°N and 150 m at 5°N. It then sloped upward to 100 m at 2°S and

then back down to 125 m at 5°S. The temperature in the upper layer between 8°N and 2°N had decreased while the temperatures to the south remained approximately the same as on 22 August 1992. The temperature field on 18 September 1992 had similar characteristics to the one on 22 August 1992. The thermocline at 5°N had shoaled back to about 100 m and the upper layer temperature between 8°N and 2°N had increased.

The temperature anomaly cross section for 22 August 1992 showed negative anomalies throughout the water column from 5°N to 5°S. The maximum negative temperature anomaly was at 75 m between 2°N and the equator. On 03 September 1992, a strong positive anomaly was evident below 75 m, between 8°N and 2°N, while the anomalies to the south and above it were negative. The deep layer positive temperature anomaly between 8°N and 2°N had been replaced by a negative anomaly by 18 September 1992. Thus, it took approximately 37 days for the negative temperature anomaly north of the equator to return.

The strong out of phase variations in near-surface and deeper temperatures during this 37 day period, and the location of these variations in the eastern and central Pacific near 5°N show that the animation provides a good representation of the tropical instability waves and mixed Rossby-gravity waves.

The cross section of temperature along 5°N, on 22 August 1992, showed the thermocline sloping from about 125 m

at 156°E to 100 m at 110°W. By 03 September 1992, the thermocline had deepened between 170°W and 140°W. This deepened thermocline propagated to the west, and by 18 September 1992 was between 170°W and 155°W.

On 22 August 1992, there was a strong negative temperature anomaly between 170°W and 155°W at 150 m, and a weak positive anomaly from 110°W to 125°W at 100 m. By 03 September 1992, the positive temperature anomaly had propagated westward to 140°W, increased in intensity, and deepened to about 200 m. Above this positive anomaly, there was a negative anomaly at 50 m. On 18 September 1992, this positive anomaly and the upper layer negative anomaly had propagated to between 170°W and 155°W. This propagation occurred at approximately 1.2 m/s. A second deep layer negative anomaly had appeared between 140°W and 125°W to the east of the positive anomaly, and a new positive anomaly had developed between 110°W and 125°W.

The westward propagation speed of the deepening thermocline and temperature anomalies, and their upper layer location, and periods provide a good representation of tropical instability waves that overlaid mixed Rossby-gravity waves.

10. FORCING MECHANISMS

There were no strong correlations between temperatures, currents, and local winds in association with

the tropical instability waves. Thus, it appears that the local winds were not a major forcing for the tropical instability waves. Previous studies have reported that tropical instability waves are driven by barotropic instability between the NECC and SEC (e.g., Legeckis 1977, Cox 1980, Hansen and Paul 1984). This could not be verified in this study because the current meter data was available only at 110°W and 140°W on the equator, away from the NECC and the area of maximum wave activity.

There was no evidence that the tropical instability and mixed Rossby-gravity waves were reflected equatorial Kelvin waves. The tropical instability and mixed Rossby-gravity waves tended to occur at 110°W too long (about two months) after the Kelvin waves had apparently reached the eastern Pacific boundary (compare Figures 19 and 31).

D. SUMMARY

The analyses of the wave activity present during the 1991-1993 El Niño showed the propagation of first baroclinic mode equatorial Kelvin waves and of tropical instability waves in association with possible mixed Rossby-gravity waves. No equatorial or off-equatorial Rossby waves were detected.

IV. CONCLUSIONS

A. SUMMARY AND DISCUSSION

Temperature, current, and wind time series were used in this study to detect and determine the properties of propagating long waves and the forcing mechanisms that generated them. The time series were measured by TOGA-TAO and EPOCS buoys located in the equatorial Pacific Ocean from 8°N to 8°S and from 110°W to 156°E. The current meter buoys were only located on the equator at 156°E, 165°E, 140°W, and 110°W. The data examined spanned from 01 January 1991 through 31 December 1993. This time period included the complete 1991-1993 El Niño event.

The time series contained numerous data gaps. The temperature time series were filled using linear interpolation and averaging procedures. The current and wind time series gaps were filled with zeroes. The major analyses of the time series were conducted only for times when there were strong wave amplitudes and minimal data gaps. The filling of these relatively short data gaps using these techniques did not seem to significantly affect the results of the analyses. However, the use of the filled data in computer animation did cause some problems in visualizing wave activity away from the areas of more complete data records. Using the filled data, we were

able to detect three types of propagating long waves.

Three episodes of propagating first baroclinic equatorial Kelvin waves were detected using temperature and current time series. These waves were most evident during September 1991-April 1992, November 1992-February 1993, and August 1993-October 1993. These waves were generally evident from 2°N to 5°S, 170°W to 110°W, and extended from 75 m to 300 m. The strongest signals occurred at the thermocline along the equator in the central Pacific. The waves had periods of 40 to 70 days, zonal wavelengths of 10,000 to 30,000 km, and eastward phase speeds of 1.9 to 6.5 m/s.

The temperature and current fluctuations for the Kelvin waves were positively correlated. When the subsurface temperature was warm the zonal surface current was eastward, and vice versa. Interation of the waves with the background flow appears to have caused differences in phase speeds. Differences in background stratification or local disturbances of the wave signal at the different buoy longitudes may also have caused these differences. The vertical shear along the equator between the SEC and EUC may explain why, at the equator, the temperature at 125 m leads temperatures at shallower depths by 4 to 6 days and lags the temperatures at deeper depths by 2 to 10 days.

The equatorial Kelvin waves appear to have been generated by westerly wind events in the western and central Pacific. There were strong positive correlations between zonal wind in

the western Pacific and: (a) the subsurface temperatures (cf. Cooper 1992) and (b) the zonal currents in the central and eastern Pacific.

Tropical instability waves were detected in the temperature time series and, to a lesser extent, in the current time series. There were three episodes of tropical instability wave activity: July 1991-January 1992, June 1992-March 1993, and June 1993-December 1993. These wave episodes occurred during the northern hemisphere summer and fall. Wave activity was evident from 8°N to 5°S and from 110°W to 170°W, with the strongest amplitudes in the eastern Pacific north of the equator but outside the equatorial wave guide. The waves had westward phase speeds from 0.5 to 1.5 m/s and zonal wavelengths of 1500 to 3000 km. The waves were detectable from the surface to approximately 250 m from 8°N to 2°N, although from 0° to 5°S they were only present in the upper 75 m. This latitudinal difference may have been caused by the greater current shear north of the equator between the SEC and the NECC. The waves in the upper layer from 8°N to 5°S had different properties than the waves located in the deeper layer from 8°N to 2°N. The waves in the upper layer had periods of 15 to 30 days while those in the deeper layer (>75 m) had periods of 25 to 30 days. There was also a strong negative correlation between temperature in the upper layer and the temperature in the deep layer. When the temperature in the upper layer was high, the deeper layer temperature was

low, and vice versa. Based on these findings the waves in the upper layer may have been of a different type then those in the deeper layer. The upper layer waves were apparently tropical instability waves (e.g., Legeckis 1977, Legeckis et al. 1983) while the deeper layer waves were possibly mixed Rossby-gravity waves identified in modeling studies by Philander (1978) and Cox (1980).

The forcing mechanism that generated the tropical instability waves and the mixed Rossby-gravity waves could not be determined. There were no strong correlations between the temperatures and local winds. No ocean current data were available in the area of maximum wave activity to use in estimating forcing mechanisms.

By using latitude-depth cross sections, the downwelling and upwelling phases of the equatorial Kelvin wave could be inferred from the three dimensional computer animation of the temperature data. The equatorial Kelvin waves were detected propagating from west to east in longitude-depth cross sections. The advection of warm western Pacific water to the east and the fluctuations in the thermocline by the equatorial Kelvin wave could also be seen.

The tropical instability waves and mixed Rossby-gravity waves could also be seen in the animation. The latitudinal-depth cross sections showed the warming of the upper layer followed by cooling, and opposite variations in the deeper layer. The fluctuation of the thermocline by the waves could

also be seen. The longitude-depth cross sections showed the same fluctuations from east to west. None of the waves could be detected using north-south cross sections because the areal resolution of the data was too coarse.

These propagating long waves were dominant features in the equatorial Pacific ocean during the 1991-1993 El Niño. They affected the SST and heat content of the ocean in different ways. The equatorial Kelvin waves warmed (cooled) the upper layer temperature by advection of warm water from the western (eastern) Pacific and by downwelling (upwelling). Based on the latitudinal extent of the detected equatorial Kelvin waves, they may well have affected the formation of tropical cyclones in the eastern Pacific, as hypothesized by Kent (1993). Further study is needed to better understand the relationship between equatorial Kelvin waves and equatorial weather conditions.

The tropical instability waves and mixed Rossby-gravity waves changed the temperature and heat content in opposing ways. When the tropical instability waves warmed the near-surface, the mixed Rossby-gravity waves cooled the water at and below the thermocline, and vice versa. These effects likely caused major changes in the heat content of the ocean and its effects on the atmosphere. It is interesting that the June to September 1992 episode of tropical instability waves corresponded to the time when the second warm phase of the El Niño was initiated. This suggests that the equatorward heat

flux associated with the tropical instability waves (see Chapter I) may have initiated this warm phase and help extend the El Niño into a second year. Additional data, especially current data, would be needed to determine if this suggestion is correct.

This study provides the first comprehensive examination of propagating long waves during the 1991-1993 El Niño. Numerous propagating equatorial Kelvin waves were detected, along with possibly the first detection of tropical instability waves and mixed Rossby-gravity waves during an El Niño using temperature time series.

B. FUTURE WORK

Further climate studies should include these long waves in order to understand the full interaction between the tropical ocean and atmosphere. Some projects that could be addressed using this data are:

(1) Examination of tropical instability waves during non-El Niño events and comparisons with those during El Niño events.

(2) Deployment of current meters in areas of strong tropical instability wave and mixed Rossby-gravity wave activity to help determine and study the forcing mechanisms that generate them.

(3) Exploration of the contribution of tropical instability waves and mixed Rossby-gravity waves to

the El Niño cycle.

(4) Integrated modeling of equatorial Kelvin waves, tropical instability waves, and mixed Rossby-gravity waves.

(5) Study of interactions between equatorial currents, Kelvin waves, tropical instability waves, and mixed Rossby-gravity waves.

(6) Verification of tropical ocean analyses against TOGA-TAO temperature, current, and wind observations.

We have conducted a brief preliminary study of temperature data from the Navy's Optimal Thermal Interpolation Scheme (OTIS) during 1991-1992. This study showed that OTIS had only a poor resolution of the equatorial long waves detected in the TOGA-TAO data.

LIST OF REFERENCES

Anonymous, 1992: *MATLAB Reference Guide*. The Mathworks, Inc, Natick, Massachusetts, pp548.

Cooper, G. A., 1992: *An Observational Study of the Local and Remote Response of the Equatorial Pacific to Westerly Wind Events During the 1991-92 El Niño*. Master's thesis, Naval Postgraduate School, Monterey, California, 103pp.

Cox, M. D., 1980: Generation and propagation of 30-day waves in a numerical model of the Pacific. *J. Phys. Oceanogr.*, **10**, 1168-1186.

Delcroix, T., J. Picaut and G. Eldin, 1991: Equatorial Kelvin and Rossby waves evidenced in the Pacific Ocean through Geosat sea level and surface current anomalies. *J. Geophys. Res.*, **96**, 3249-3262.

Eriksen, C. C., M. B. Blumenthal, S. P. Hayes and P. Ripa, 1983: Wind-generated equatorial Kelvin waves observed across the Pacific Ocean. *J. Phys. Oceanogr.*, **13**, 1622-1640.

Giese, B. S. and D. E. Harrison, 1990: Aspects of the Kelvin wave response to episodic wind forcing. *J. Geophys. Res.*, **95**, 7289-7312.

Gill, A. E., 1982: *Atmosphere and Ocean Dynamics*. Academic Press, Orlando, Florida, 662pp.

Gordon, L. J., 1992: *Analysis of a Simulation of the Seasonal Cycle in the Tropical Pacific Ocean in an Eddy-Resolving Global Ocean Model*. Master's thesis, Naval Postgraduate School, Monterey, California, 75pp.

Graham, N. E. and W. B. White, 1988: The El Niño cycle: A natural oscillator of the Pacific Ocean-atmosphere system. *Science*, **240**, 1293-1302.

Halpern, D., R. A. Knox and D. S. Luther, 1988: Observations of 20-day period meridional current oscillations in the upper ocean along the Pacific equator. *J. Phys. Oceanogr.*, **18**, 1514-1534.

Hansen, D. V. and C. A. Paul, 1984: Genesis and effects of long waves in the equatorial Pacific. *J. Geophys. Res.*, **89**, 10,431-10,440.

Harrison, D. E. and P. S. Schopf, 1984: Kelvin-wave-induced anomalous advection and the onset of surface warming in El Niño events. *Mon. Wea. Rev.*, **112**, 923-933.

Hayes, S. P., L. J. Mangum, J. Picaut, A. Sumi and K. Takeuchi, 1991: TOGA-TAO: A moored array for real-time measurements in the tropical Pacific Ocean. *Bull. Amer. Meteor. Soc.*, **72**, 339-347.

Hibbard, B., B. Paul, D. Santek, A. Battaiola and V. Maria-Francoise, 1993: *VIS 5D Software*. Space Science and Engineering Center, University of Wisconsin-Madison.

Johnson, E. S. and M. J. McPhaden, 1993: Structure of intraseasonal Kelvin waves in the equatorial Pacific Ocean. *J. Phys. Oceanogr.*, **23**, 608-625.

Kent, J. E., 1993: *Air-Sea Interaction Patterns in the Equatorial Pacific*. Master's thesis, Naval Postgraduate School, Monterey, California, 189pp.

Kessler, W. S., 1990: Observations of long Rossby waves in the northern tropical Pacific. *J. Geophys. Res.*, **95**, 5183-5217.

Knox, R. A. and D. Halpern, 1982: Long range Kelvin wave propagation of transport variations in Pacific Ocean equatorial currents. *J. Mar. Res.*, **40**, 329-339.

Kousky, V. E., 1991: *Climate Diagnostic Bulletin* (February-December), Climate Analysis Center, U.S. Department of Commerce, Washington, D. C., **91/2-91/12**.

Kousky, V. E., 1992: *Climate Diagnostic Bulletin* (January-December), Climate Analysis Center, U.S. Department of Commerce, Washington, D. C., **92/1-92/12**.

Kousky, V. E., 1993: *Climate Diagnostic Bulletin* (January-December), Climate Analysis Center, U.S. Department of Commerce, Washington, D. C., **93/1-93/12**.

Legeckis, R., 1977: Long waves in the eastern equatorial Pacific Ocean: a view from a geostationary satellite. *Science*, **197**, 1179-1181.

Legeckis, R., W. Pichel and G. Nesterczuk, 1983: Equatorial long waves in geostationary satellite observations and in a multichannel sea surface temperature analysis. *Bull. Amer. Meteor. Soc.*, **64**, 133-139.

Legeckis, R., 1984: Long waves in the eastern equatorial Pacific during 1983. *EOS, Trans. AGU.*, **65**, 229.

Little, J. N. and L. Shure, 1992: *Signal Processing Toolbox for use with MATLAB.* The Mathworks, Inc, Natick, Massachusetts, pp164.

Lukas, R., S. P. Hayes and K. Wyrtki, 1984: Equatorial sea level response during the 1982-1983 El Niño. *J. Geophys. Res.*, **89**, 10,425-10,430.

Matsuno, T., 1966: Quasi-geostrophic motions in the equatorial area. *J. Meteor. Soc. Japan*, **44**, 25-42.

McPhaden, M. J., J. A. Proehl and L. M. Rothstein, 1986: The interaction of equatorial Kelvin waves with realistically sheared zonal currents. *J. Phys. Oceanogr.*, **16**, 1499-1515.

McPhaden, M. J., J. A. Proehl and L. M. Rothstein, 1987: On the structure of low-frequency equatorial waves. *J. Phys. Oceanogr.*, **17**, 1555-1559.

McPhaden, M. J., H. P. Freitag, S. P. Hayes, B. A. Taft, Z. Chen and K. Wyrtki, 1988: The response of the equatorial Pacific Ocean to a westerly wind burst in May 1986. *J. Geophys. Res.*, **93**, 10,589-10,603.

McPhaden, M. J., 1993: TOGA-TAO and the 1991-93 El Niño-Southern Oscillation event. *Oceanography*, **6**, 36-44.

Miller, L., R. E. Cheney and B. C. Douglas, 1988: GEOSAT altimeter observations of Kelvin waves and the 1986-87 El Niño. *Science*, **239**, 52-54.

Mysak, L. A., 1986: El Niño, interannual variability, and fisheries in the northeast Pacific Ocean. *Can. J. Fish. Aquat. Sci.*, **43**, 464-497.

Périgaud, C., 1990: Sea level oscillations observed with Geosat along the two shear fronts of the Pacific North Equatorial Countercurrent. *J. Geophys. Res.*, **95**, 7239-7248.

Philander, S. G. H., 1978: Forced oceanic waves. *Rev. Geophys & Space Phys.*, **16**, 15-46.

Philander, S. G. H., 1981: The response of equatorial oceans to a relaxation of the trade winds. *J. Phys. Oceanogr.*, **11**, 176-189.

Philander, S. G. H., D. Halpern, D. Hansen, R. Legeckis, L. Miller, C. Paul, R. Watts, R. Weisberg and M. Wimbush, 1985: Long waves in the equatorial Pacific Ocean. *EOS, Trans. AGU.*, **66**, 154.

Philander, S. G. H., W. J. Hurlin and R. C. Pacanowski, 1986: Properties of long equatorial waves in models of the seasonal cycle in the tropical Atlantic and Pacific Oceans. *J. Geophys. Res.*, **91**, 14,207-14,211.

Seigel, A. D., 1985: A comment on long waves in the Pacific Ocean. *J. Phys. Oceanogr.*, **15**, 1881-1883.

Weddle, C. A., 1993: *The Effect of Westerly Wind Bursts on a Tropical Ocean General Circulation Model.* Master's thesis, Naval Postgraduate School, Monterey, California, 120pp.

Weisberg, R. H., A. Horigan and C. Collin, 1979: Equatorially trapped Rossby-gravity wave propagation in the Gulf of Guinea. *J. Mar. Res.*, **37**, 67-86.

White, W. B., 1977: Annual forcing of baroclinic long waves in the tropical north Pacific Ocean. *J. Phys. Oceanogr.*, **7**, 50-61.

White, W. B. and C-K Tai, 1992: Reflection of interannual Rossby waves at the maritime western boundary of the tropical Pacific. *J. Geophys. Res.*, **97**, 14,305-14,322.

Wyrtki, K., 1975: El Niño-the dynamic response of the equatorial Pacific Ocean to atmospheric forcing. *J. Phys. Oceanogr.*, **5**, 572-584.

This page intentionally left blank.

FIGURES

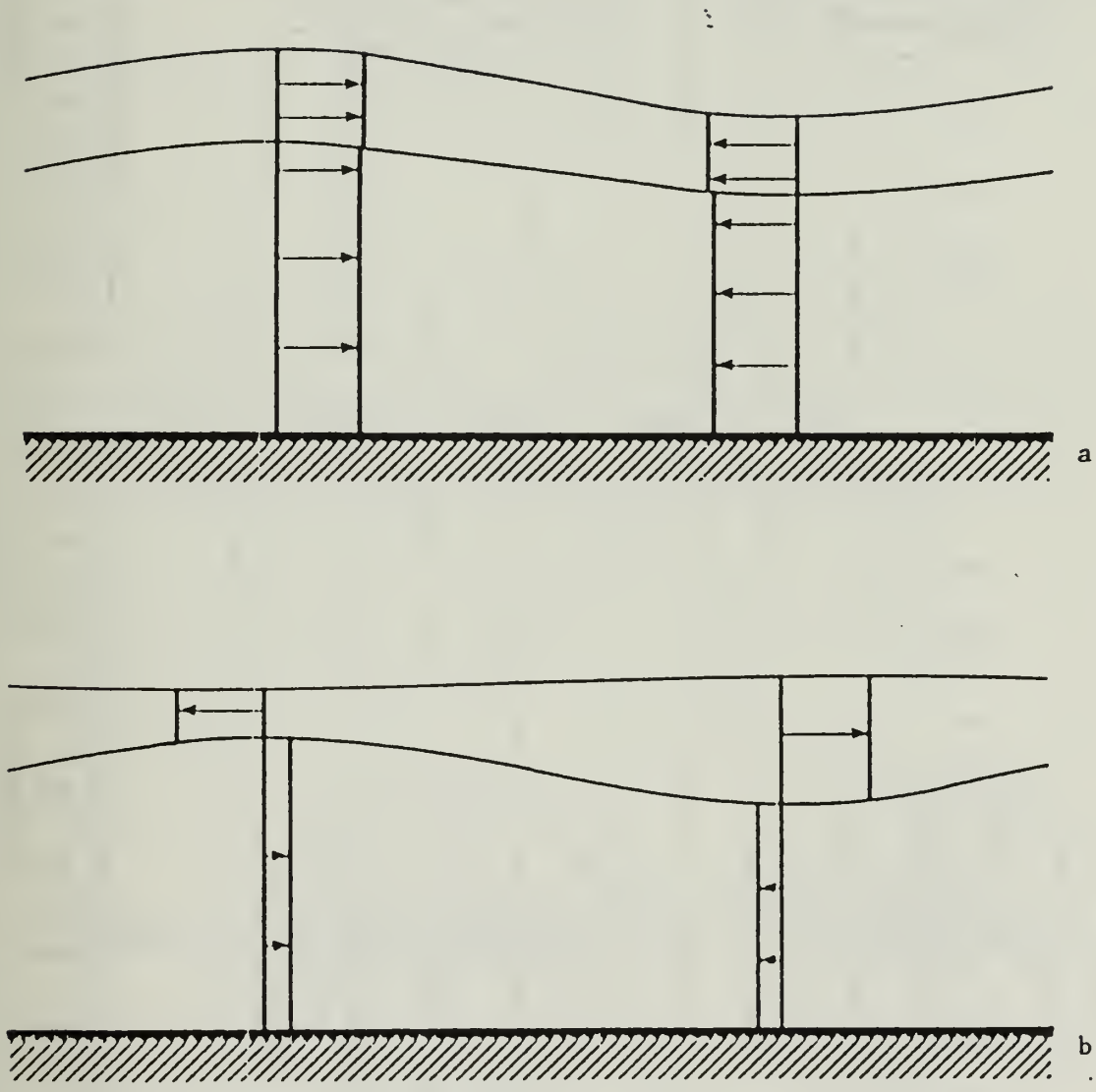

Fig. 1. Schematic of waves propagating from left to right. (a) barotropic waves, (b) baroclinic wave. From Gill (1982).

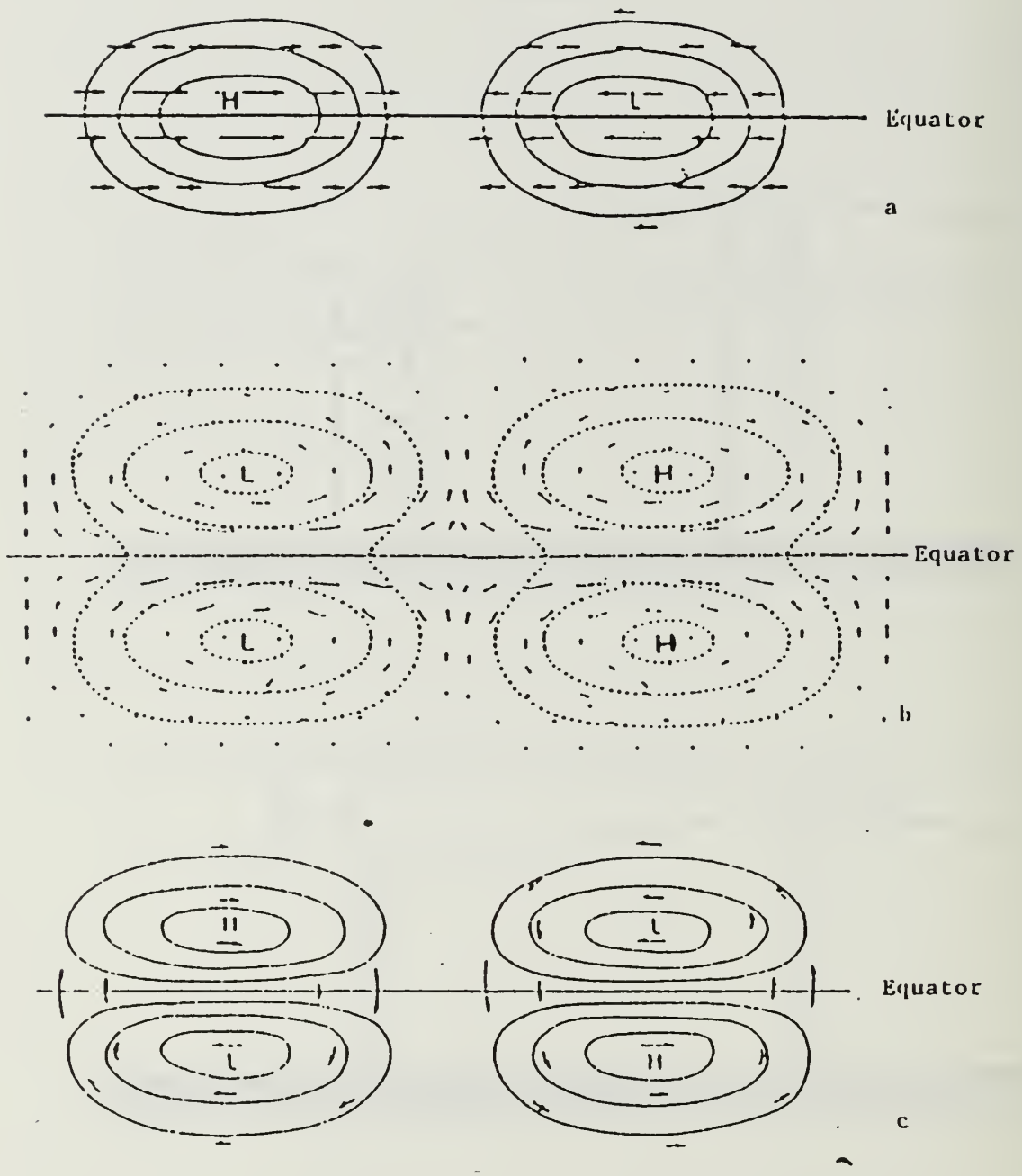

Fig. 2. Schematic latitude-longitude plots of velocity and pressure distributions in a horizontal plane for equatorial: a) Kelvin wave, b) Rossby wave, c) mixed Rossby-gravity wave. From Matsuno (1966).

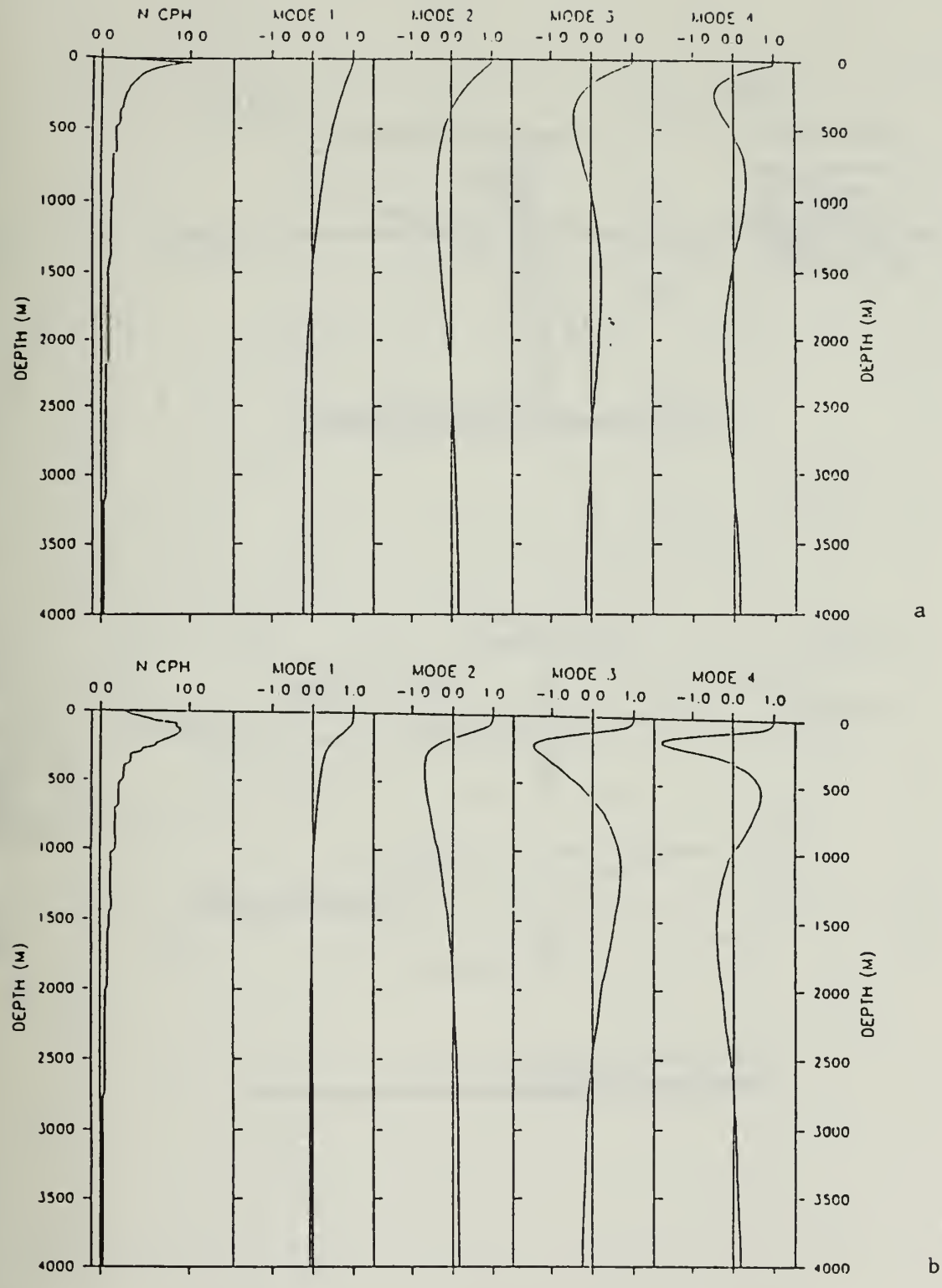

Fig. 3. The buoyancy profile (N) and the zonal velocity structure functions of the first four baroclinic modes for the density stratification: a) of the eastern Pacific, b) at 160°E. From Giese and Harrison (1990).

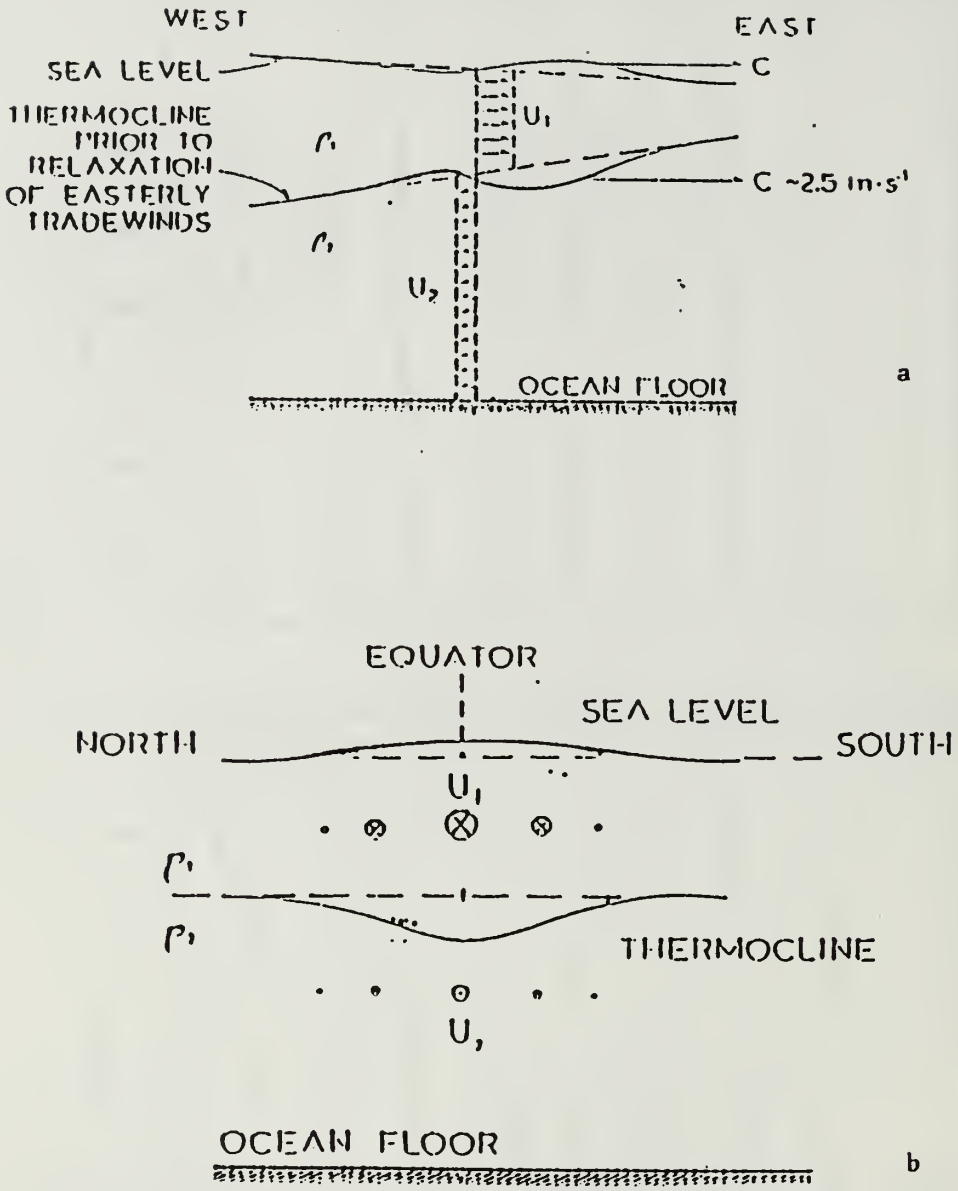

Fig. 4. Schematic views of vertical structure of downwelling phase of first baroclinic equatorial Kelvin wave, (a) view looking north, (b) view looking east. From Mysak (1986).

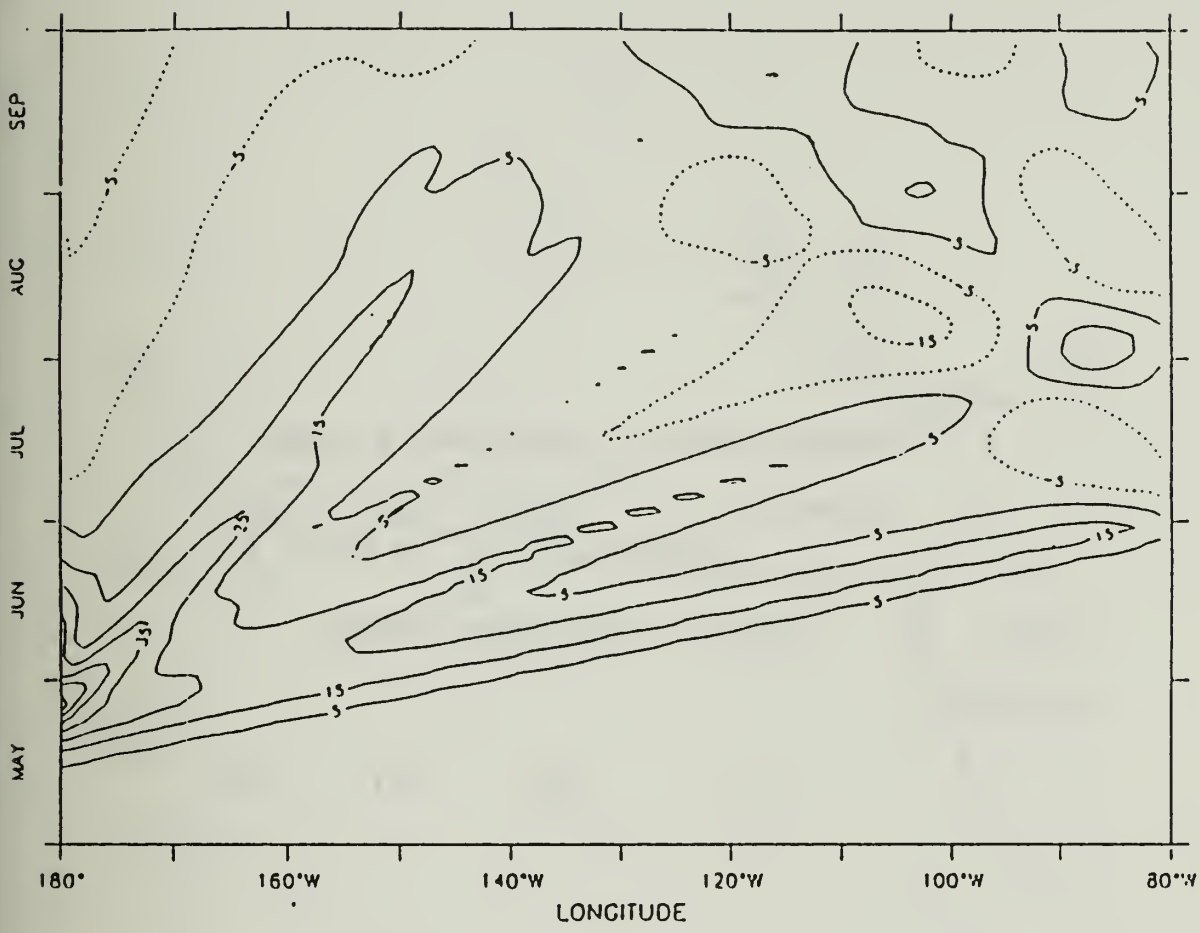

Fig. 5. Time-longitude plot of ocean model zonal velocity (cm/s). Solid contour, showing eastward propagation, are for the first four baroclinic Kelvin wave modes (caption continued on next page).

Fig. 5. (Continued, see figure on previous page) Dotted contours, showing westward propagation, are for the first two Rossby wave modes. From Giese and Harrison (1990).

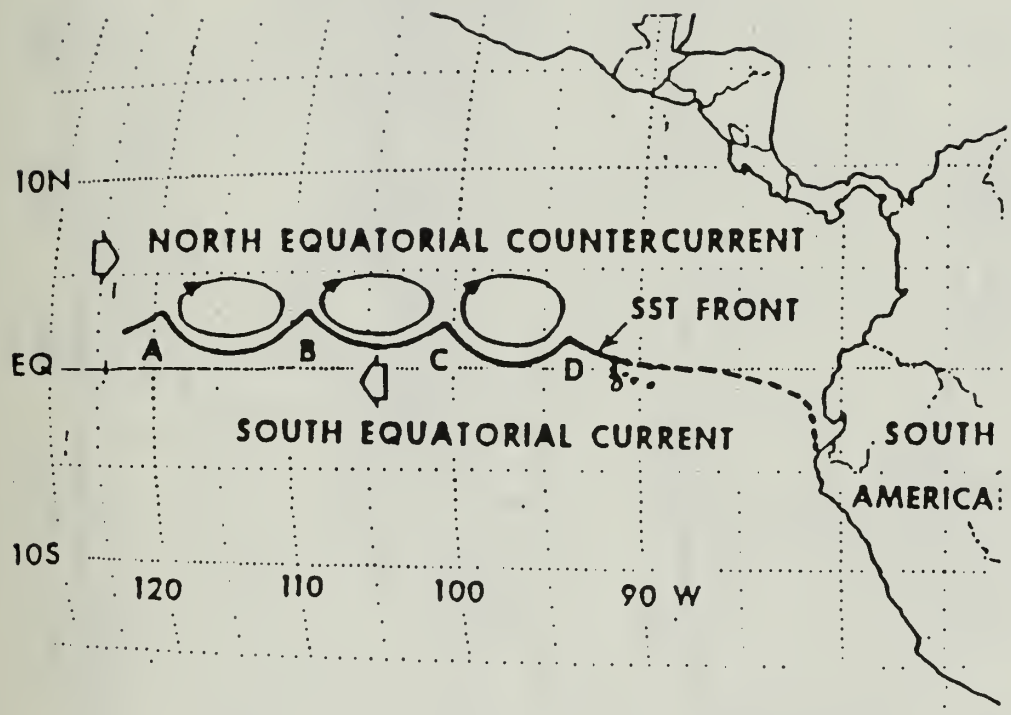

Fig. 6. Schematic of wave-like sea surface temperature fronts in the eastern equatorial Pacific. Associated anticyclonic eddies estimated from drifting buoy tracks. From Legeckis et al. (1983).

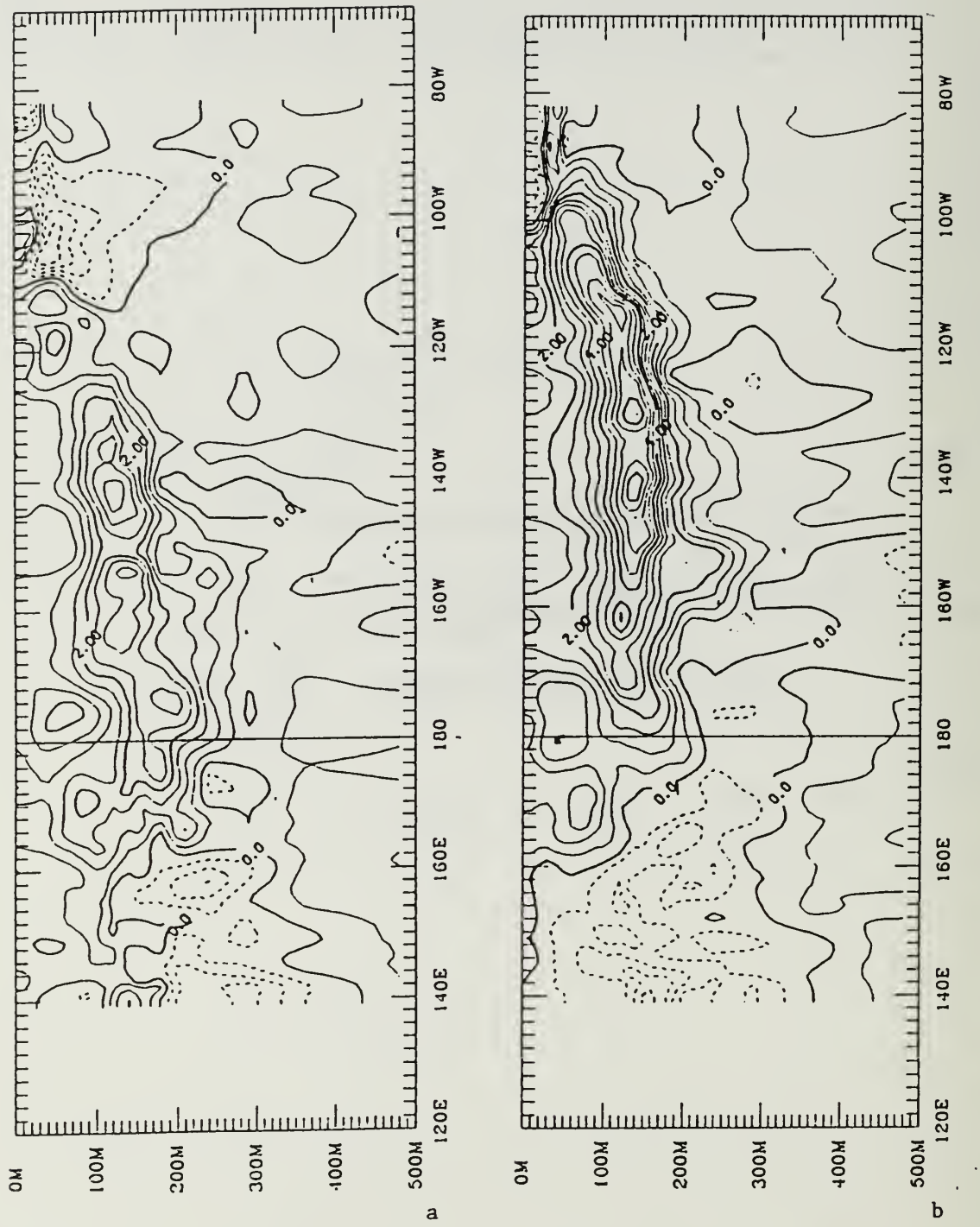

Fig. 7. Equatorial ocean temperature anomalies for: a) September 1991, b) October 1991. Contour interval is 0.5°C. Positive (negative) anomalies are indicated by solid (dashed) contours. From Kousky (1991).

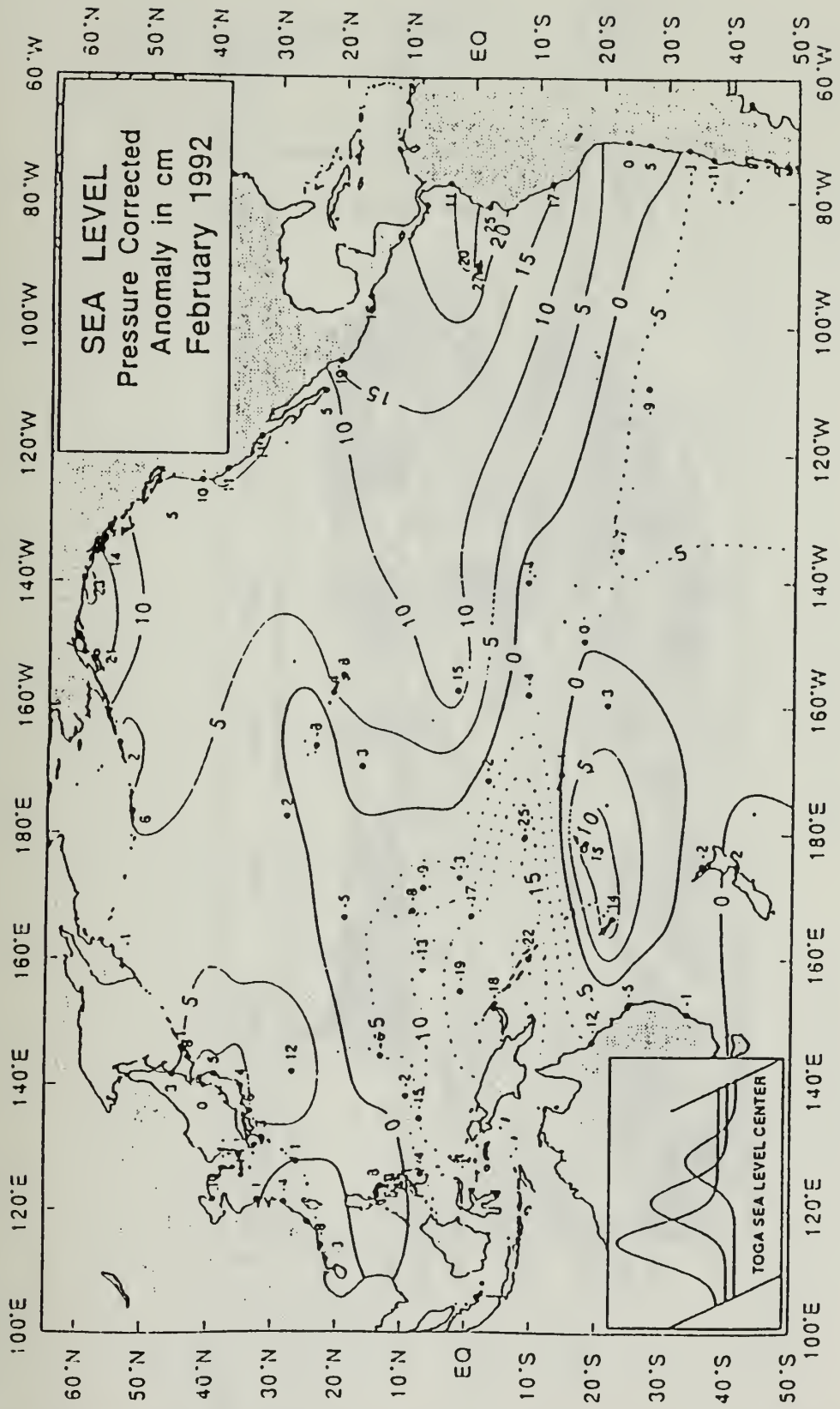

Fig. 8. Sea level anomaly for February 1992, adjusted for atmospheric pressure. From K. Wyrtki, TOGA Sea Level Center, University of Hawaii at Manoa, Honolulu HI; contained in Kousky (1992).

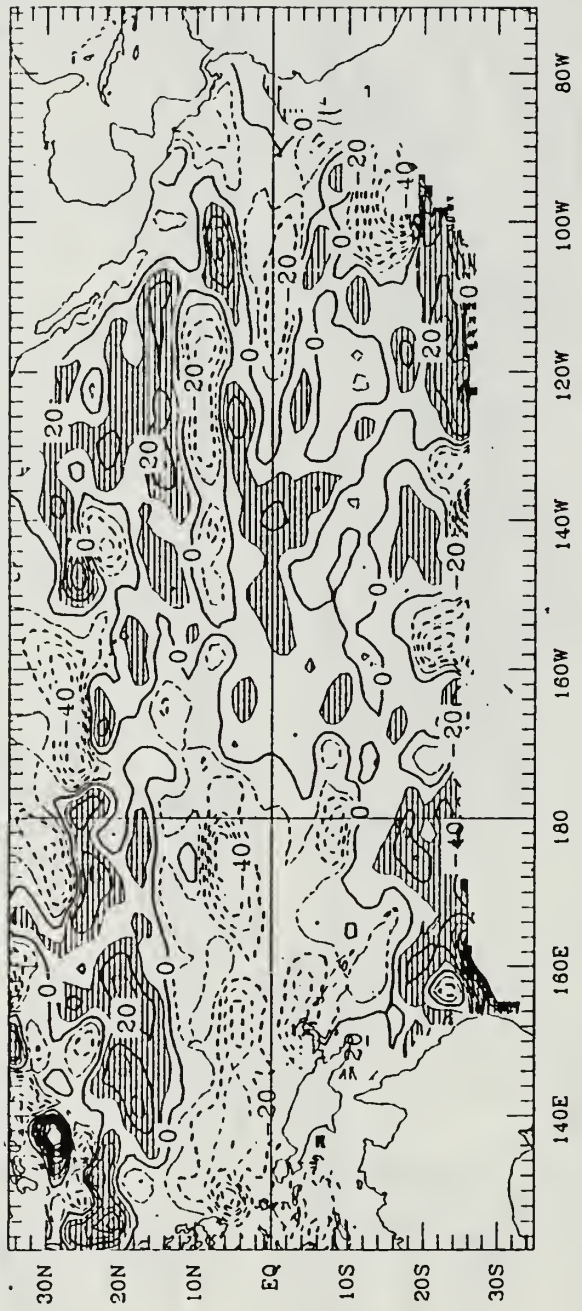

Fig. 9. Anomaly in the depth of the 20°C isotherm for the four week period ending 18 September 1993. From Kousky (1993).

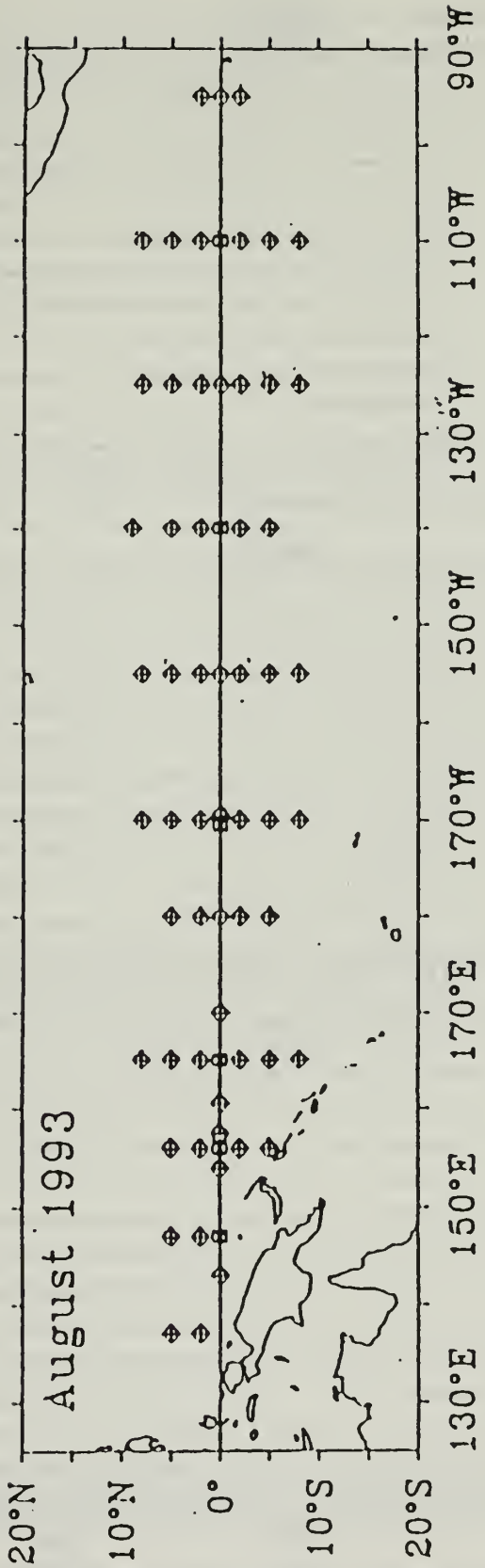

Fig. 10. The TOGA-TAO moored buoy array in August 1993. Atlas moorings, ◊ and current-meter moorings, □ . From McPhaden (1993).

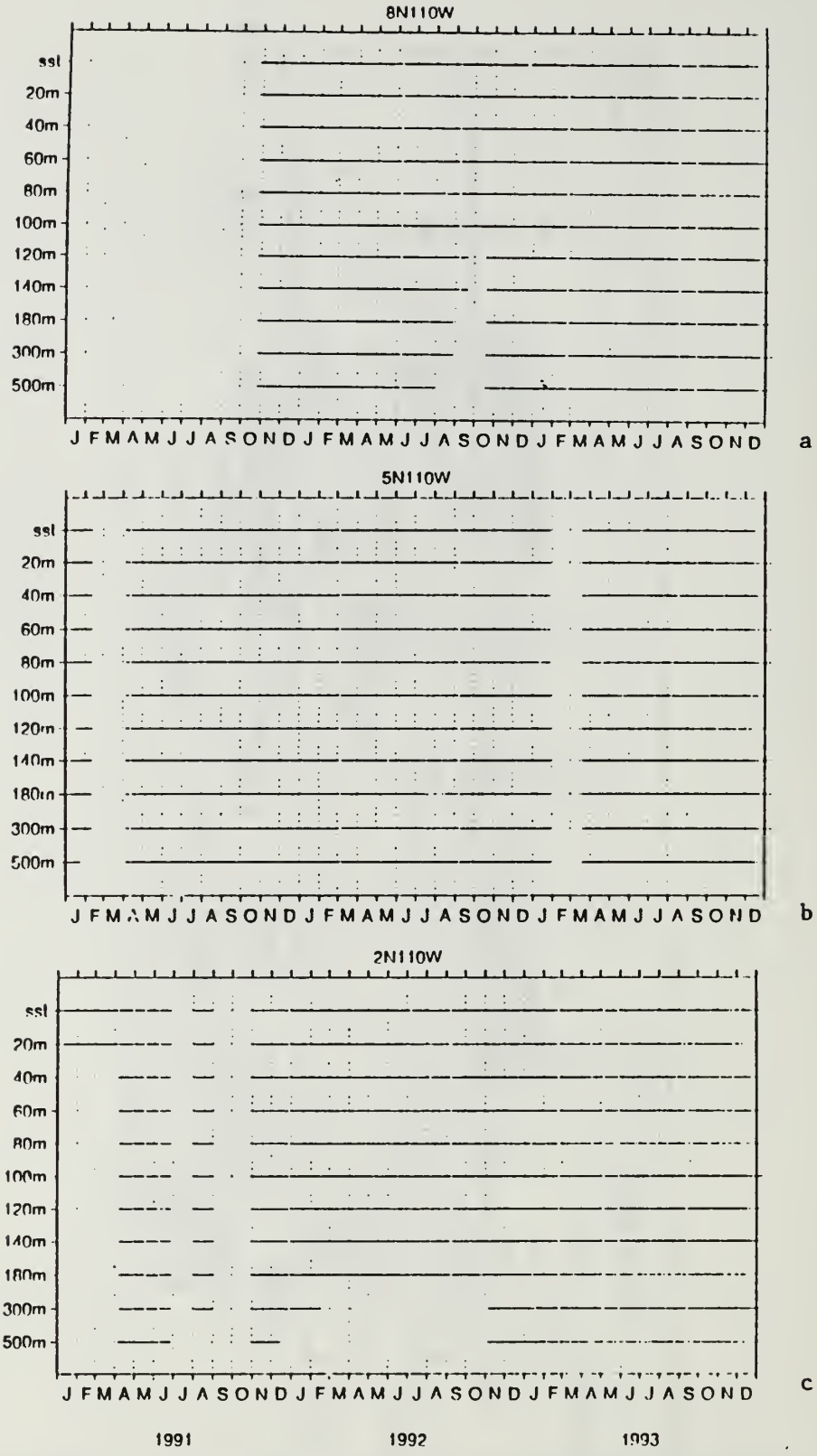

Fig. 11. Periods when temperature data was available (solid lines) for ATLAS and EPOCS buoys located at: a) 8°N 110°W, b) 5°N 110°W, c) 2°N 110°W,

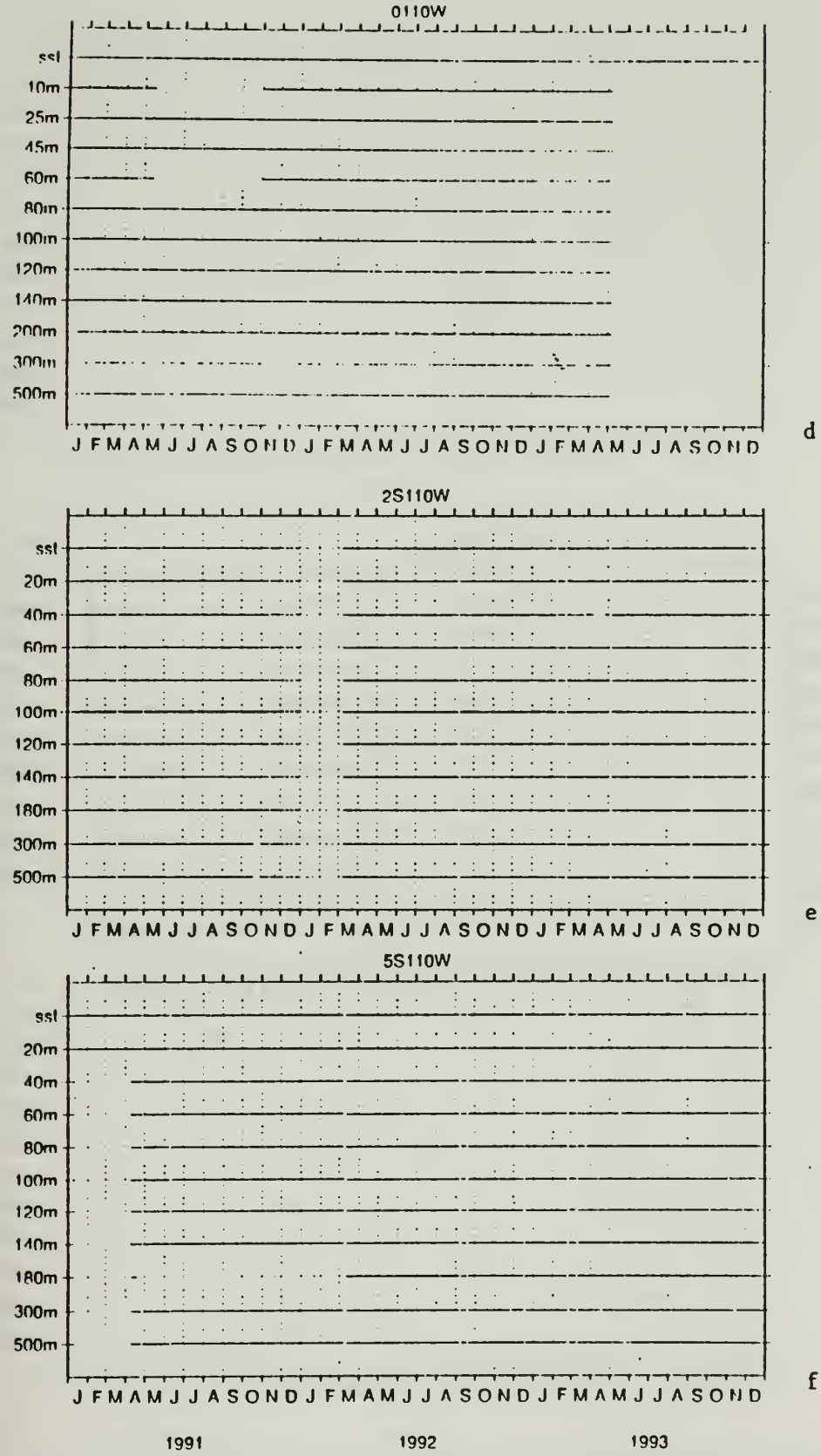

Fig. 11. (Continued) d) 0° 110°W, e) 2°S 110°W, f) 5°S 110°W,

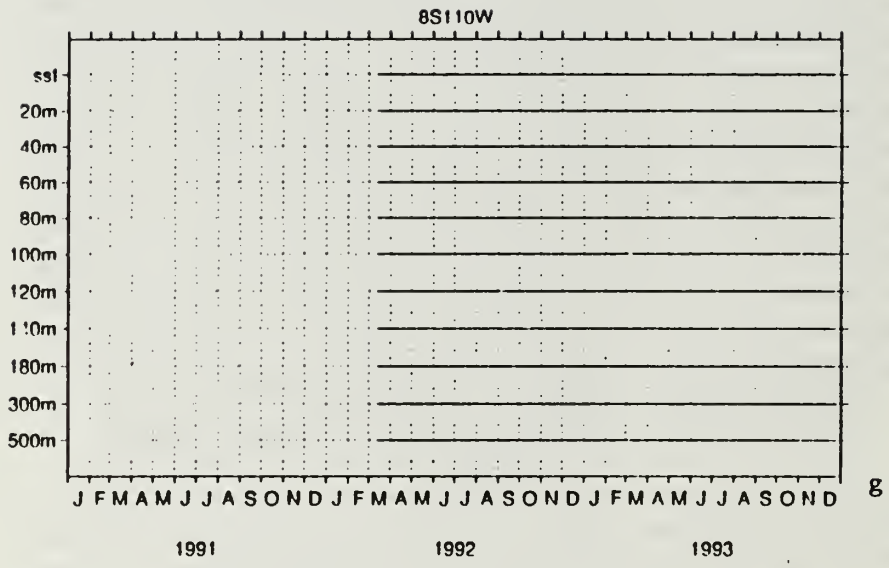

Fig. 11. (Continued) g) 8°S 110°W,

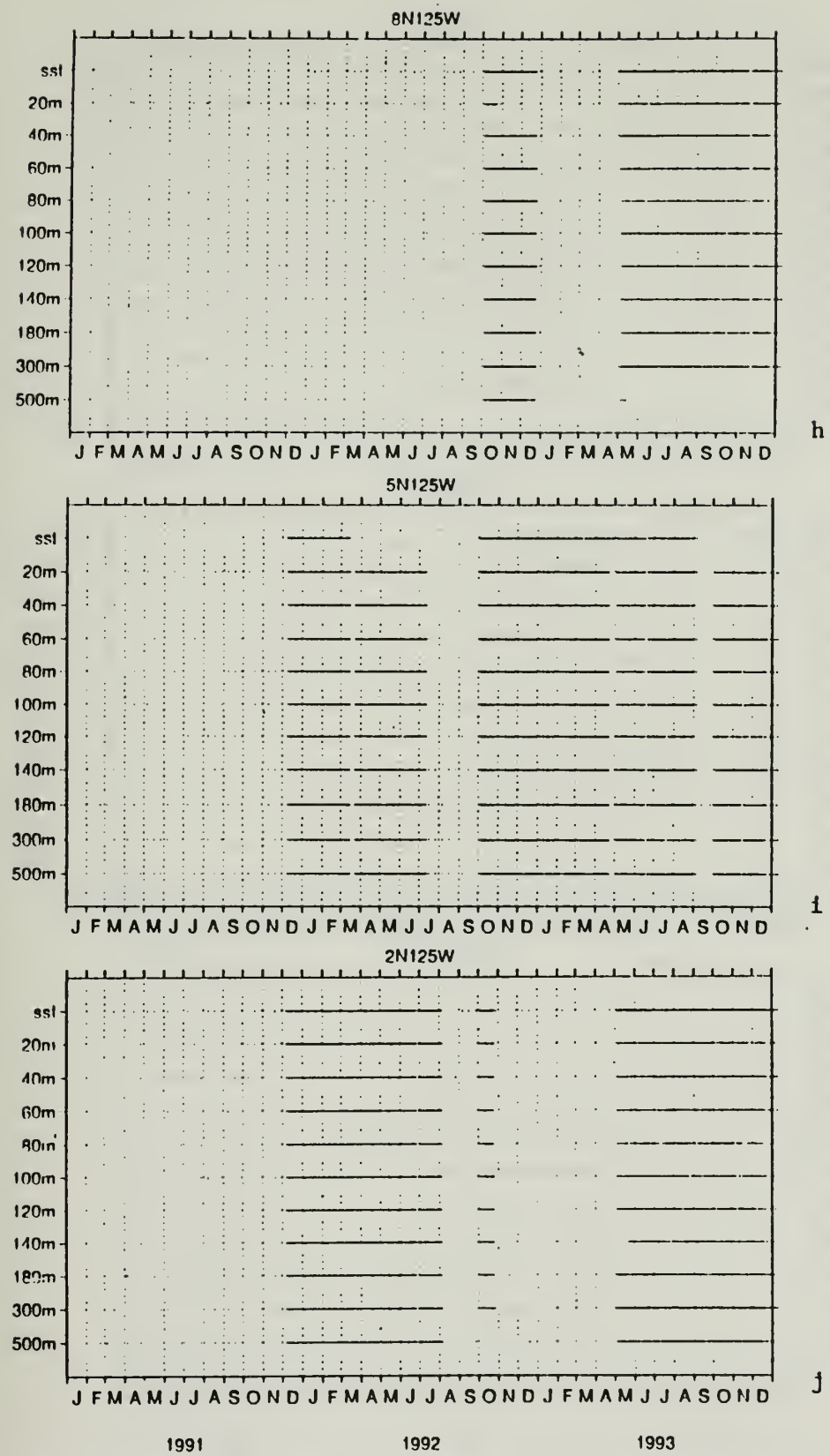

Fig. 11. (Continued) h) 8°N 125°W, i) 5°N 125°W, j) 2°N 125°W,

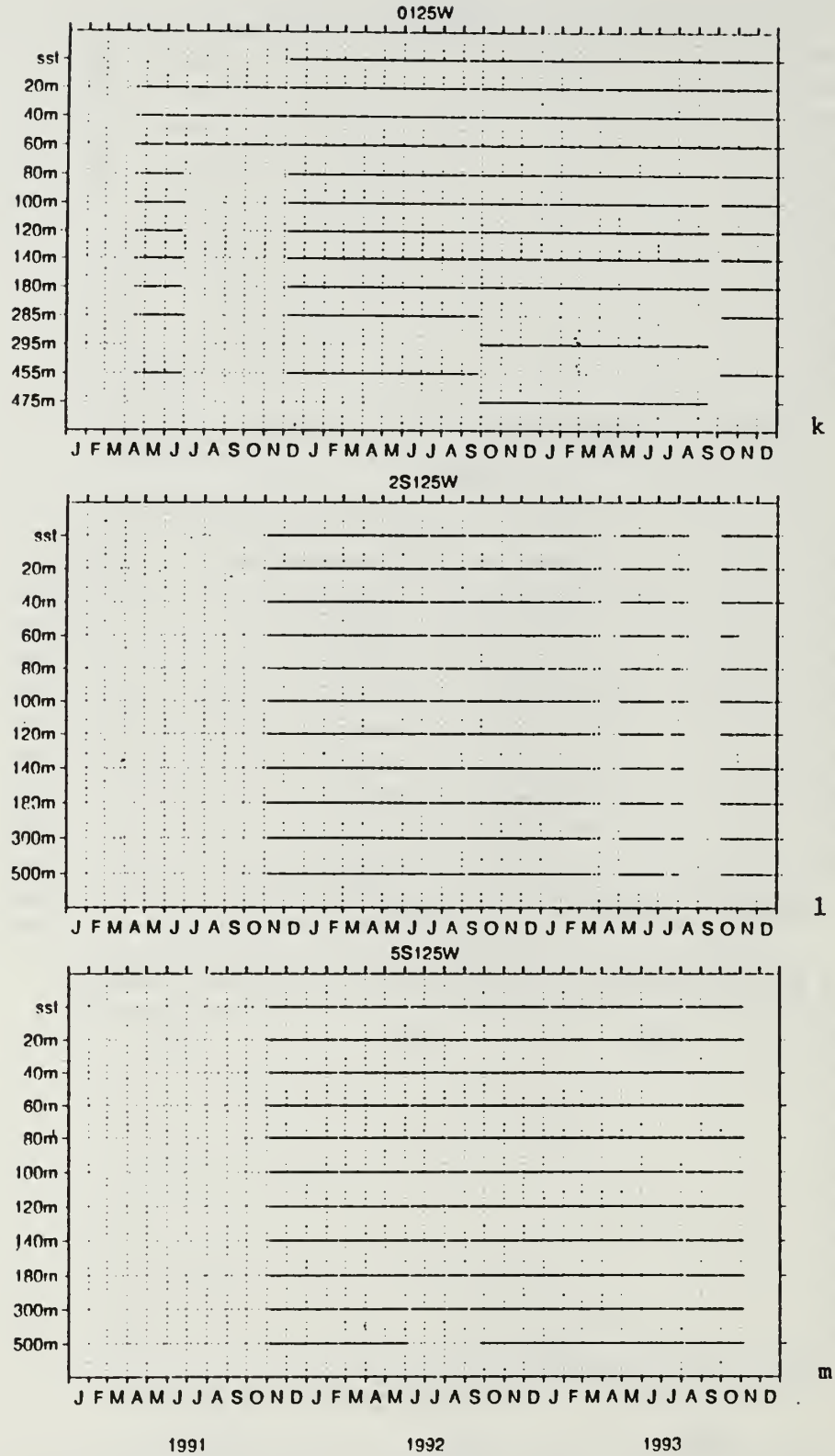

Fig. 11. (Continued) k) 0° 125°W, l) 2°S 125°W, m) 5°S 125°W,

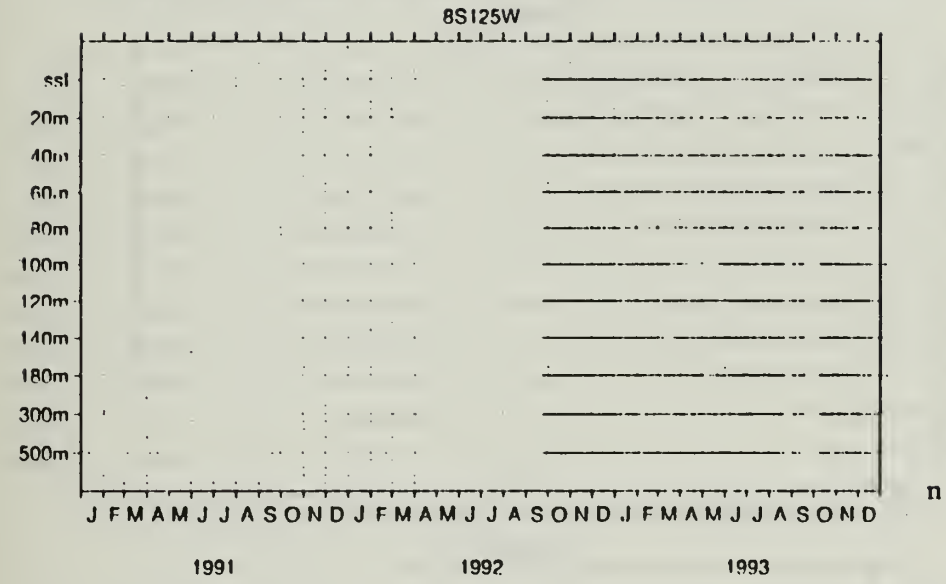

Fig. 11. (Continued) n) 8°S 125°W,

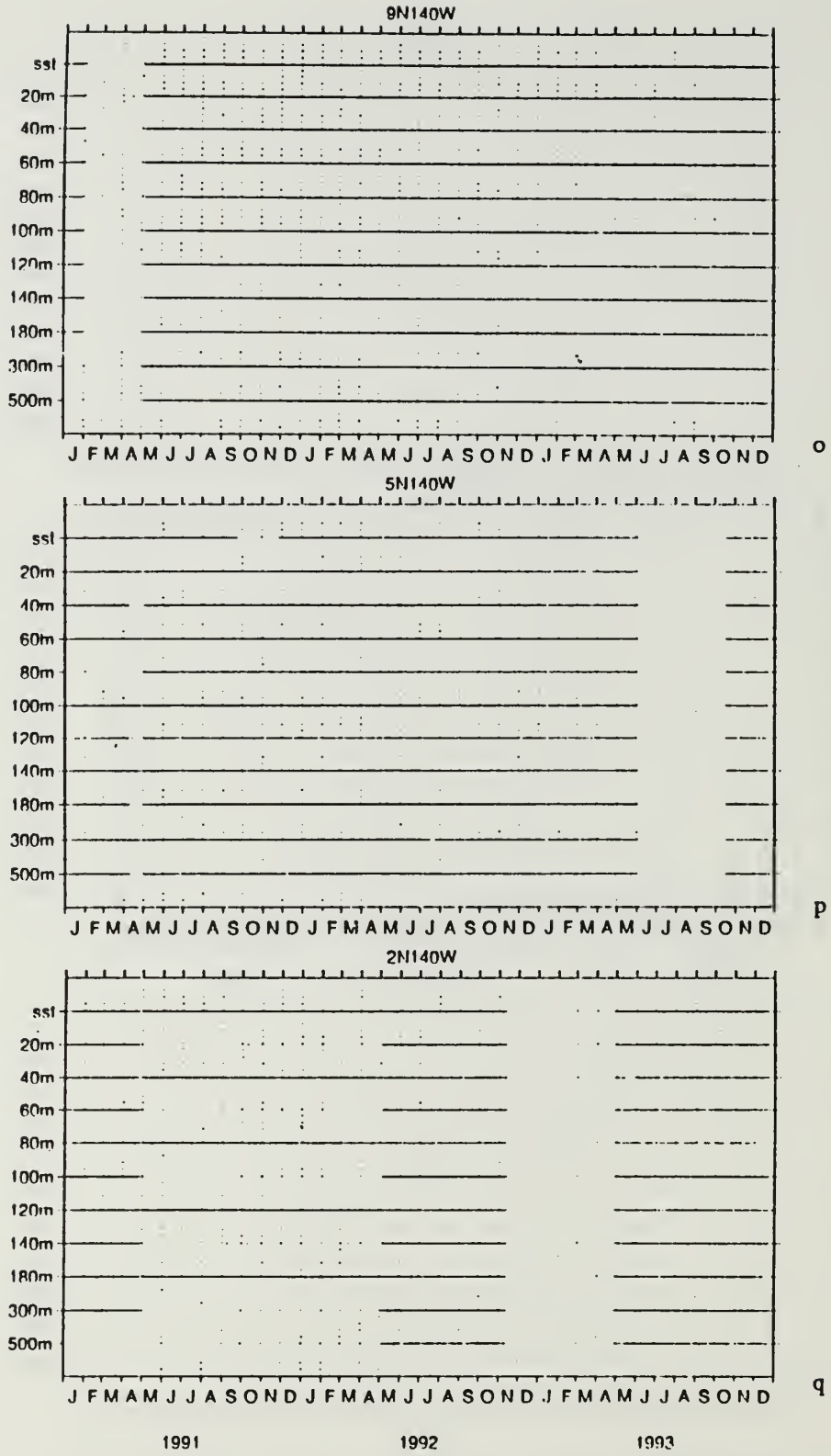

Fig. 11. (Continued) o) 9°N 140°W, p) 5°N 140°W, q) 2°N 140°W,

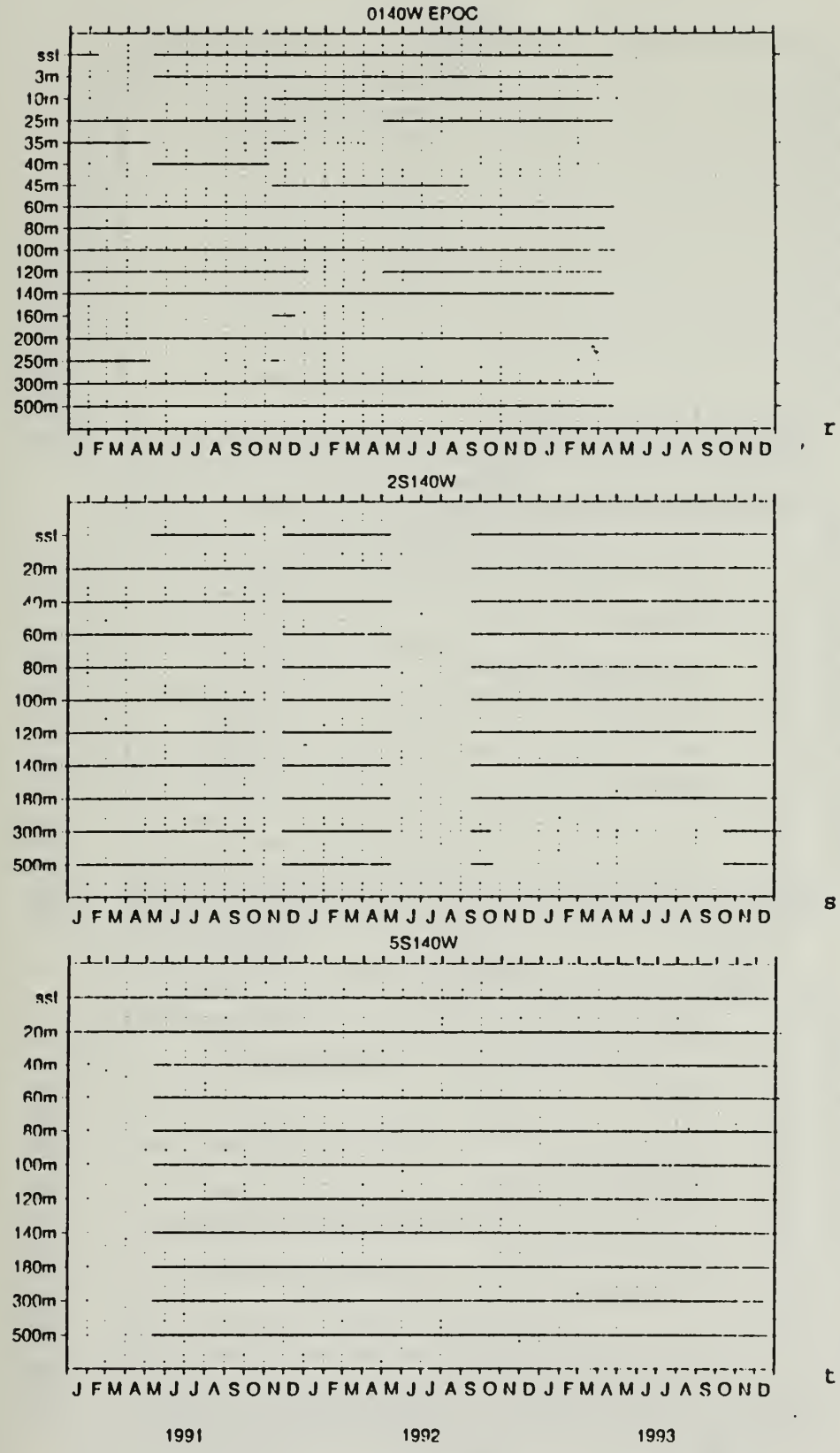

Fig. 11. (Continued) r) 0° 140°W, s) 2°S 140°W, t) 5°S 140°W,

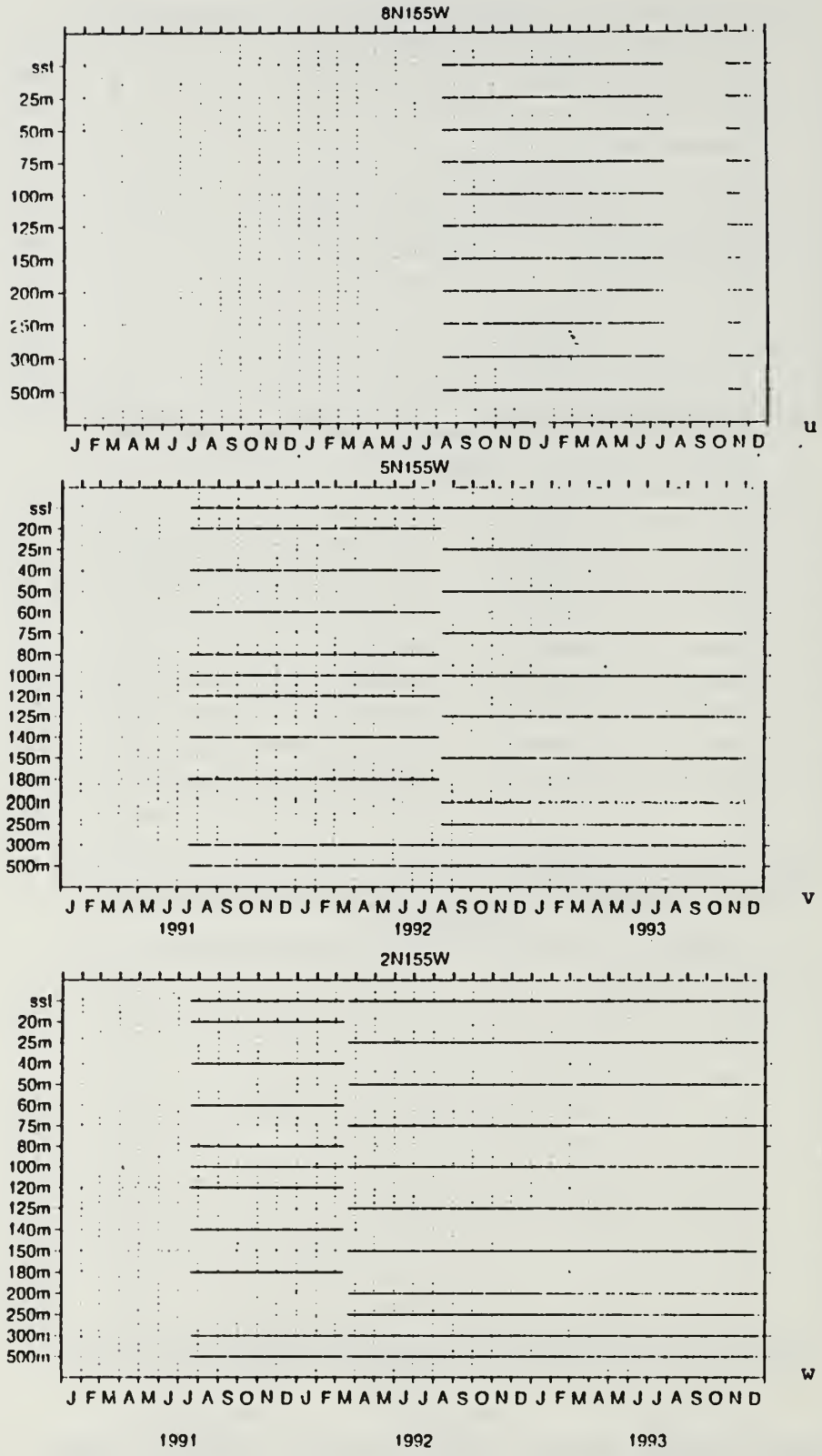

Fig. 11. (Continued) u) 8°N 155°W, v) 5°N 155°W, w) 2°N 155°W,

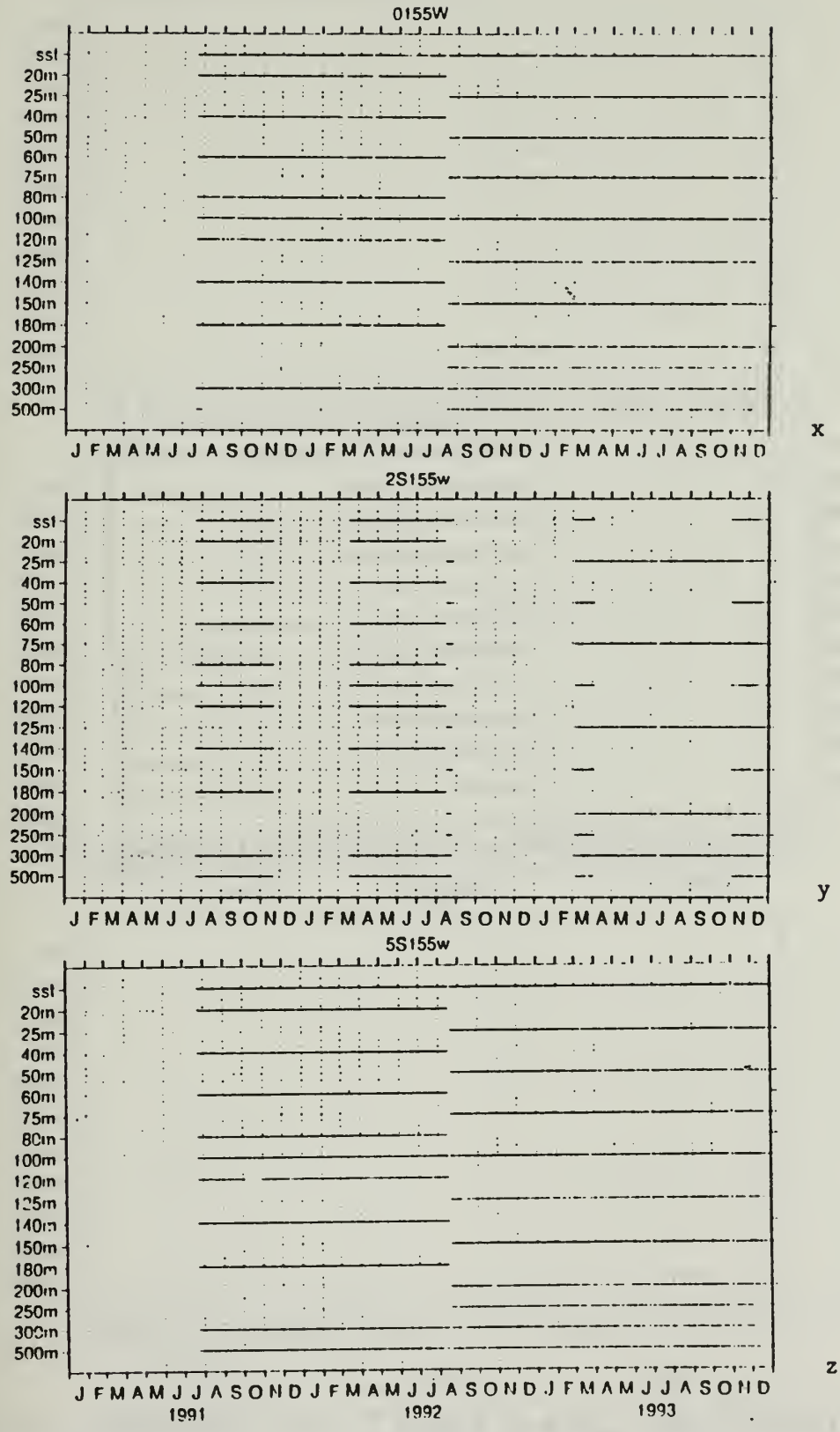

Fig. 11. (Continued) x) 0° 155°W, y) 2°S 155°W, z) 5°S 155°W,

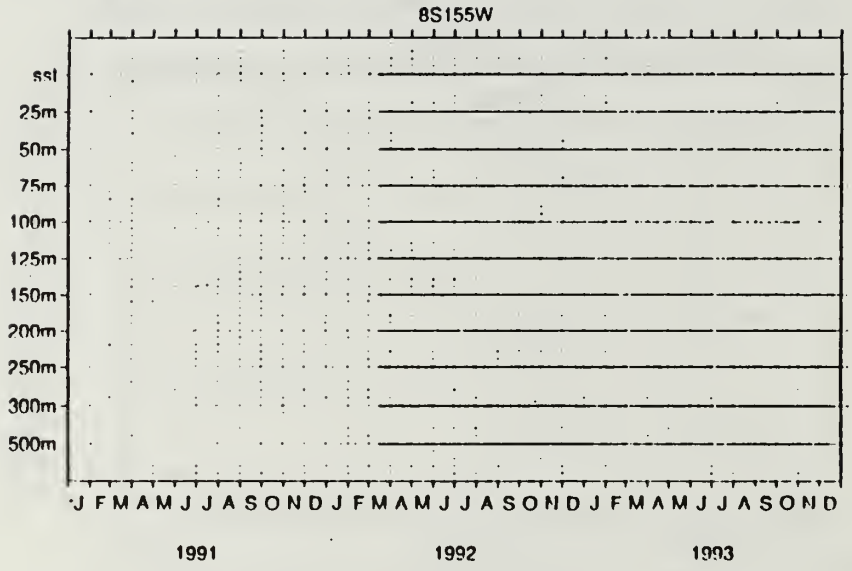

aa

Fig. 11. (Continued) aa) 8°S 155°W,

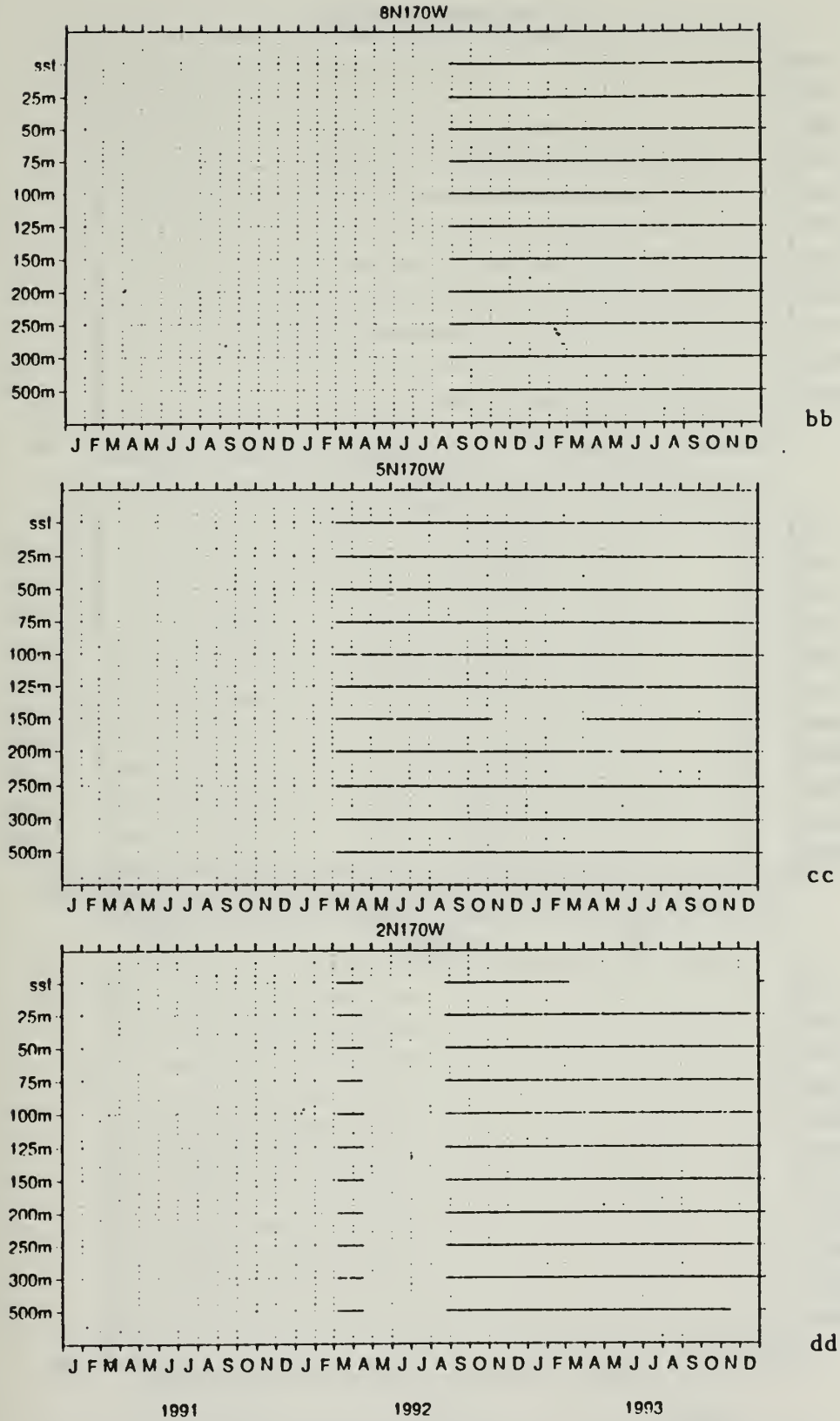

Fig. 11. (Continued) bb) 8°N 170°W, cc) 5°N 170°W, dd) 2°N 170°W,

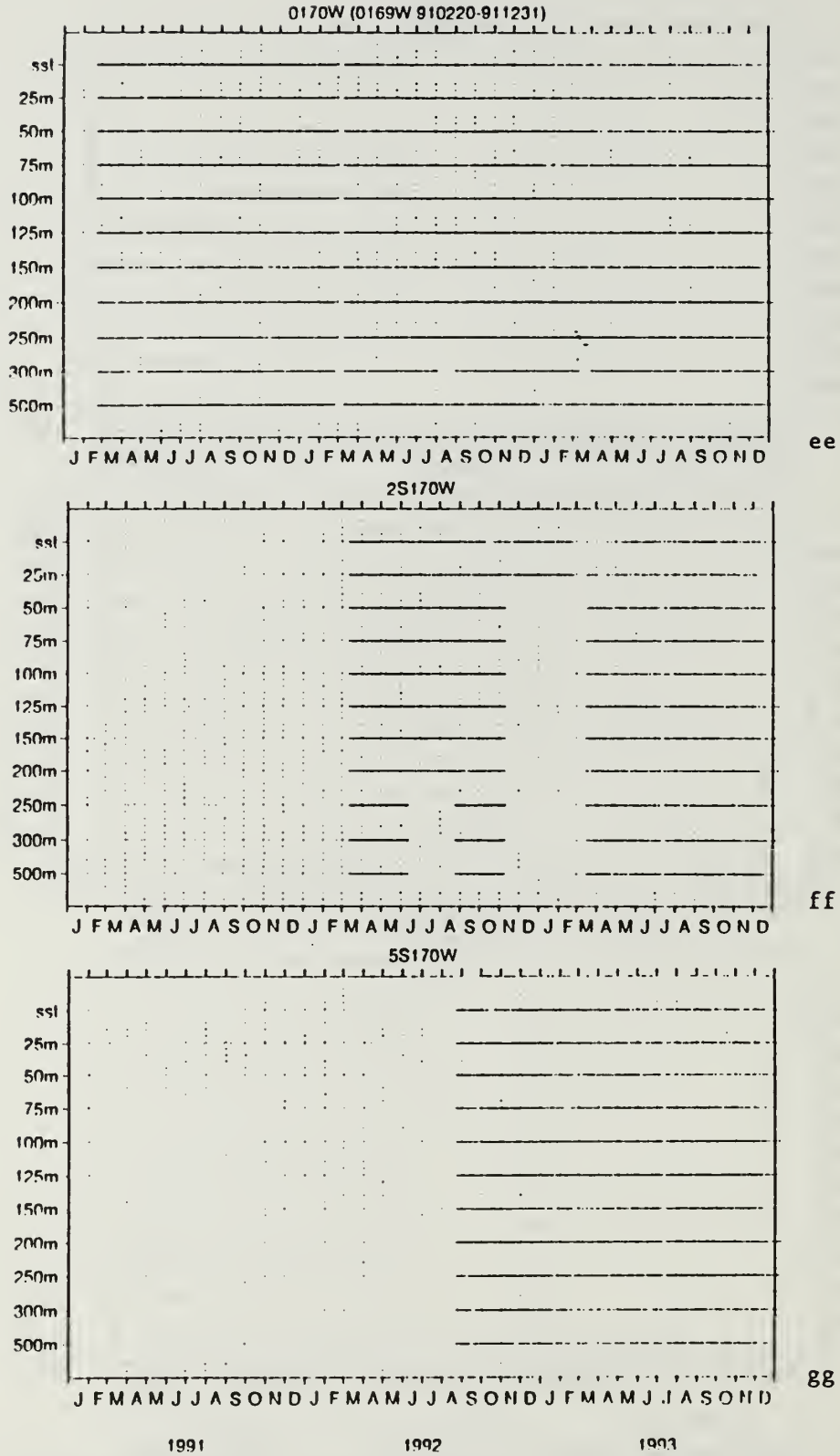

Fig. 11. (Continued) ee) 0° 170°W, ff) 2°S 170°W, gg) 5°S 170°W,

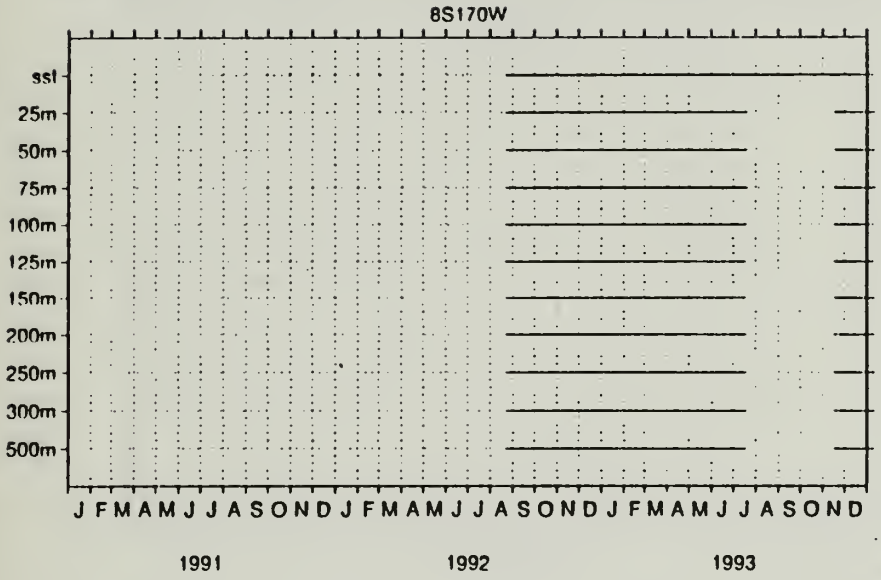

hh

Fig. 11. (Continued) hh) 8°S 170°W,

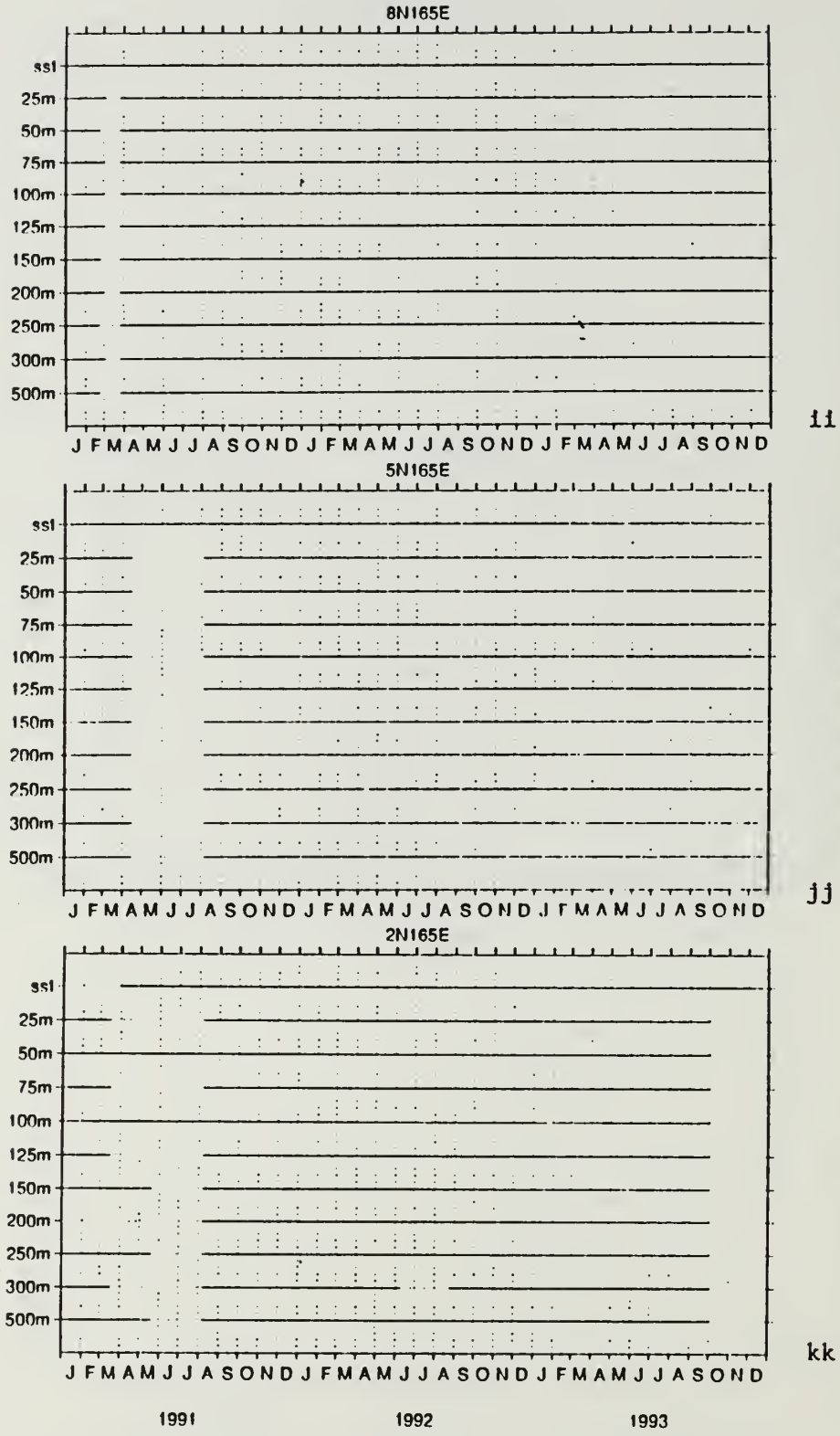

Fig. 11. (Continued) ii) 8°N 165°E, jj) 5°N 165°E, kk) 2°N 165°E,

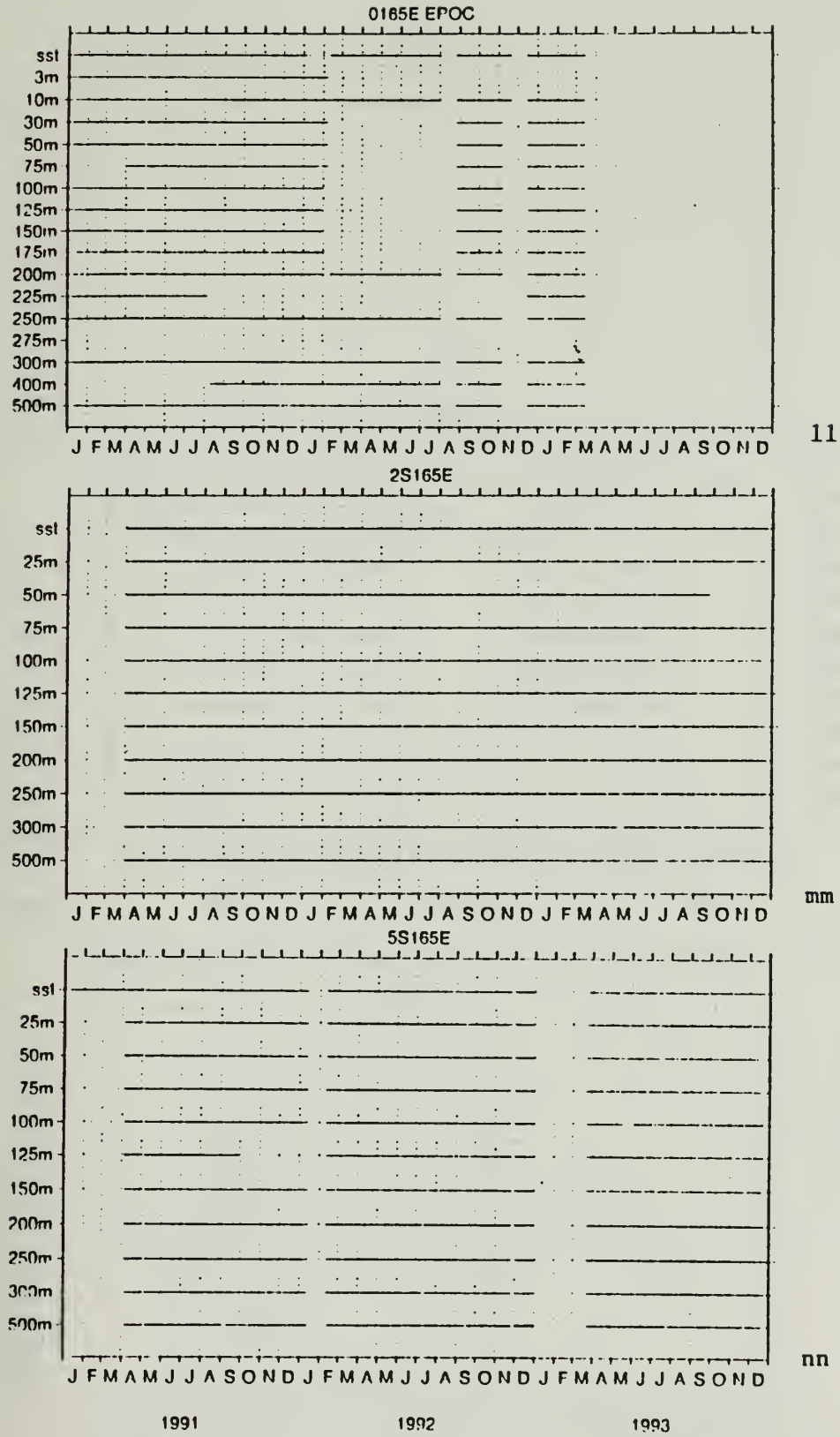

Fig. 11. (Continued) 11) 0° 165°E, mm) 2°S 165°E, nn) 5°S 165°E,

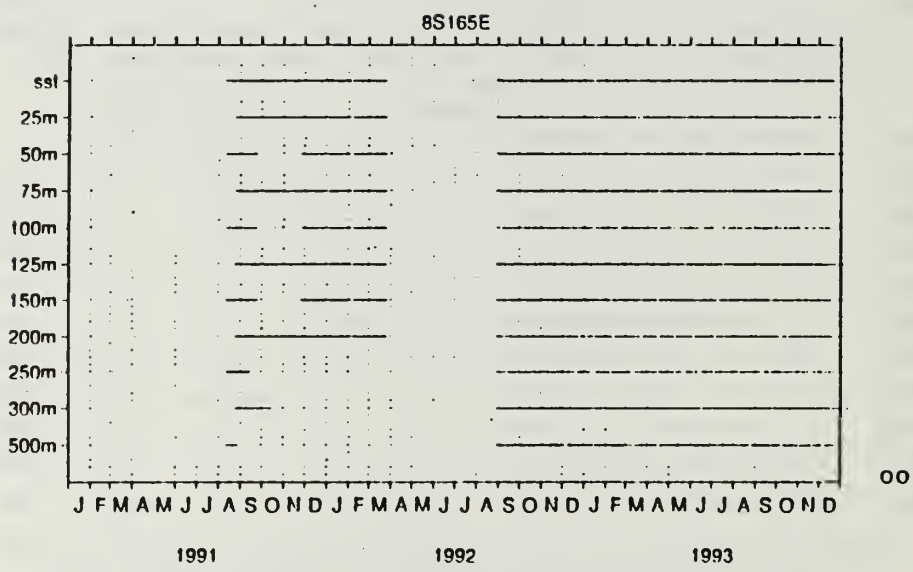

Fig. 11. (Continued) oo) 8°S 165°E,

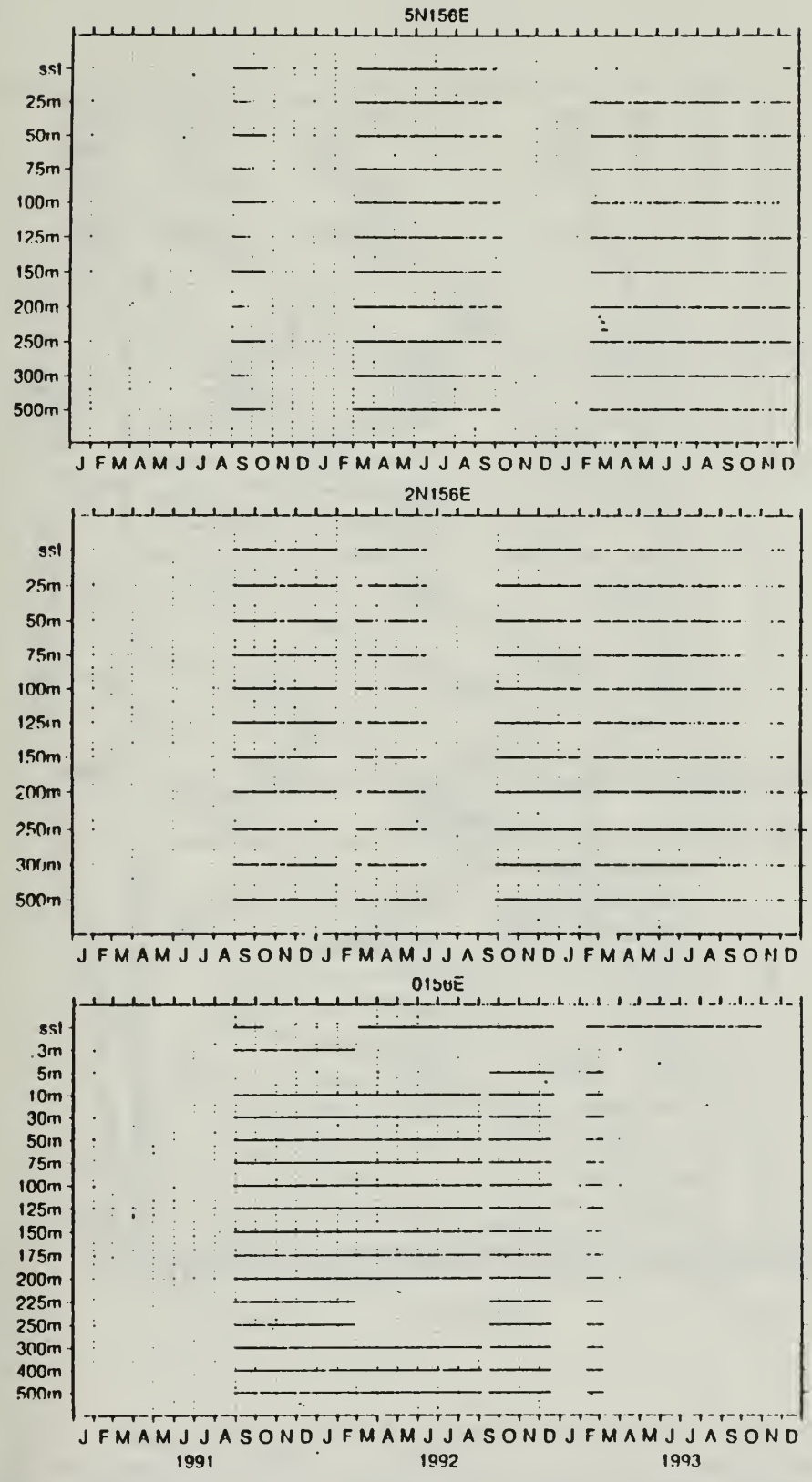

Fig. 11. (Continued) pp) 5°N 156°E, qq) 2°N 156°E, rr) 0° 156°E,

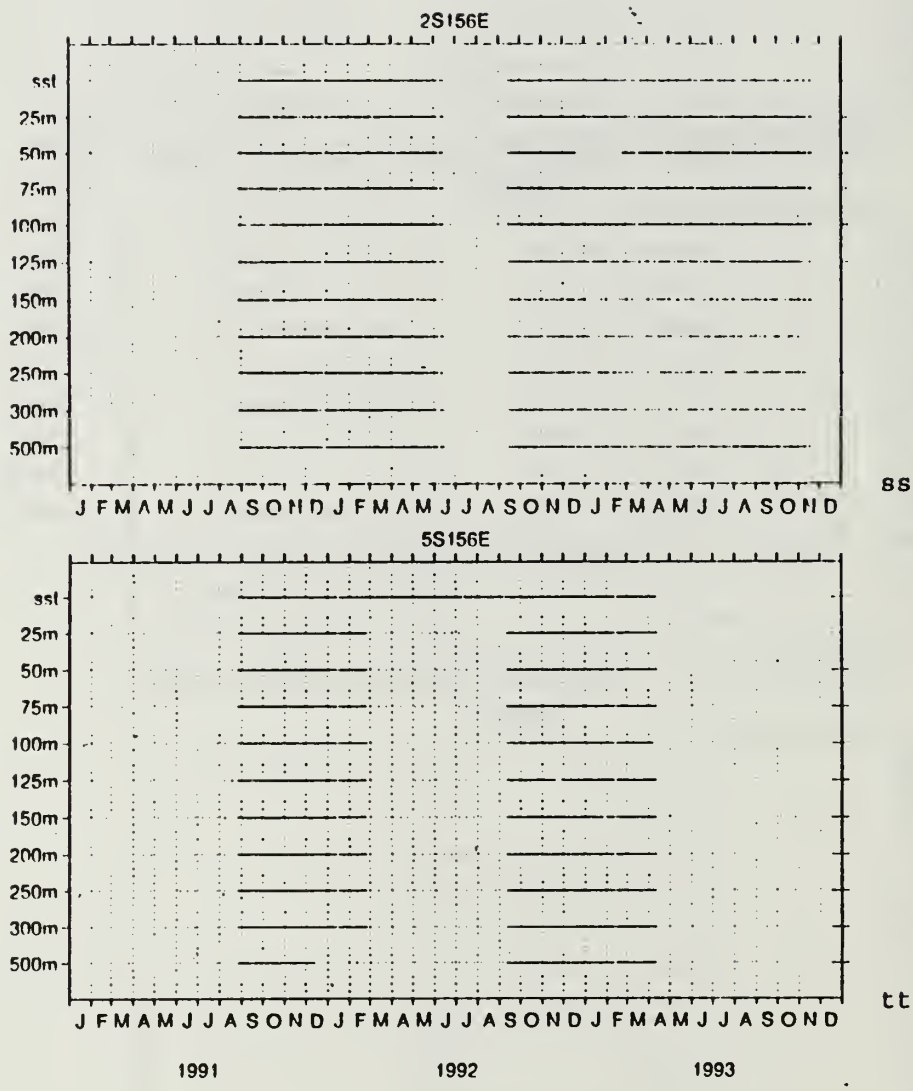

Fig. 11. (Continued) ss) 2°S 156°E, tt) 5°S 156°E.

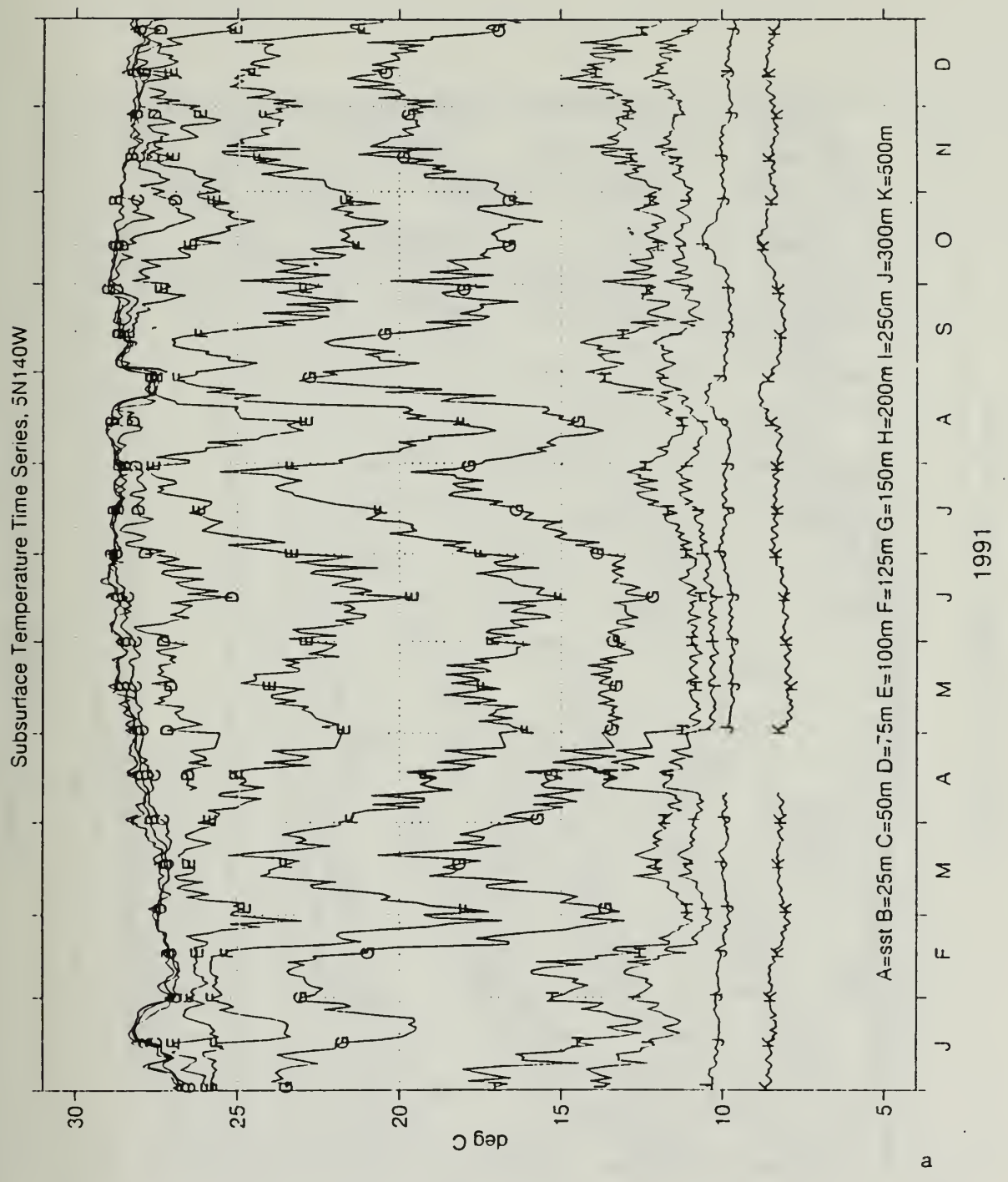

Fig. 12. Ocean temperature time series for fixed depths at 5°N 140°W for a) 1991, b) 1992, c) 1993. Letters on curve indicate depths: A=1m, B=25m, C=50m, D=75m, E=100m, F=125m, G=150m, H=200m, I=250m, J=300m, and K=500m.

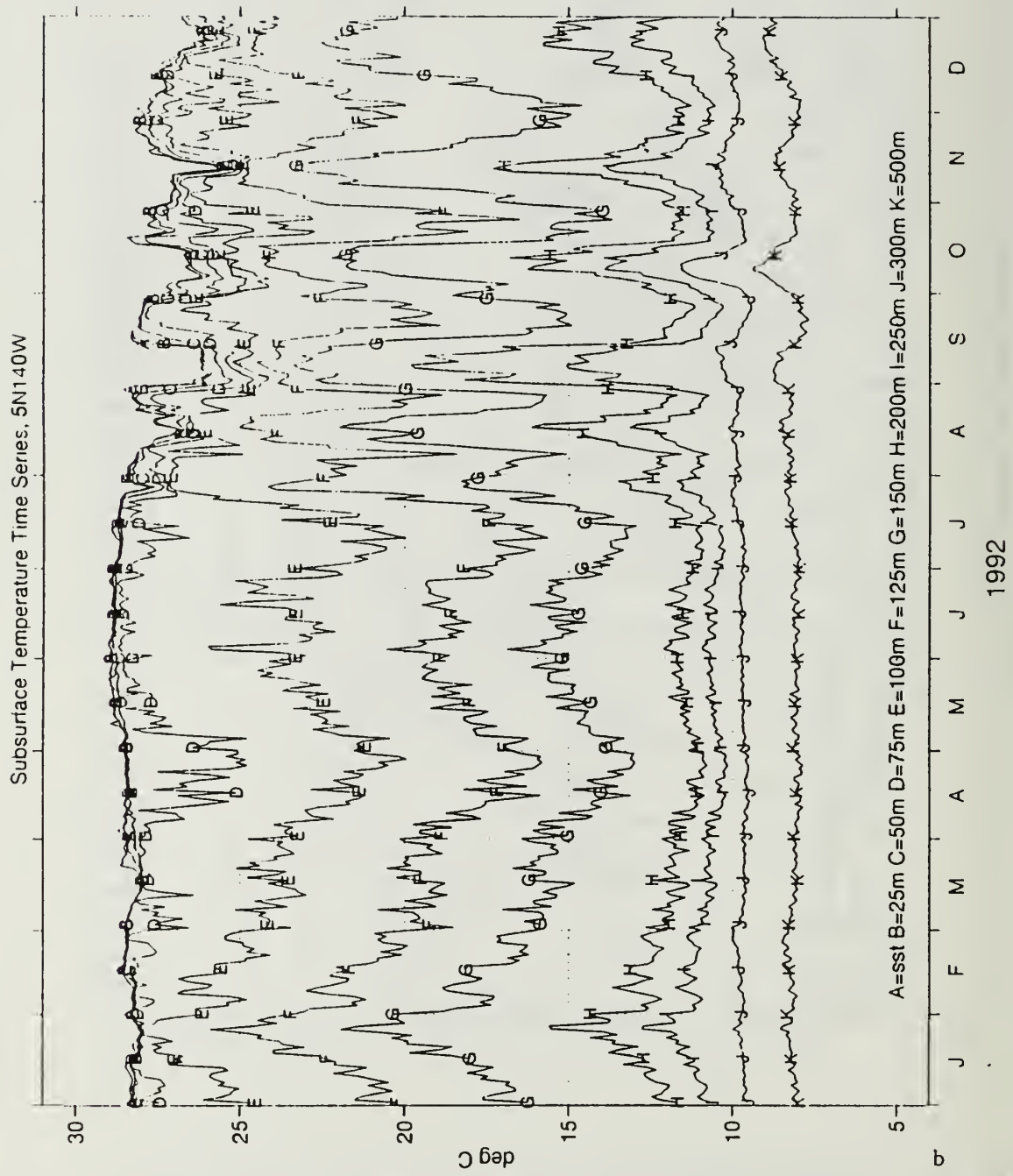

Fig. 12. (Continued).

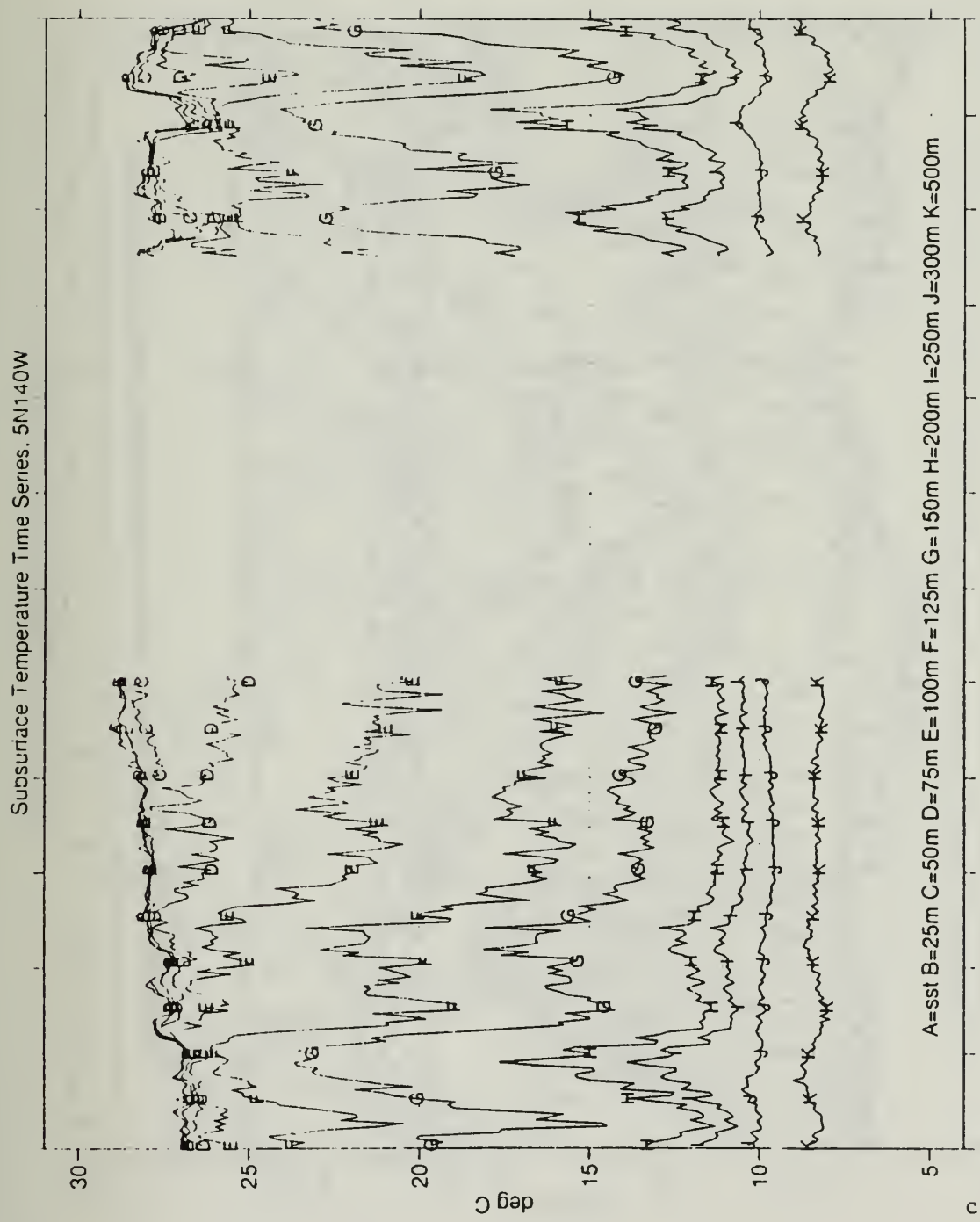

Fig. 12. (Continued).

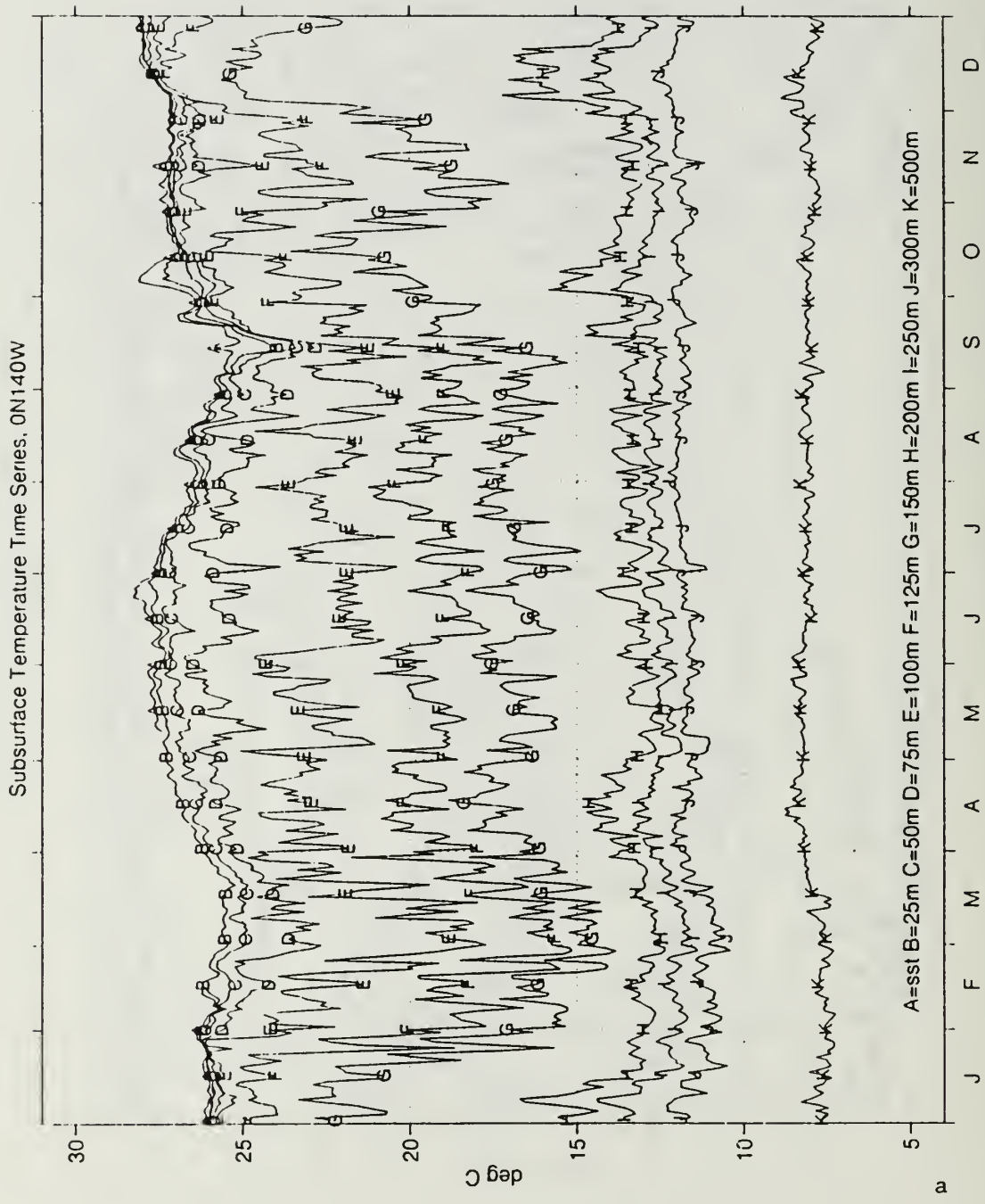

Fig. 13. Same as Fig. 12, except at 0° 140°W.

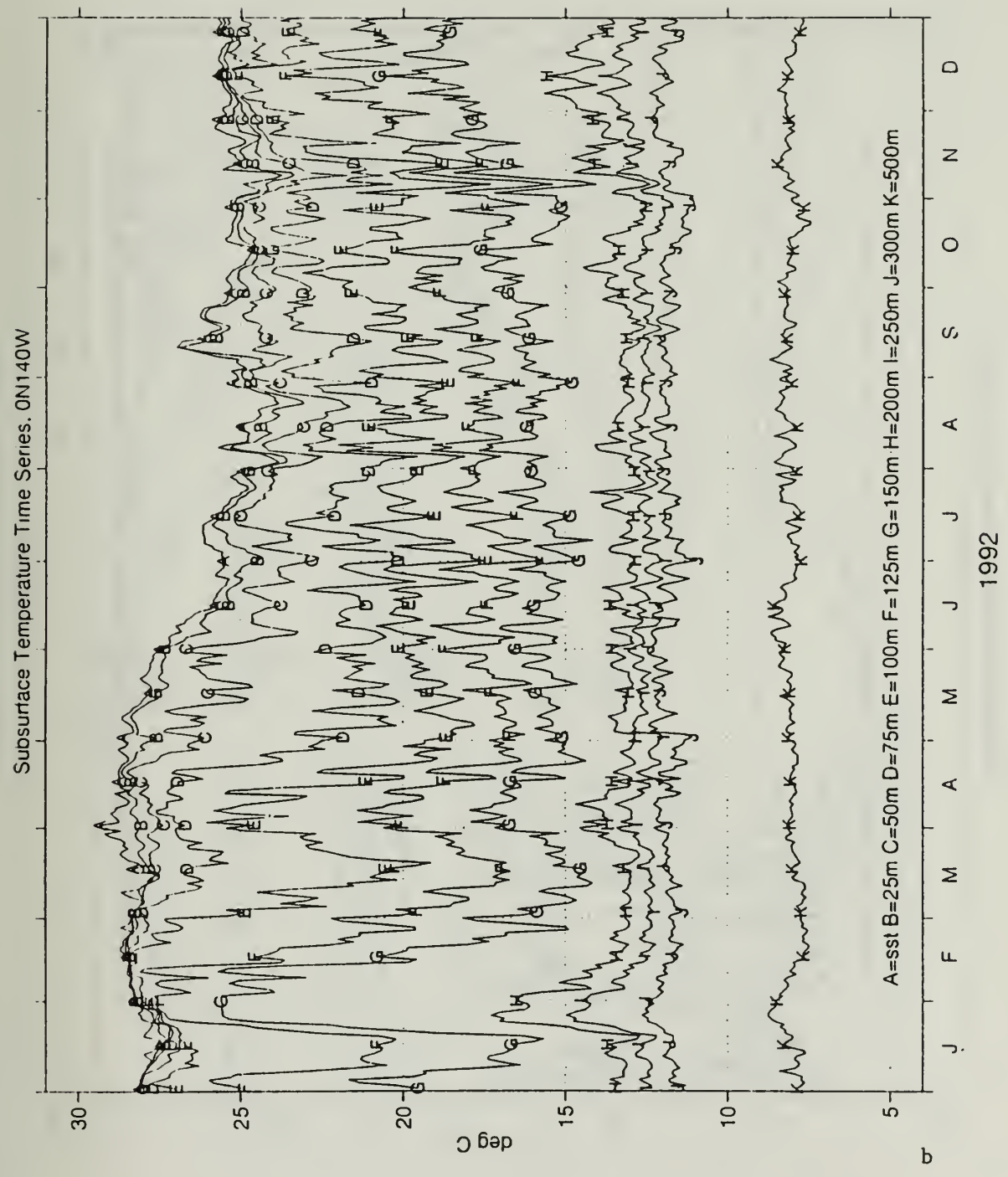

Fig. 13. (Continued).

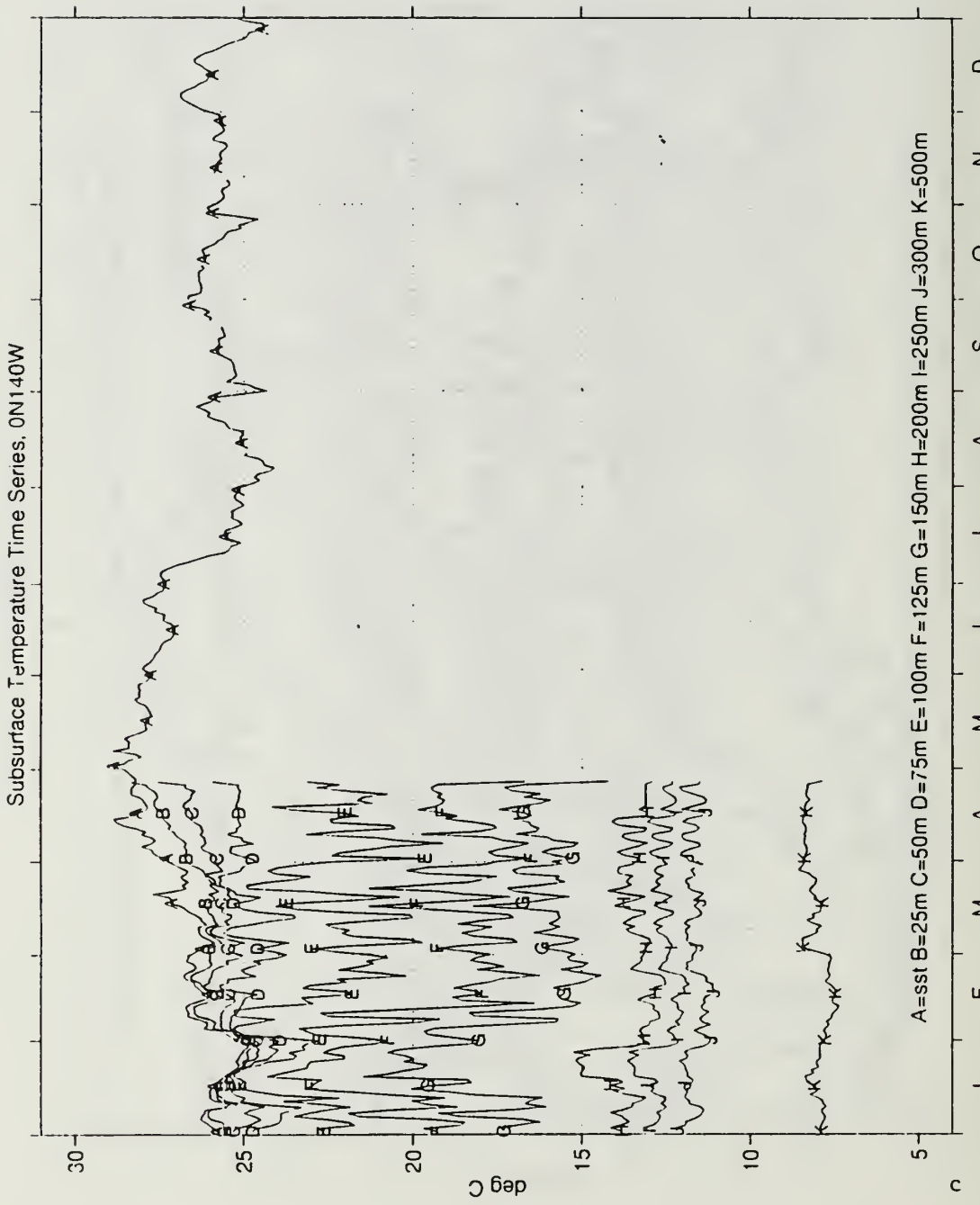

Fig. 13. (Continued).

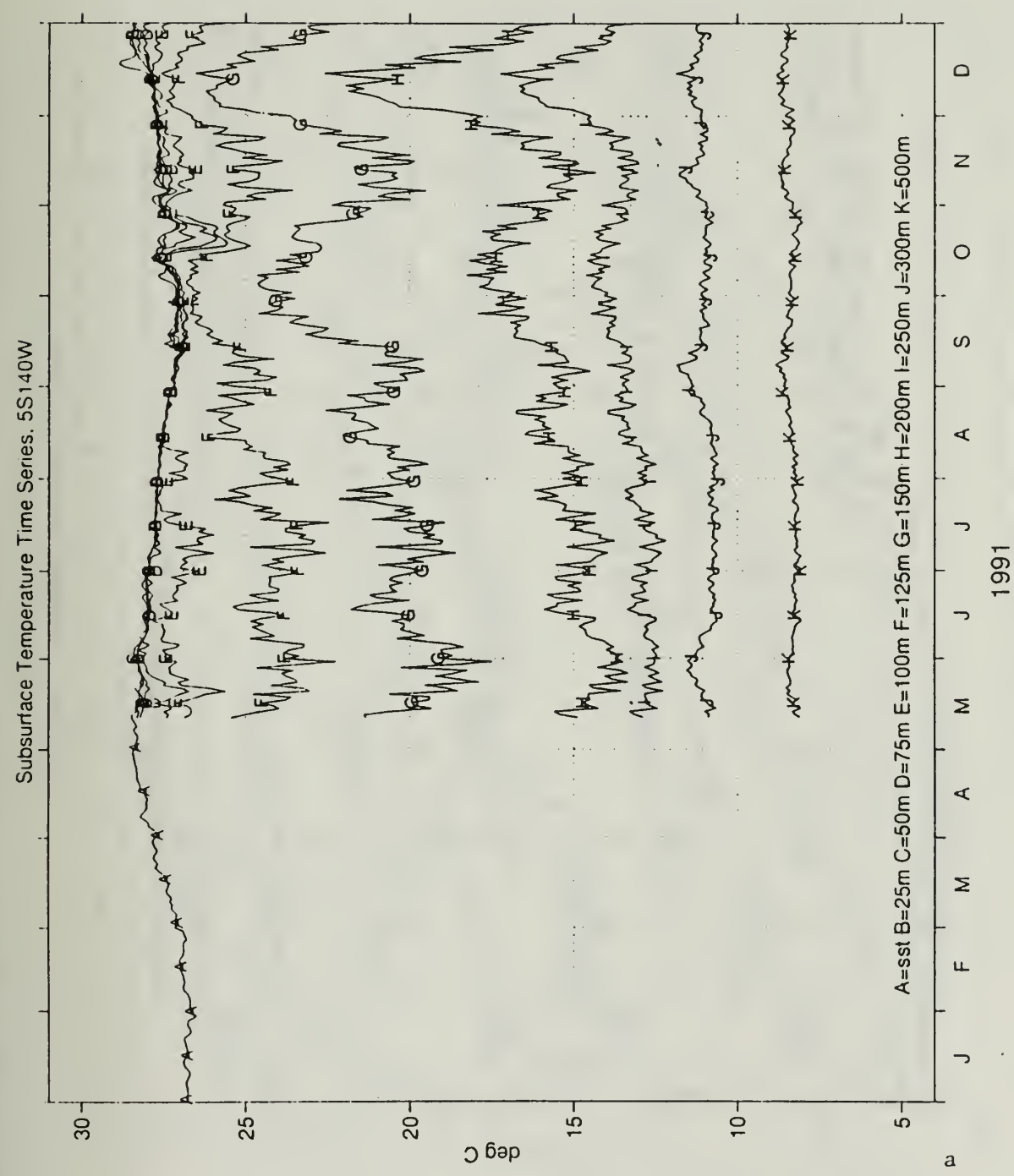

Fig. 14. Same as Fig. 12, except at 5°S 140°W.

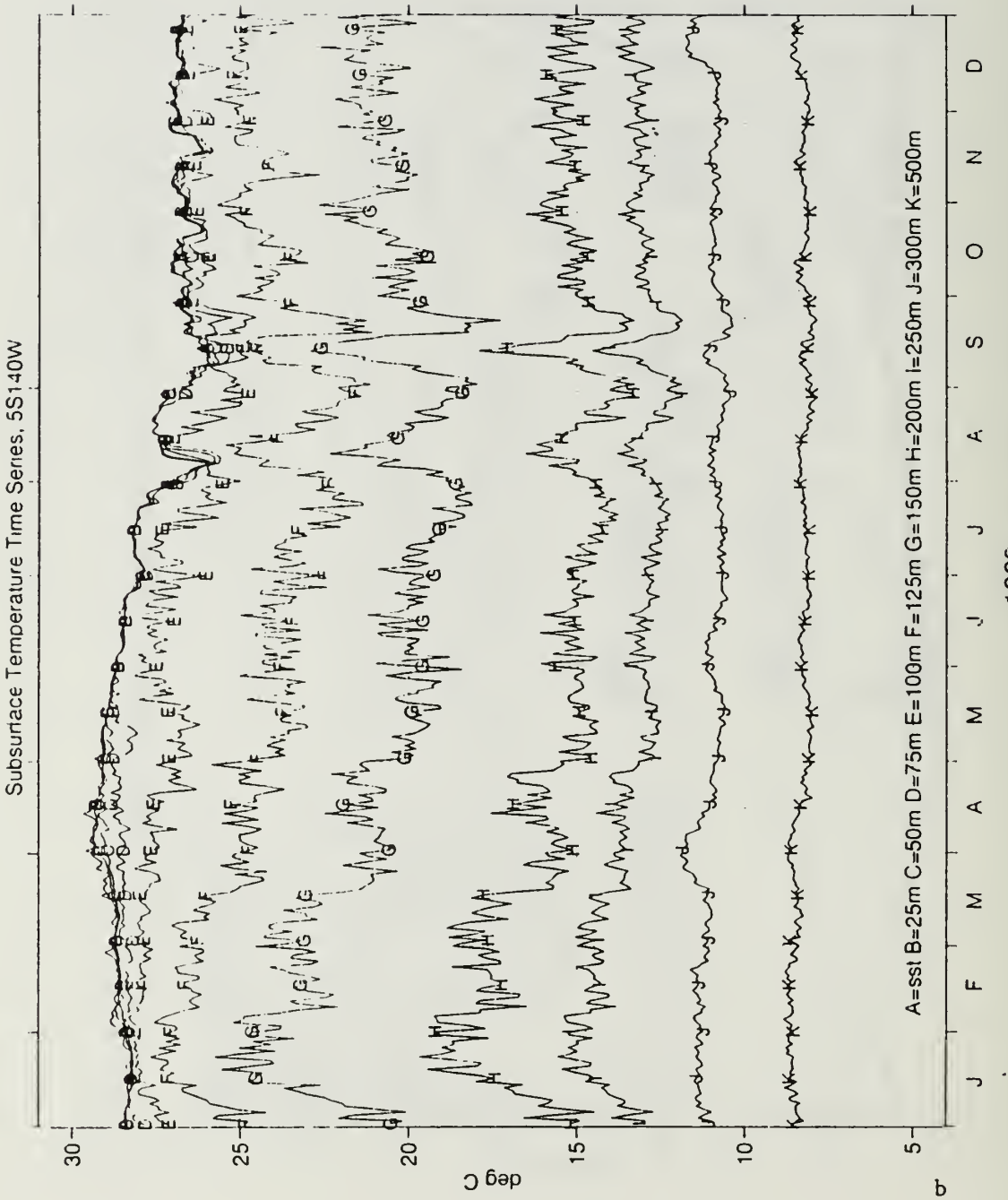

Fig. 14. (Continued).

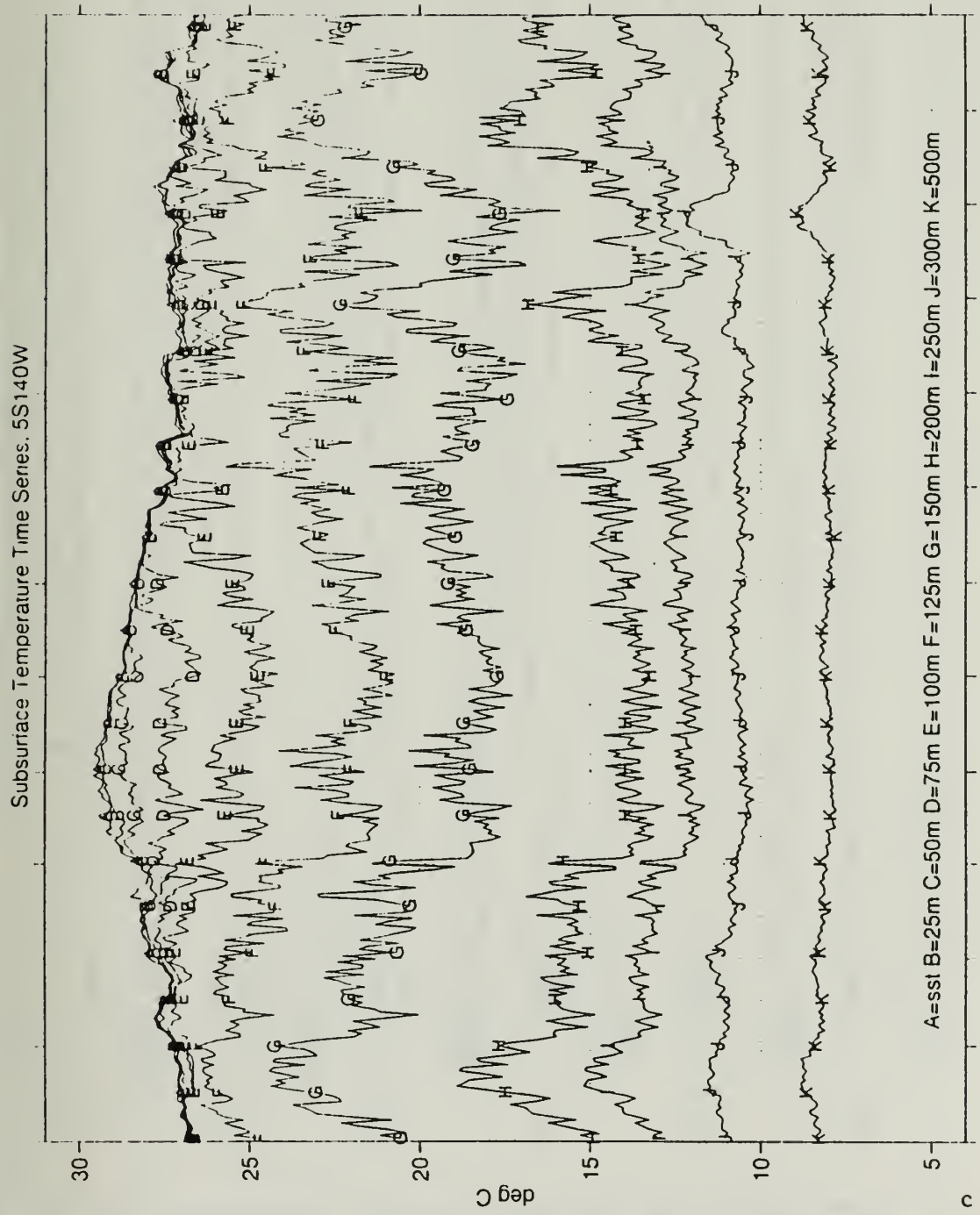

Fig. 14. (Continued).

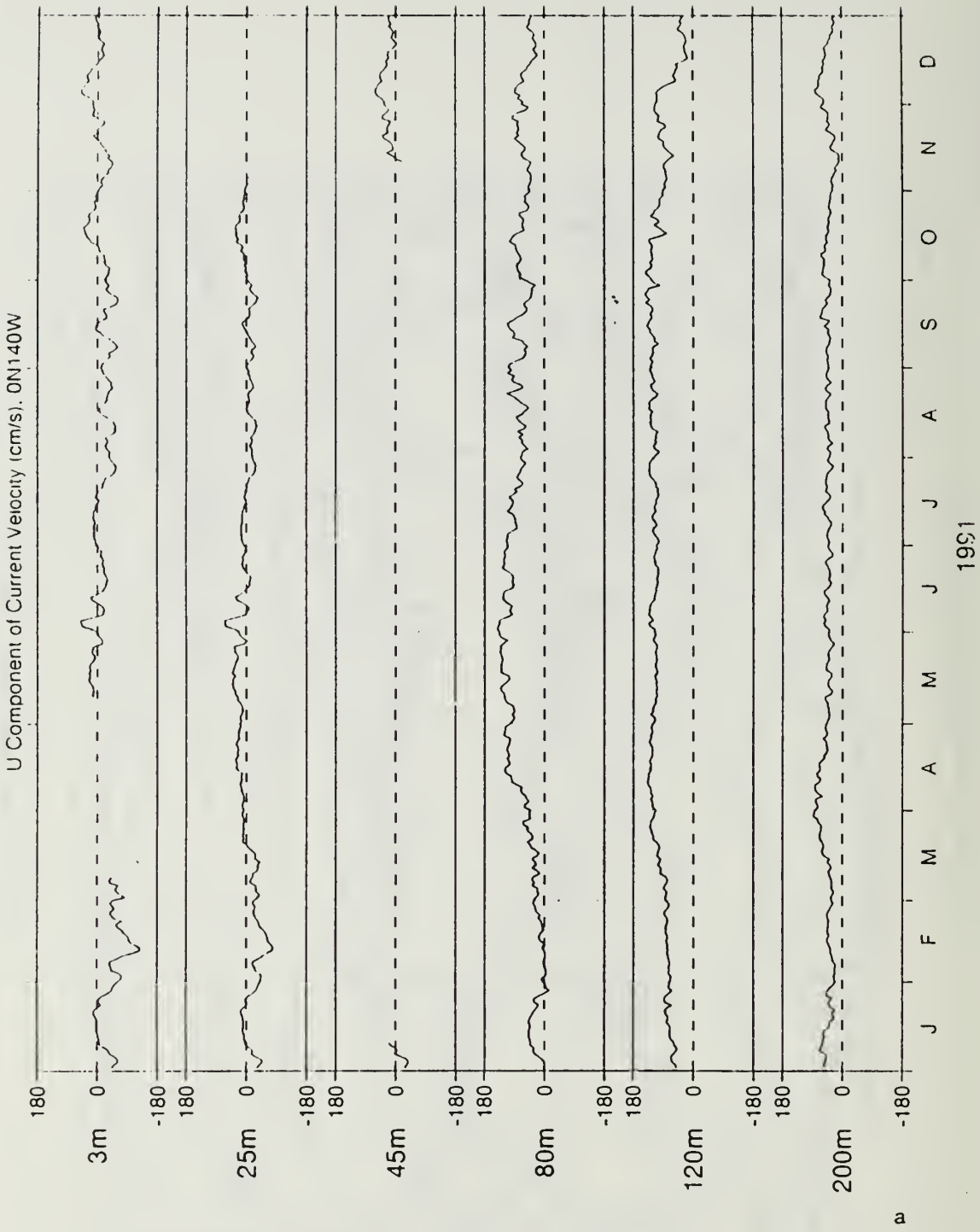

Fig. 15. Time series of current velocity components at 0° 140°W. Speed scale range is -180 to 180 cm/s. Zonal velocity component shown in: a) for 1991, b) for 1992, c) for 1993.

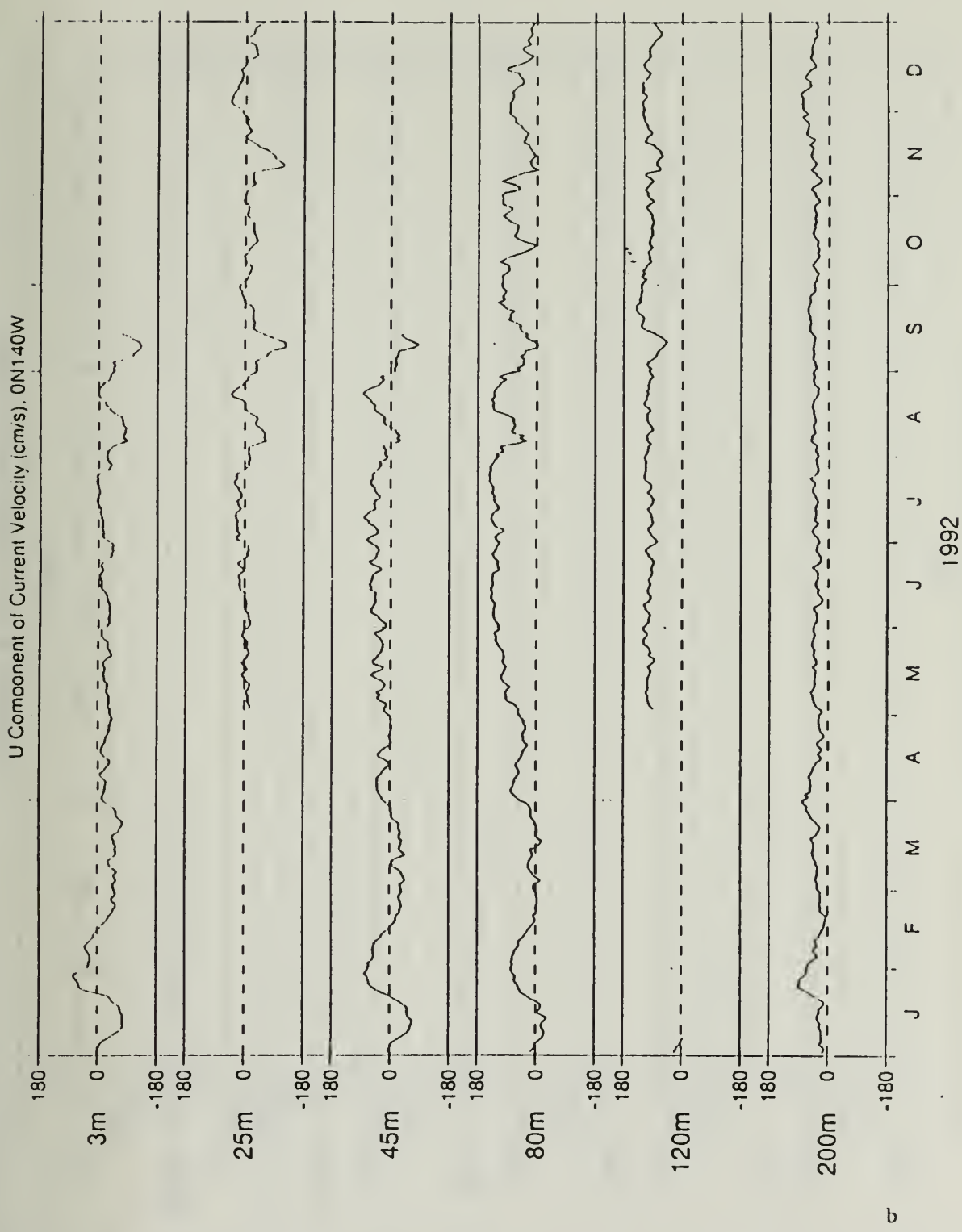

Fig. 15. (Continued) Speed scale range is -180 to 180 cm/s. Positive (negative) speeds indicate eastward (westward) currents.

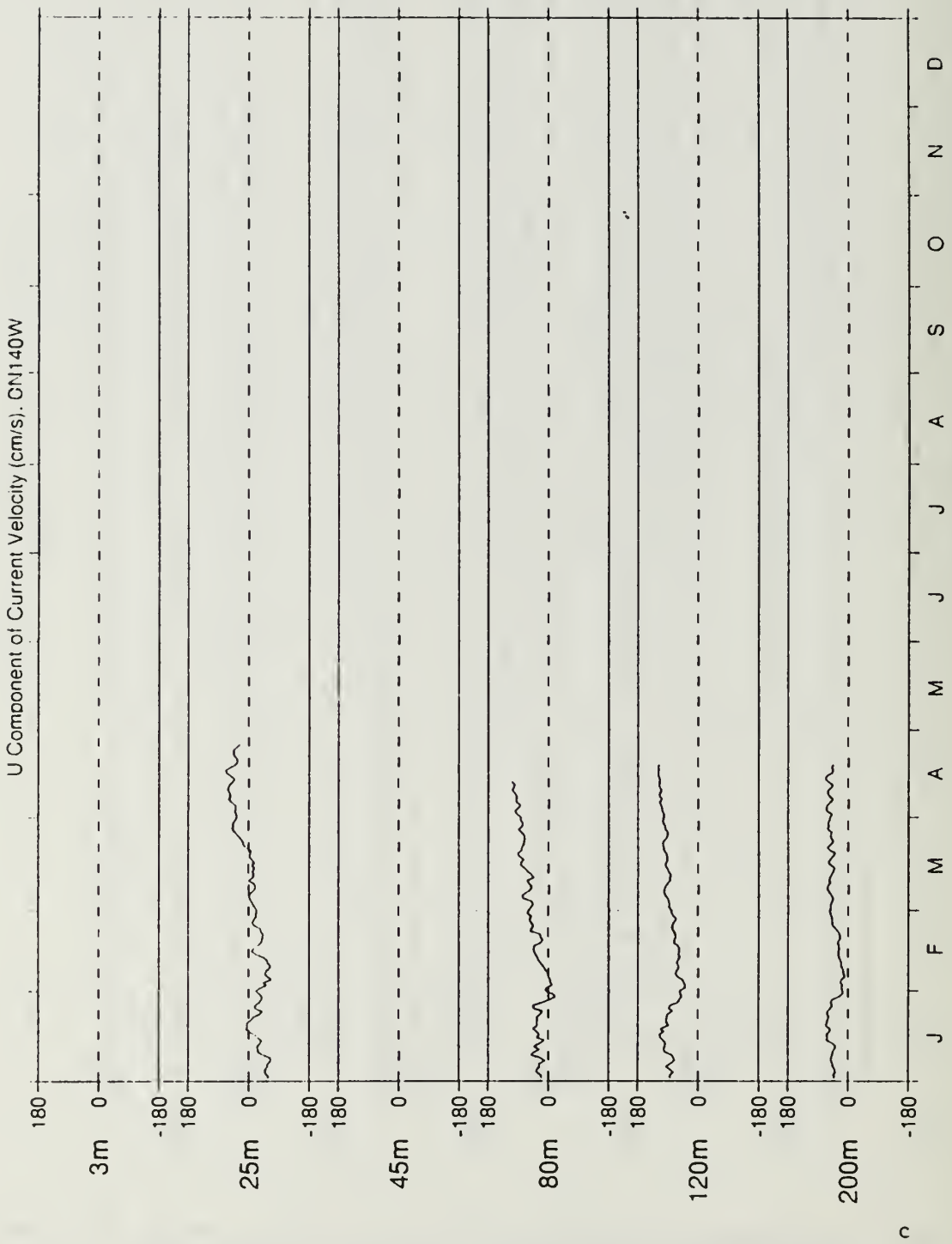

Fig. 15. (Continued).

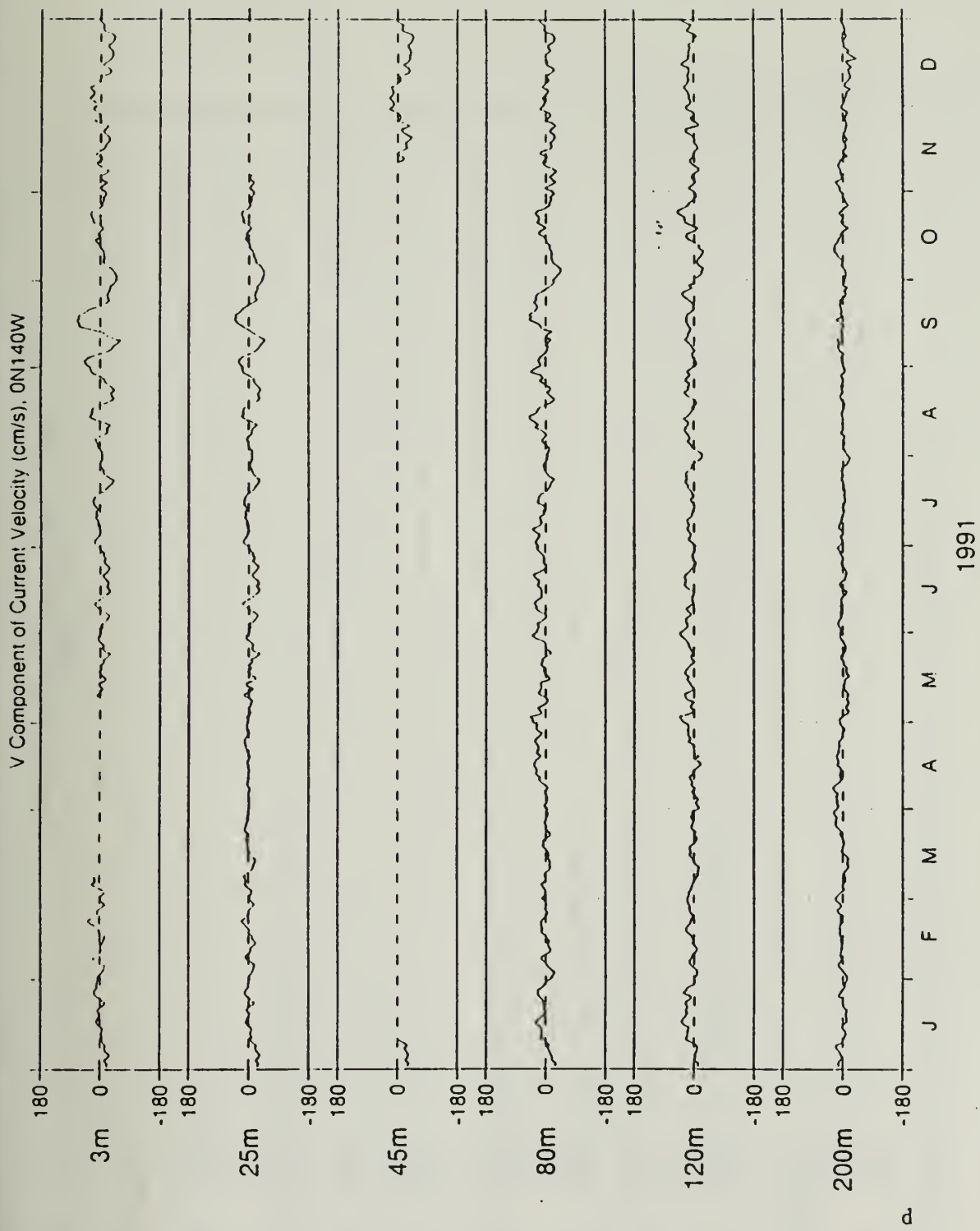

Fig. 15. (Continued) Meridional velocity component shown in: d) for 1991, e) for 1992, f) for 1993. Positive (negative) speeds indicate northward (southward) currents.

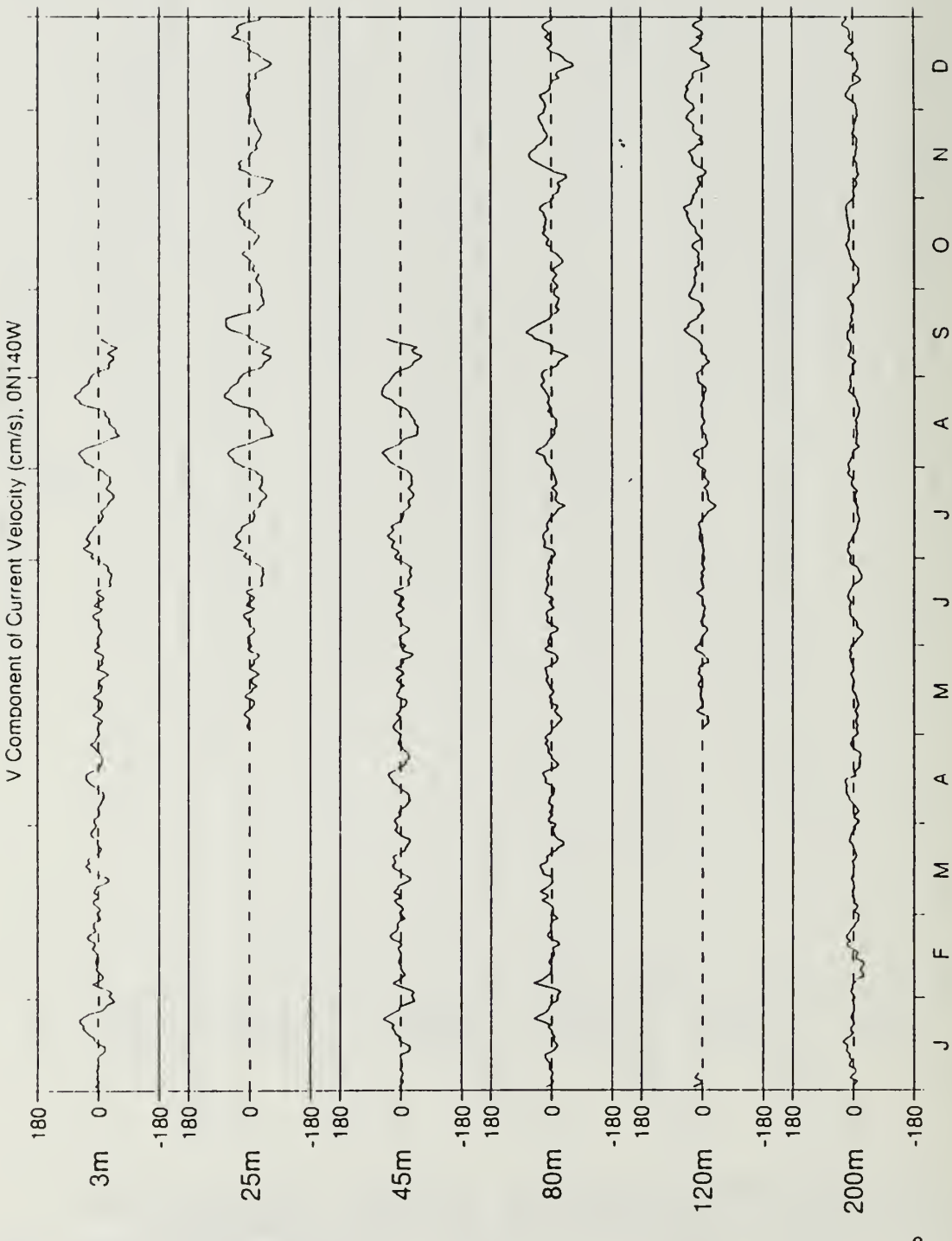

Fig. 15. (Continued).

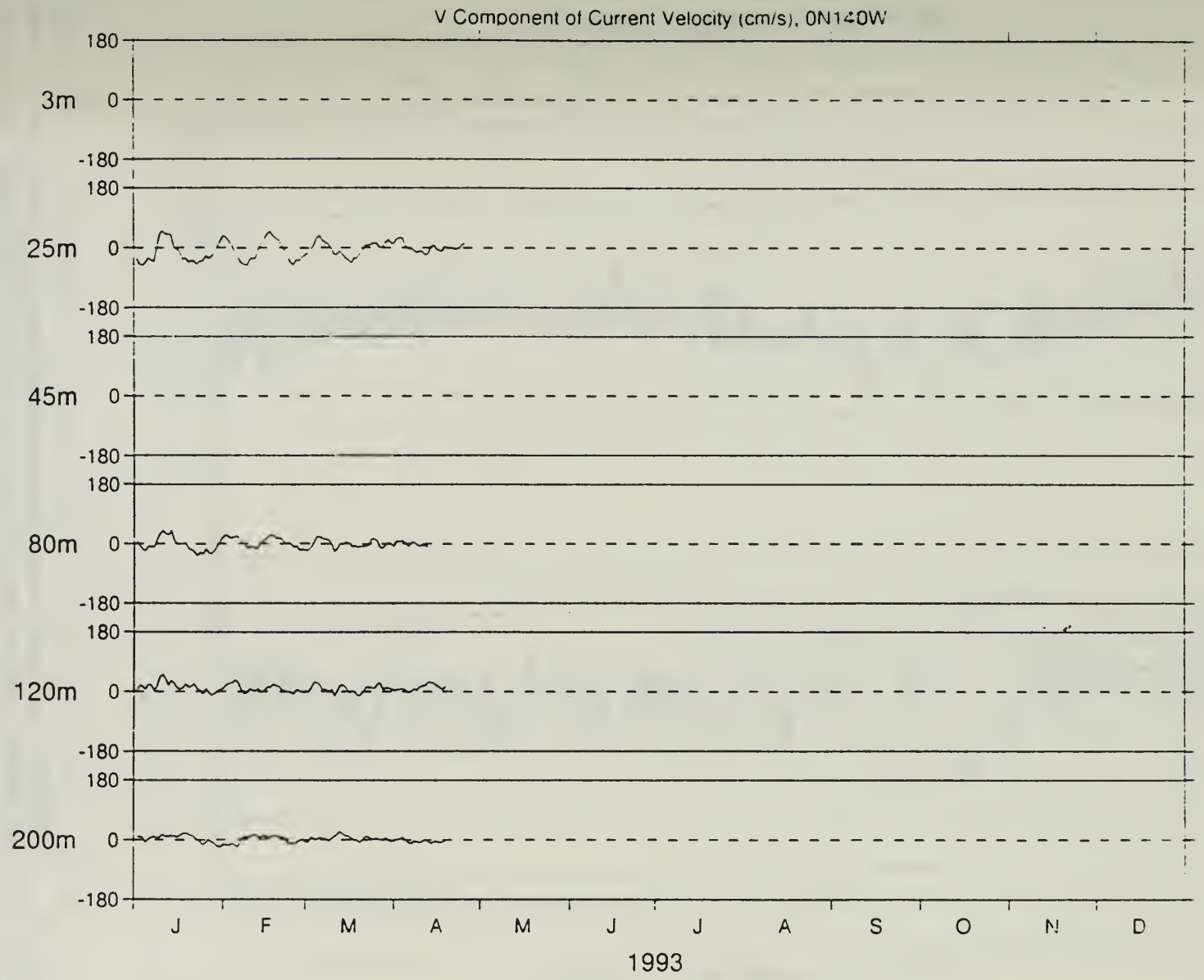

Fig. 15. (Continued).

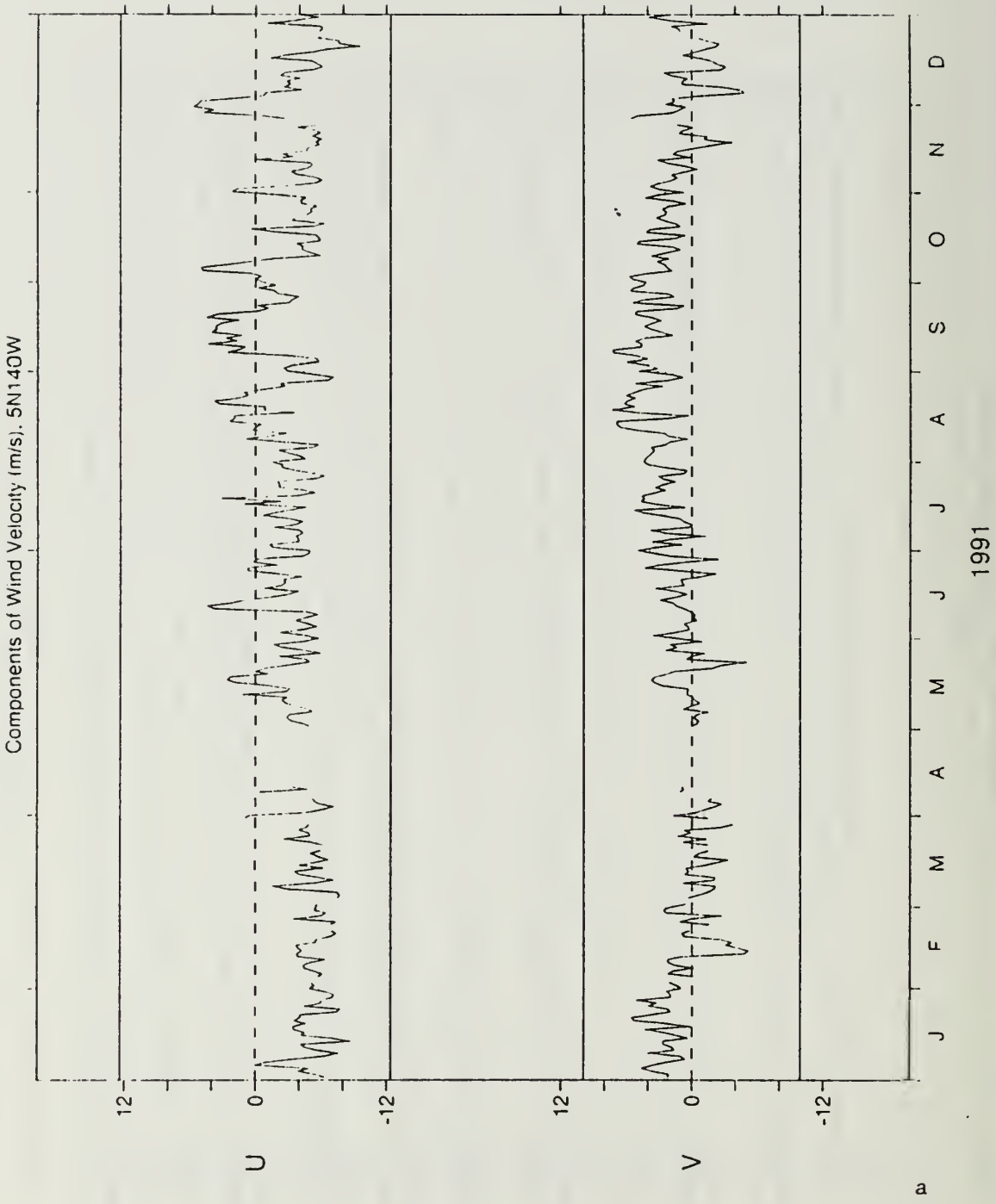

Fig. 16. Time series of zonal (U) and meridional (V) components of wind velocity at 5°N 140°W for: a) 1991, b) 1992, c) 1993.

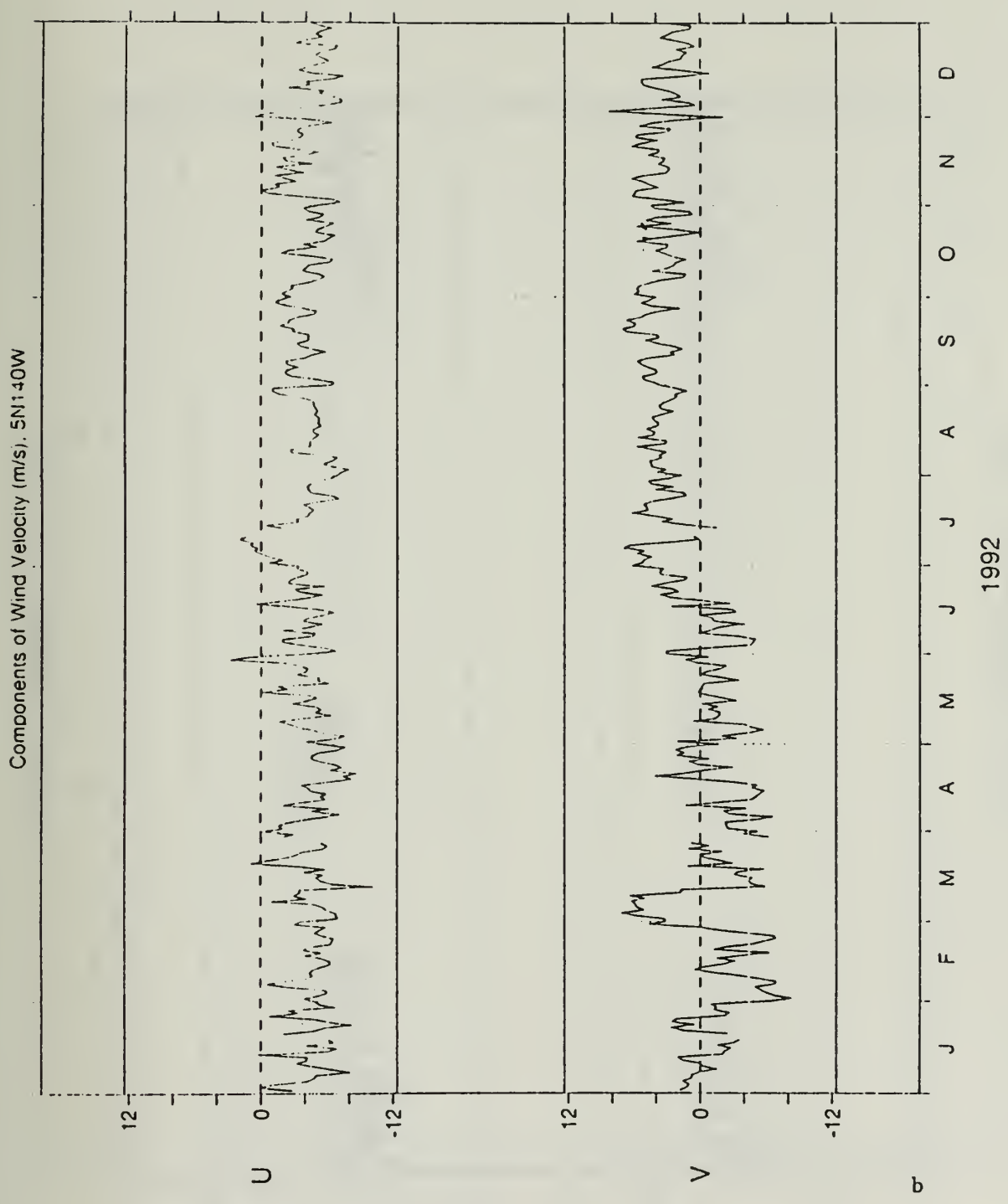

Fig. 16. (Continued) Speed scale range is -12 to 12 m/s. For U component, positive (negative) speeds indicate westerly (easterly) winds. For V component, positive (negative) speeds indicate southerly (northerly) winds.

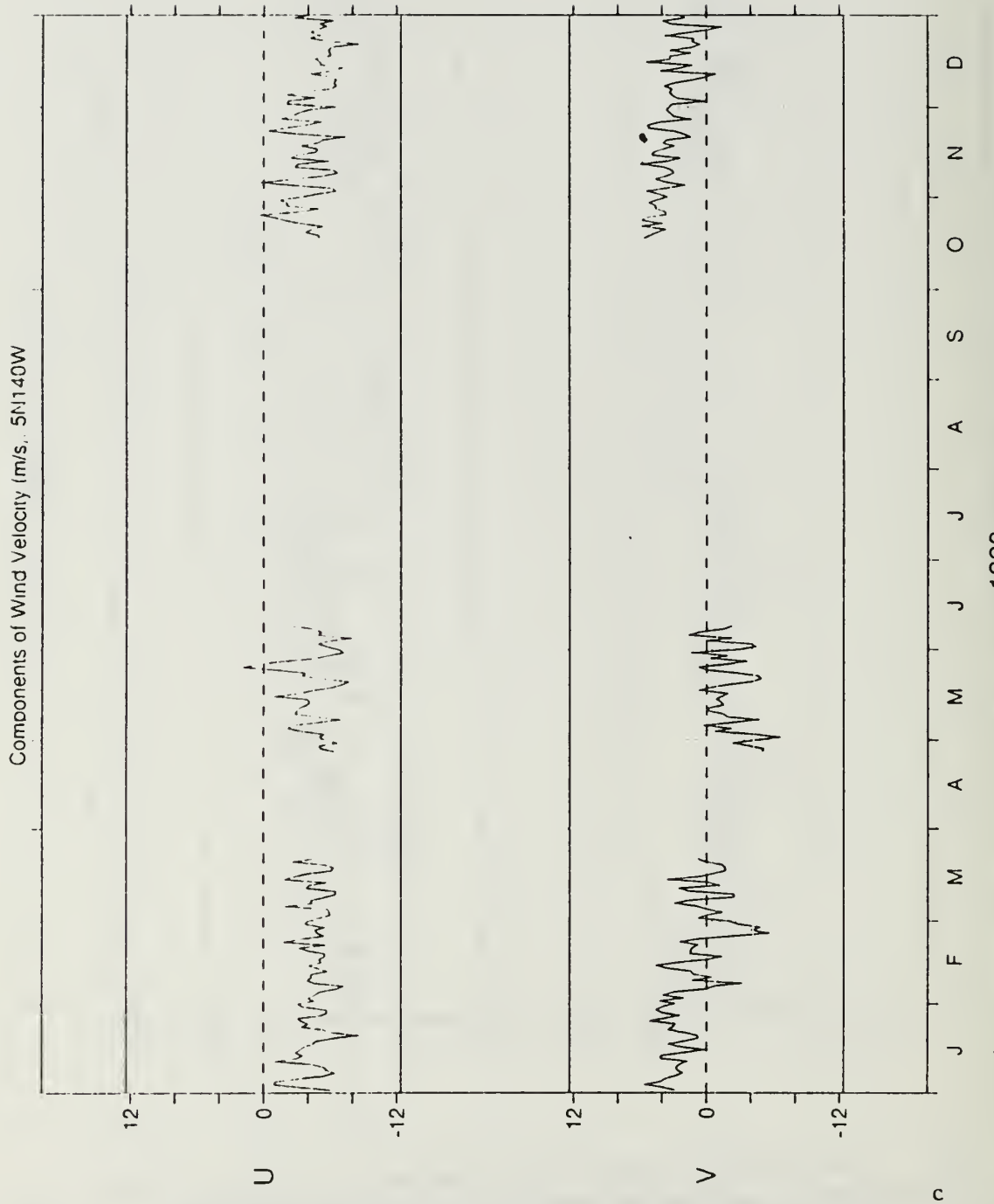

Fig. 16. (Continued).

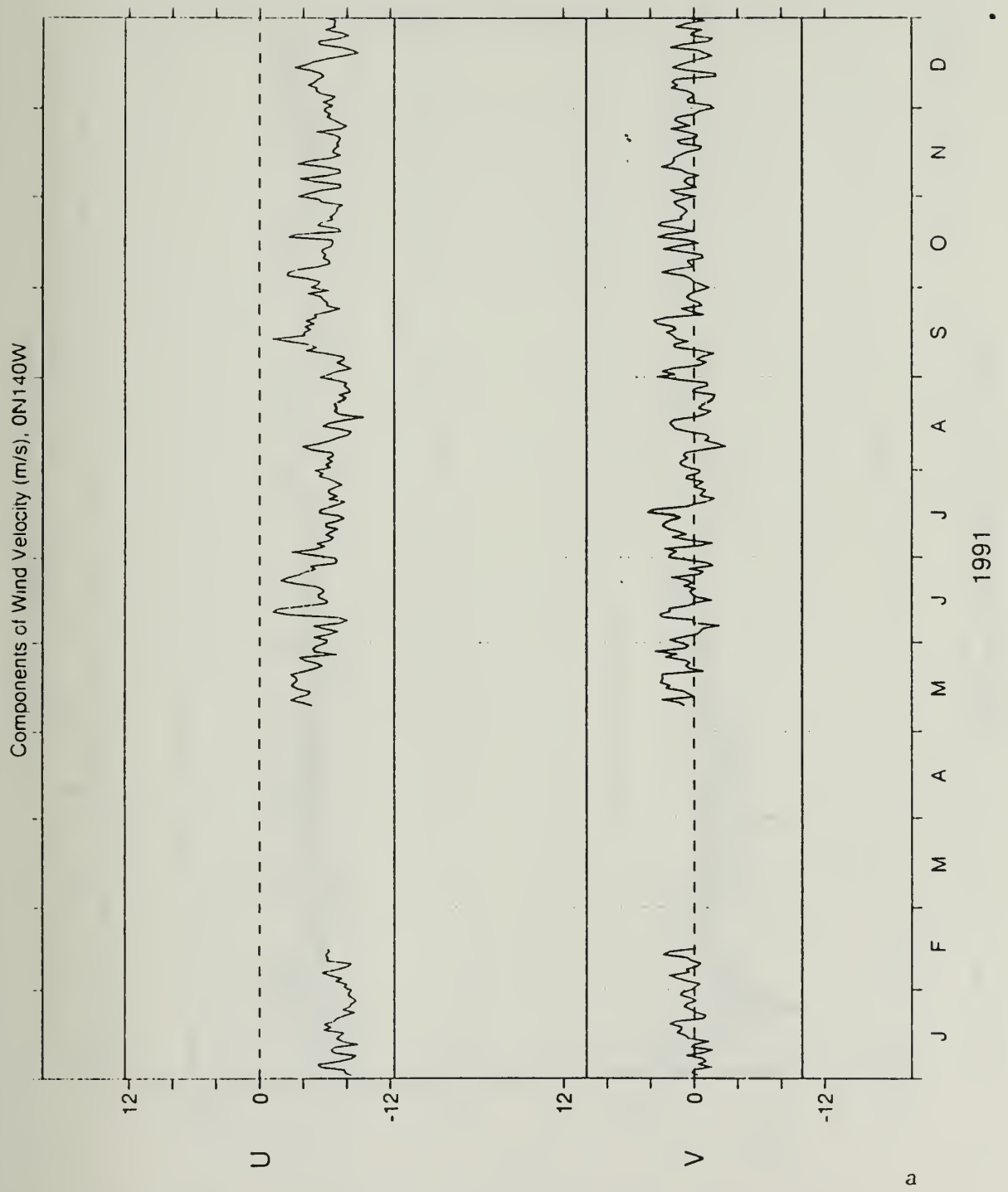

Fig. 17. Same as Fig. 16, except for 0° 140°W.

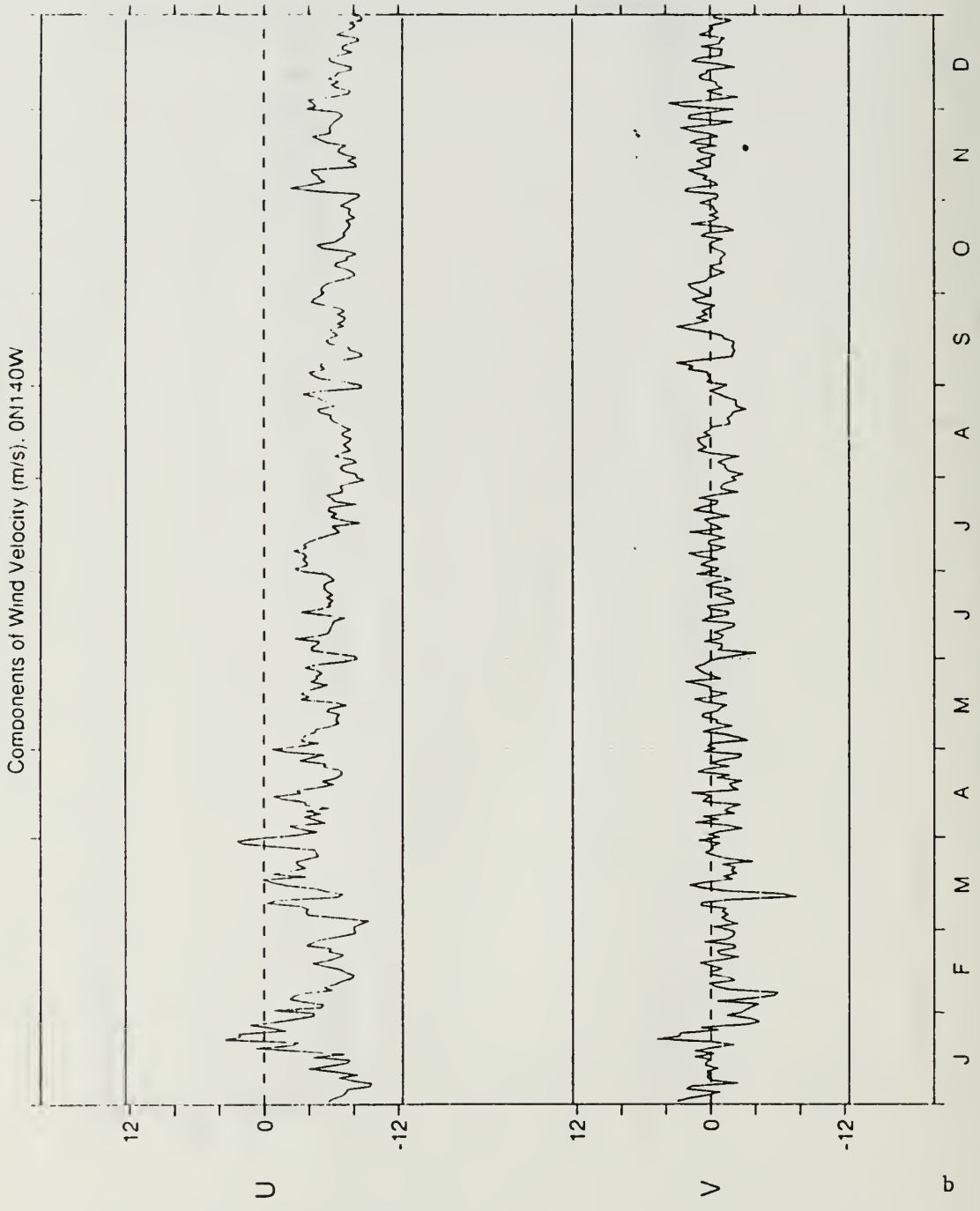

Fig. 17. (Continued).

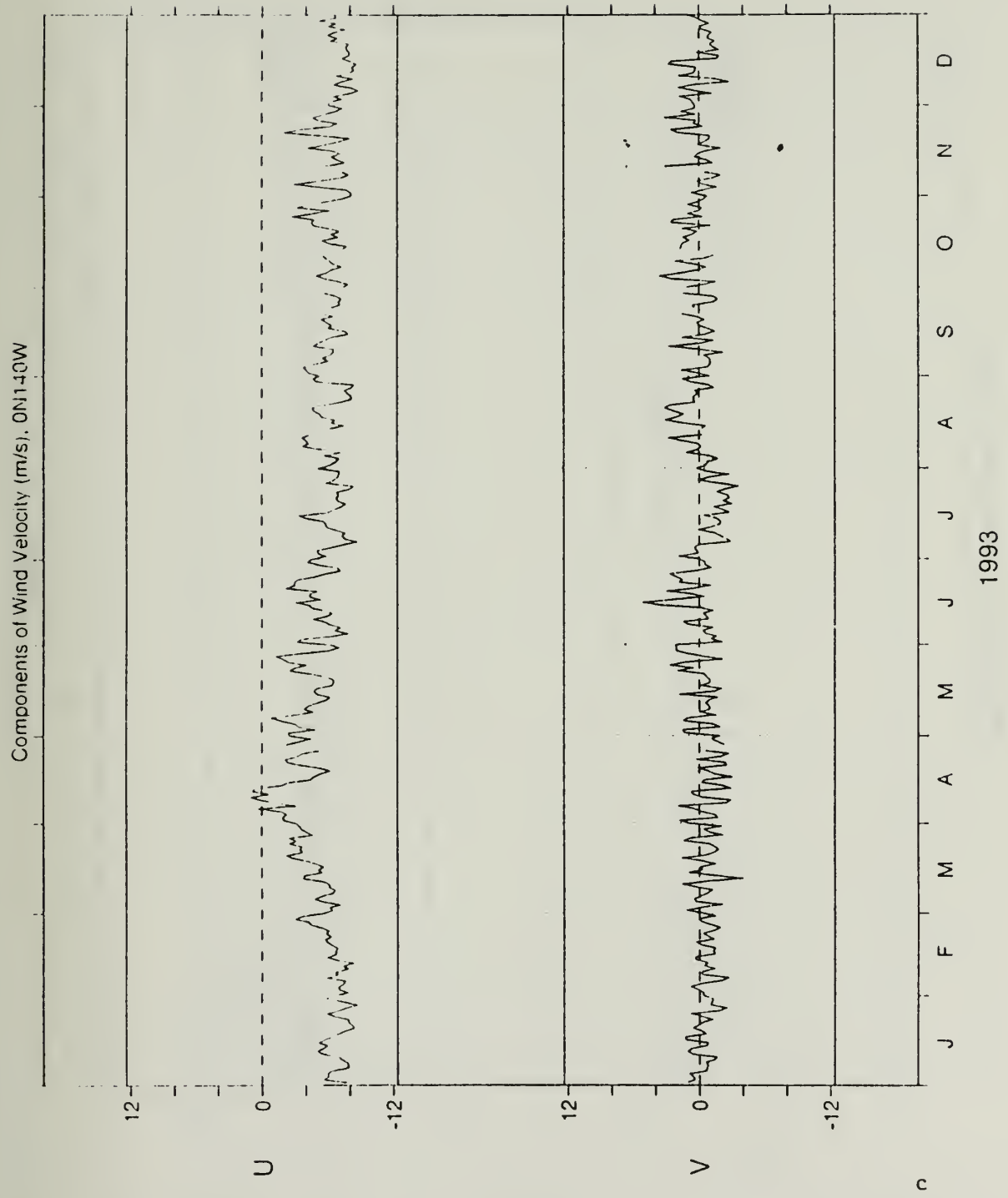

Fig. 17. (Continued).

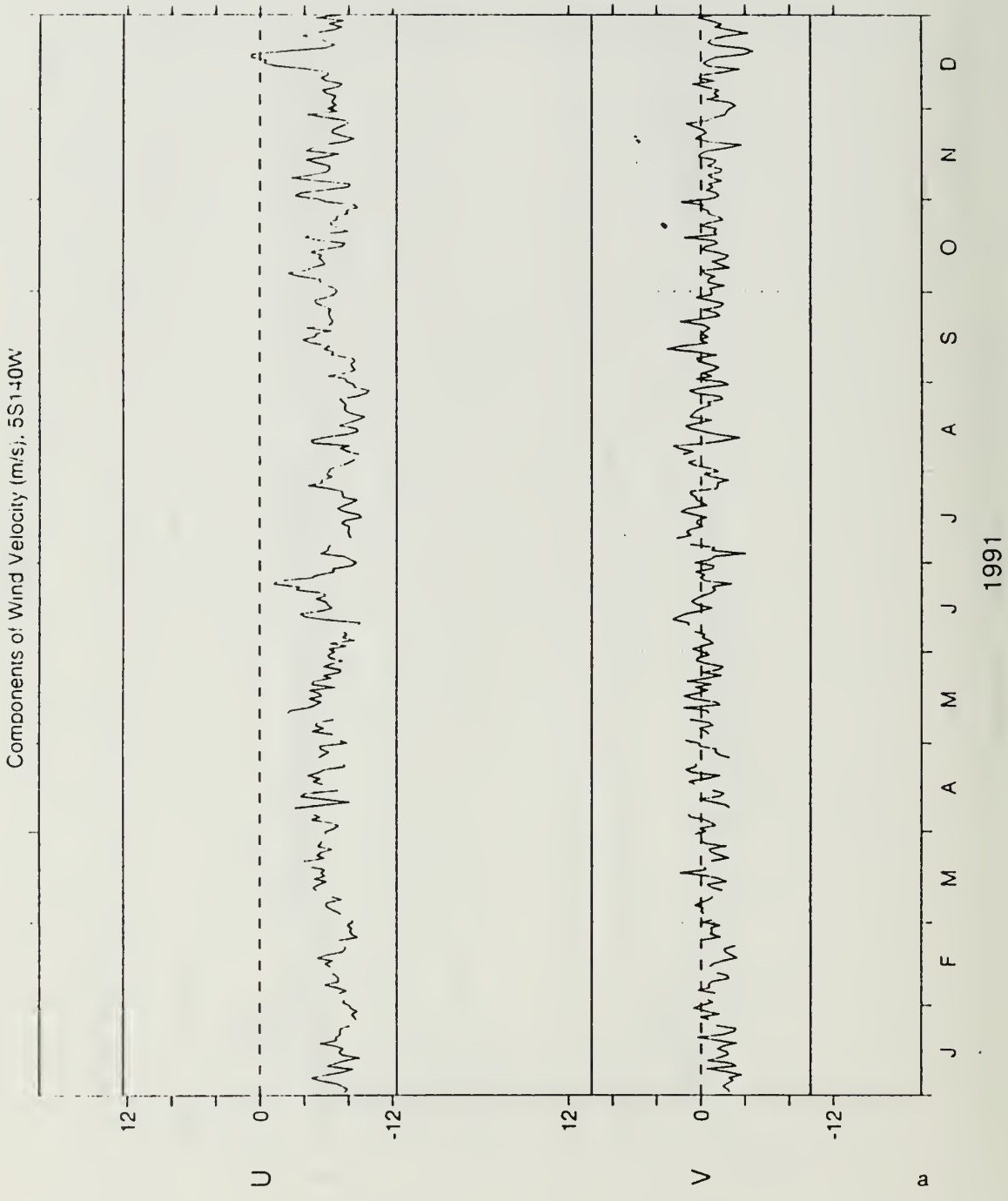

Fig. 18. Same as Fig. 16, except for 5°S 140°W.

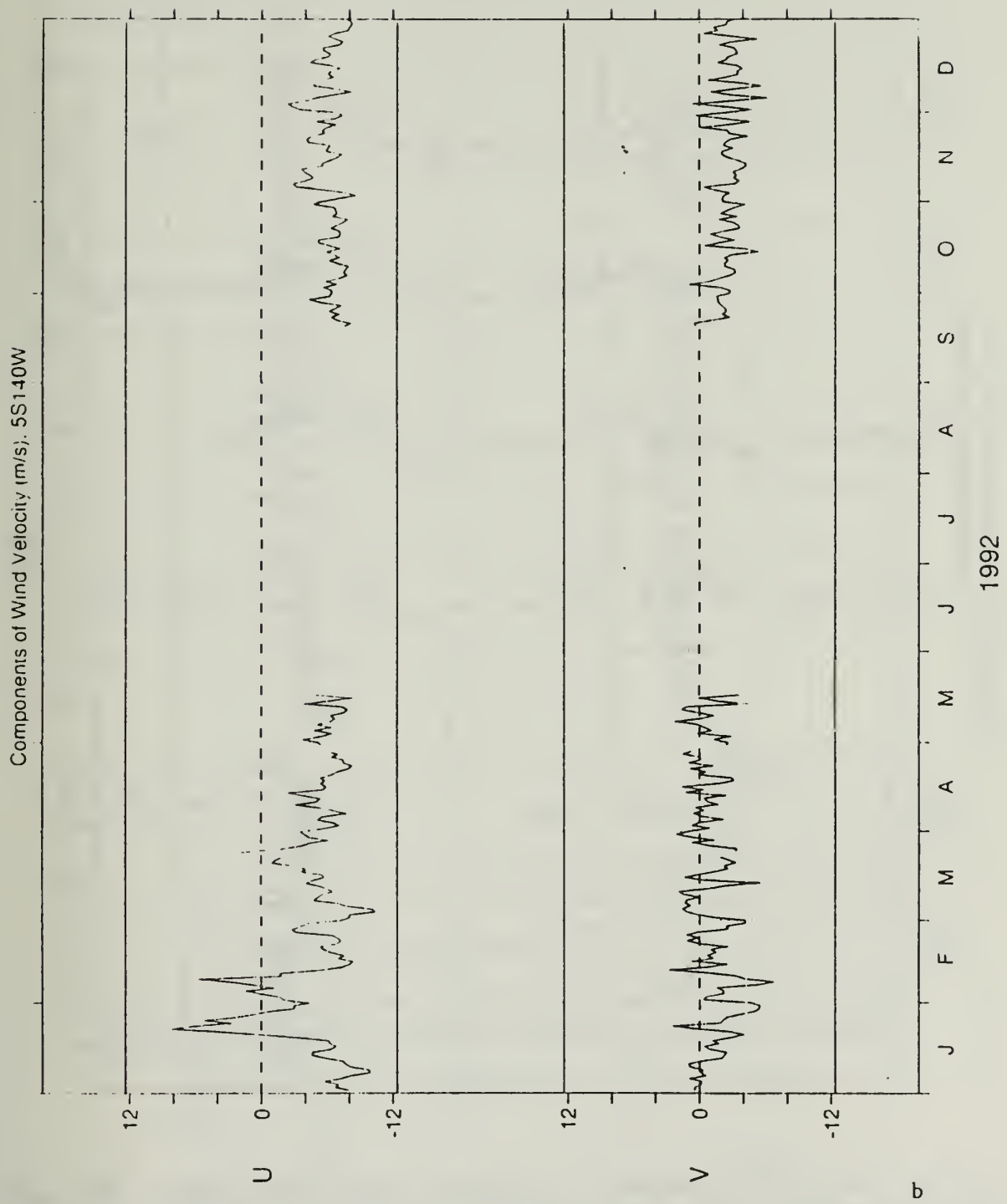

Fig. 18. (Continued).

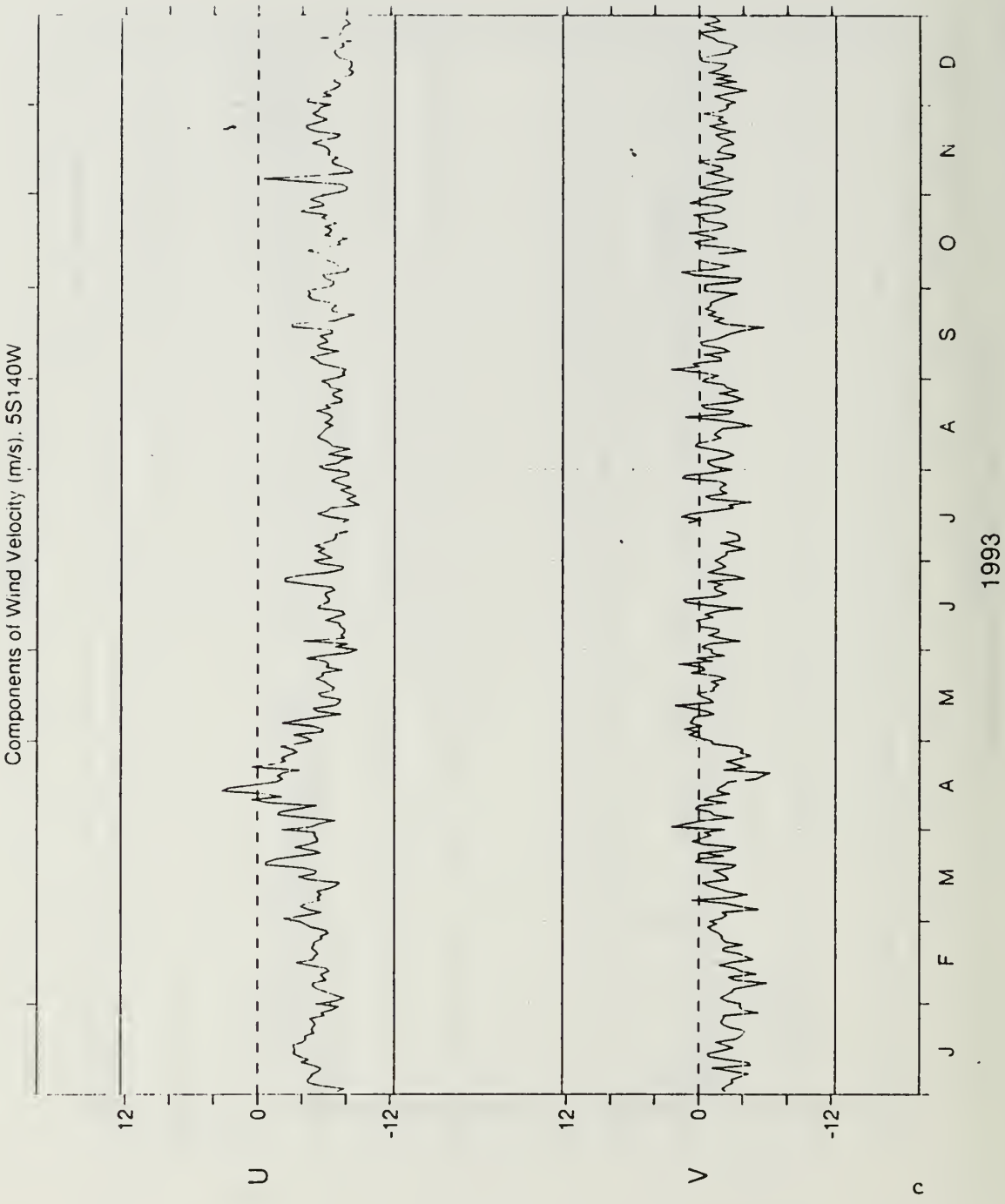

Fig. 18. (Continued).

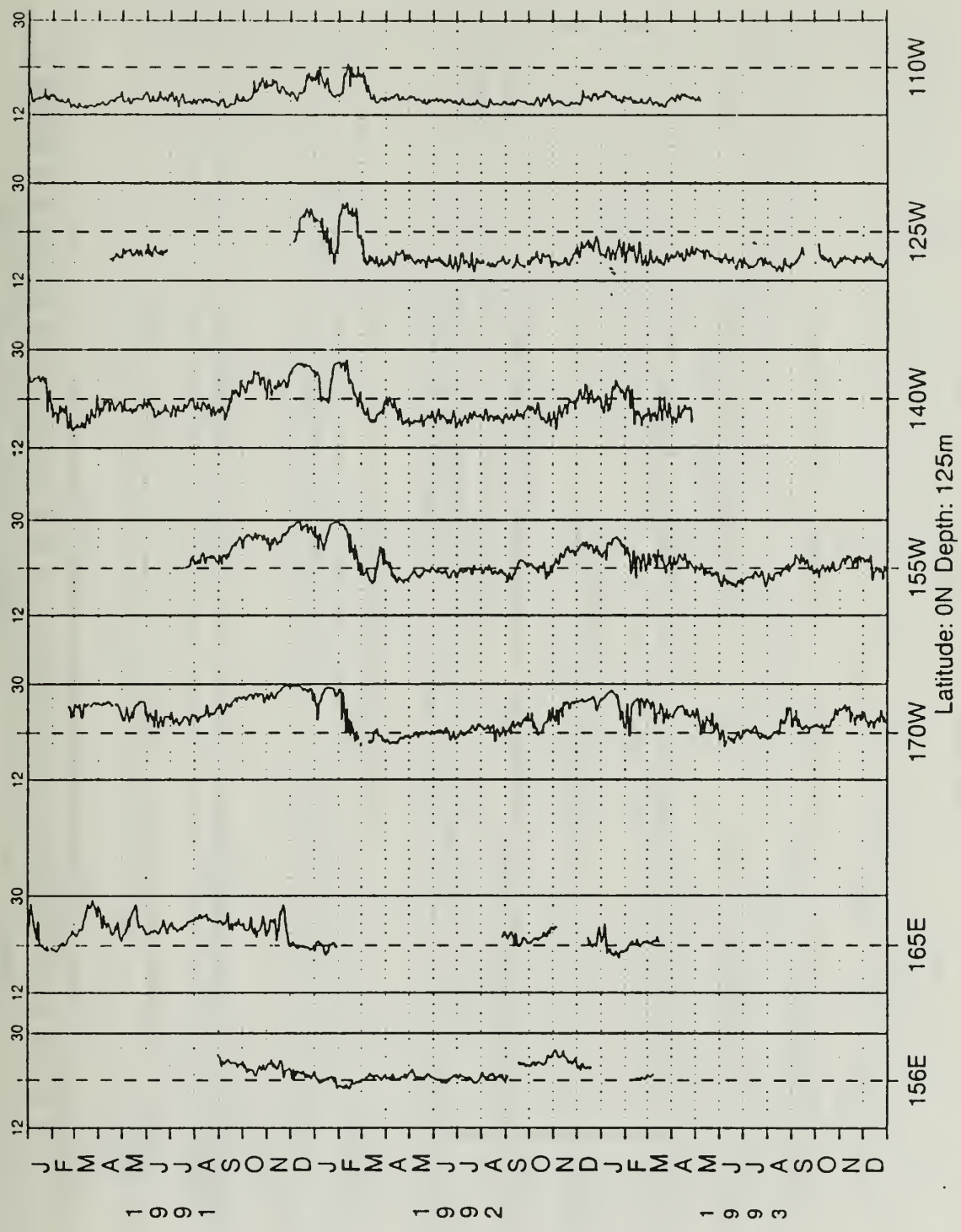

Fig. 19. Time-longitude display of temperature time series along the equator at 125m. Temperature scale range is 12 to 30°C.

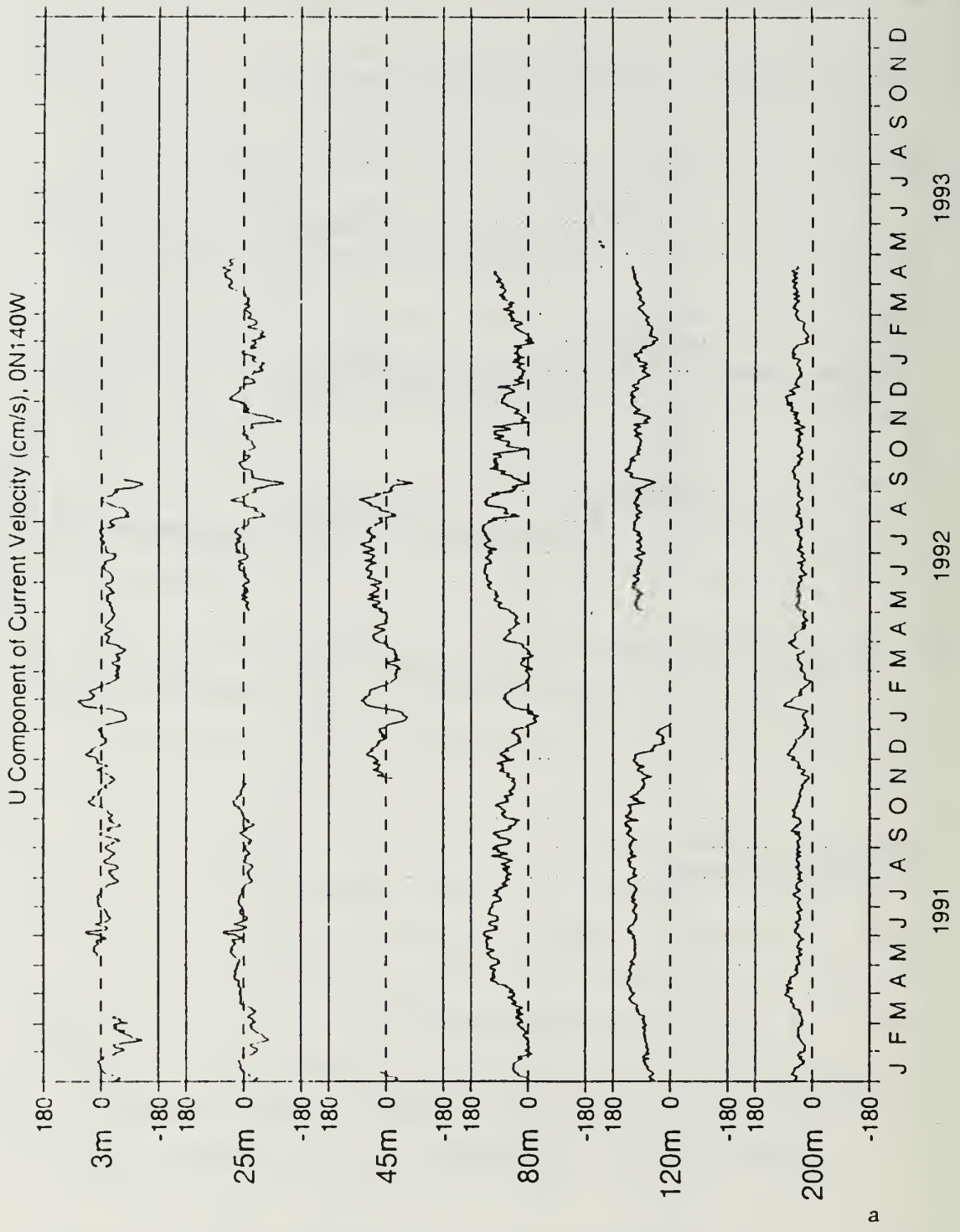

Fig. 20. Time series of current velocity components at 0° 140°W for: a) zonal component, b) meridional component. Speed scale range is -180 to 180 cm/s.

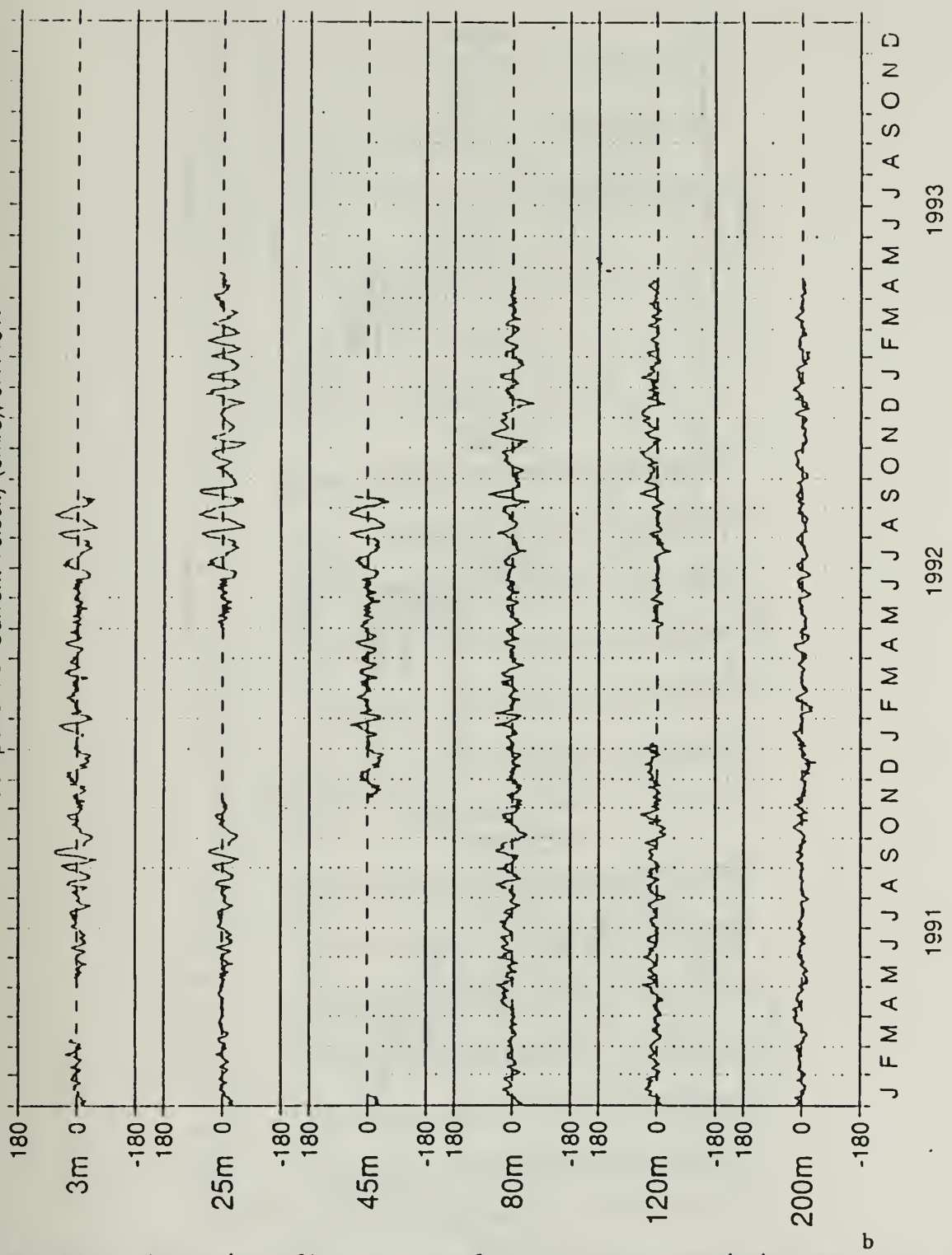

Fig. 20. (Continued) For zonal currents, positive (negative) speeds indicate eastward (westward) currents. For meridional currents, positive (negative) speeds indicate northward (southward) currents.

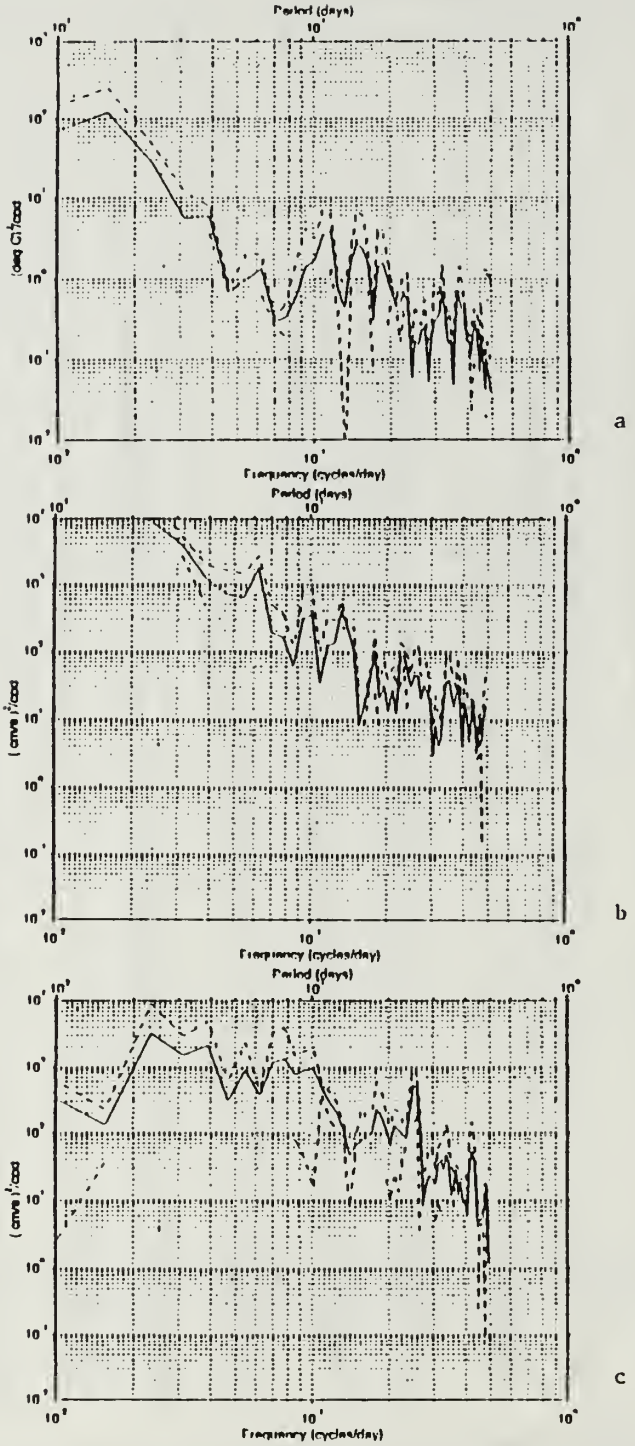

Fig. 21. Frequency spectrum at 0° 140°W from 31 Aug 91-31 May 92 for linearly detrended: a) temperature at 125m, b) zonal current at 3m, c) meridional current at 3m. Dashed curves show the 95% confidence interval.

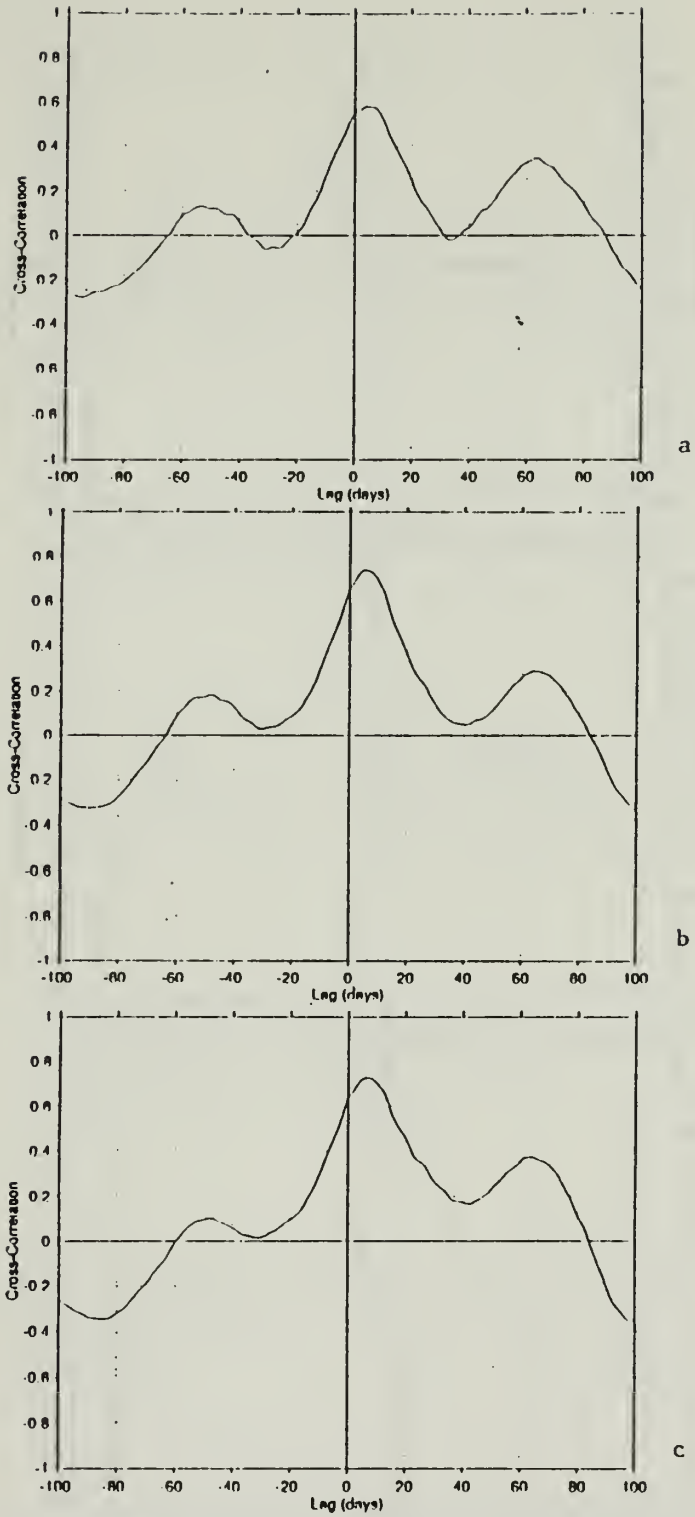

Fig. 22. Cross-correlations between linearly detrended temperature at different depths at 0° 140°W during 31 Aug 91-31 May 92 between: a) 125m/1m, b) 125m/25m, c) 125m/50m, d) 125m/75m, e) 125m/100m, f) 125m/150m,

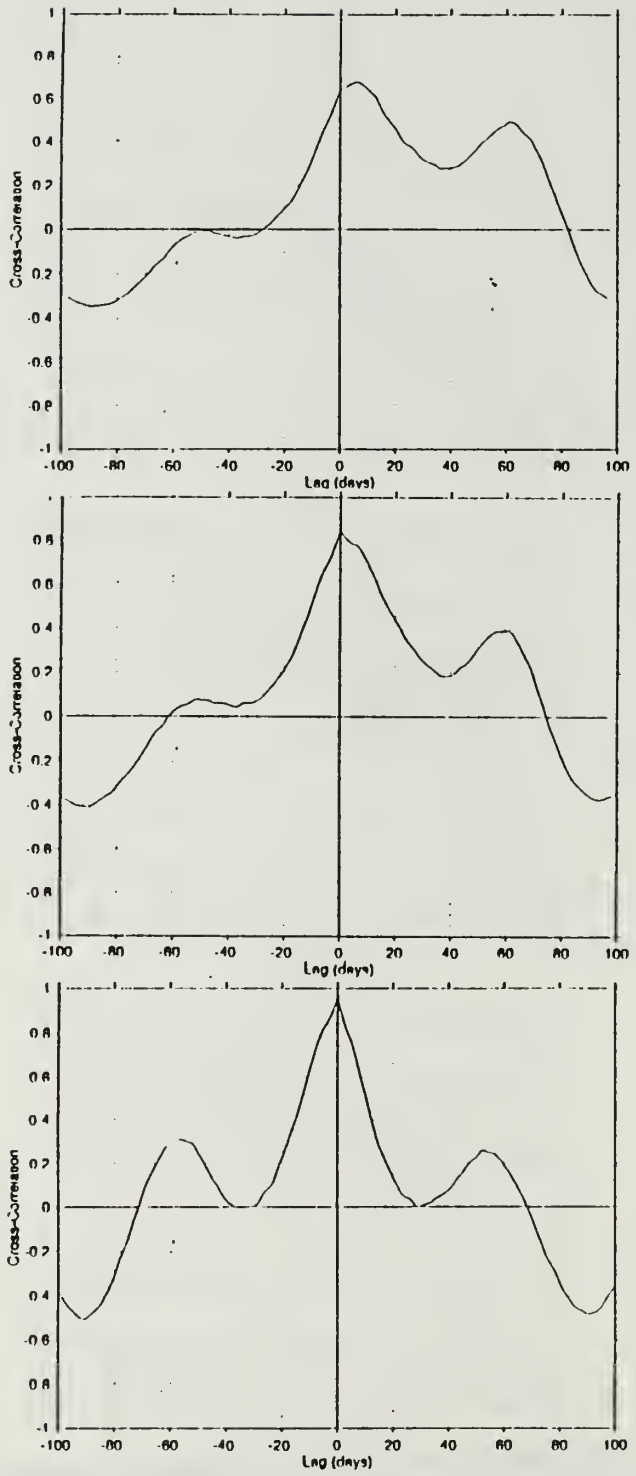

Fig. 22. (Continued) g) 125m/200m, h) 125m/250m, i) 125m/300m, j) 125m/500m. Positive (negative) lag means that the second time series lags (leads) the first.

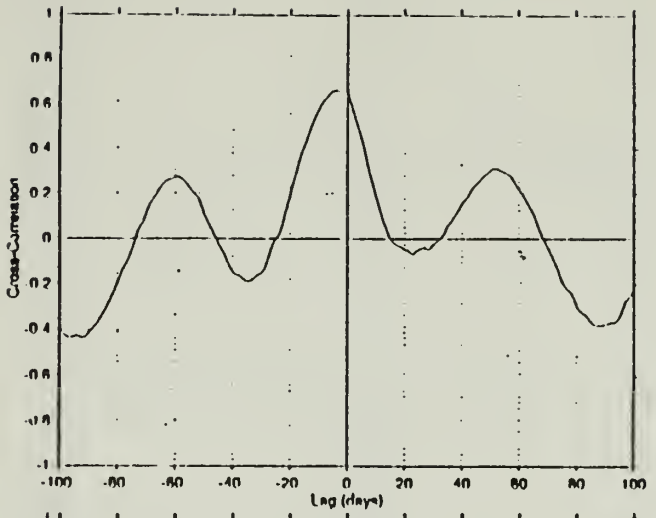

g

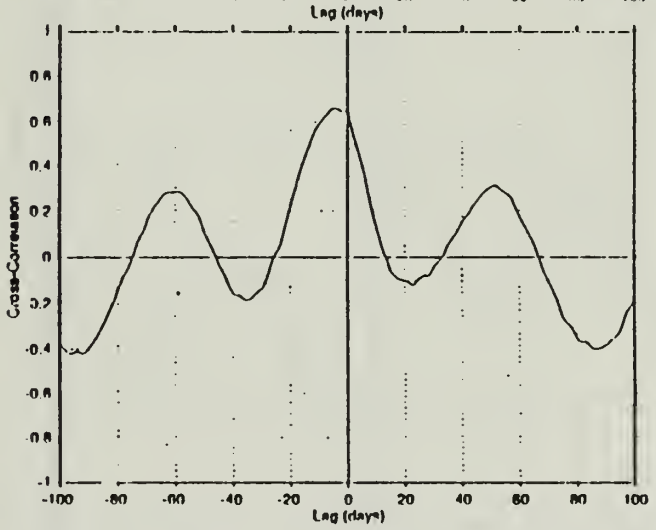

h

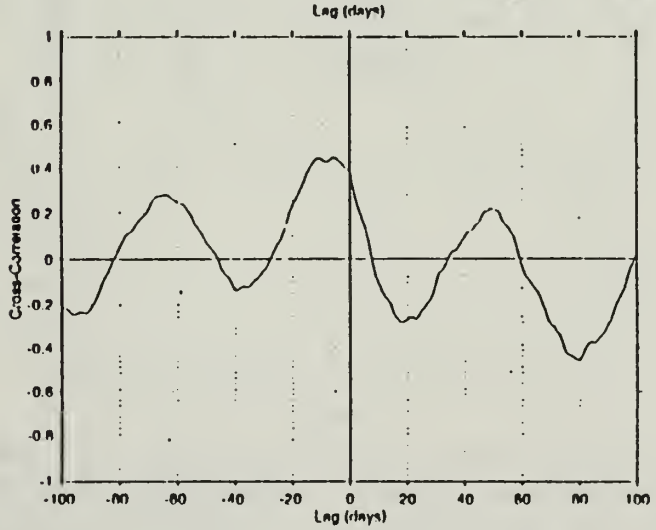

i

Fig. 22. (Continued).

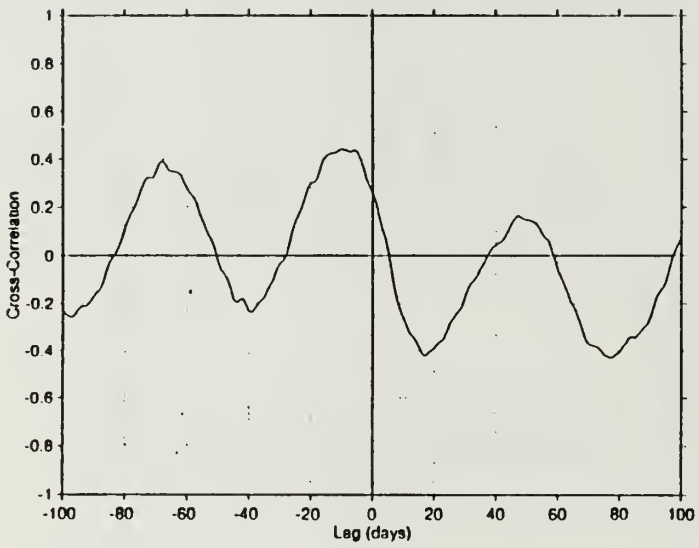

j

Fig. 22. (Continued).

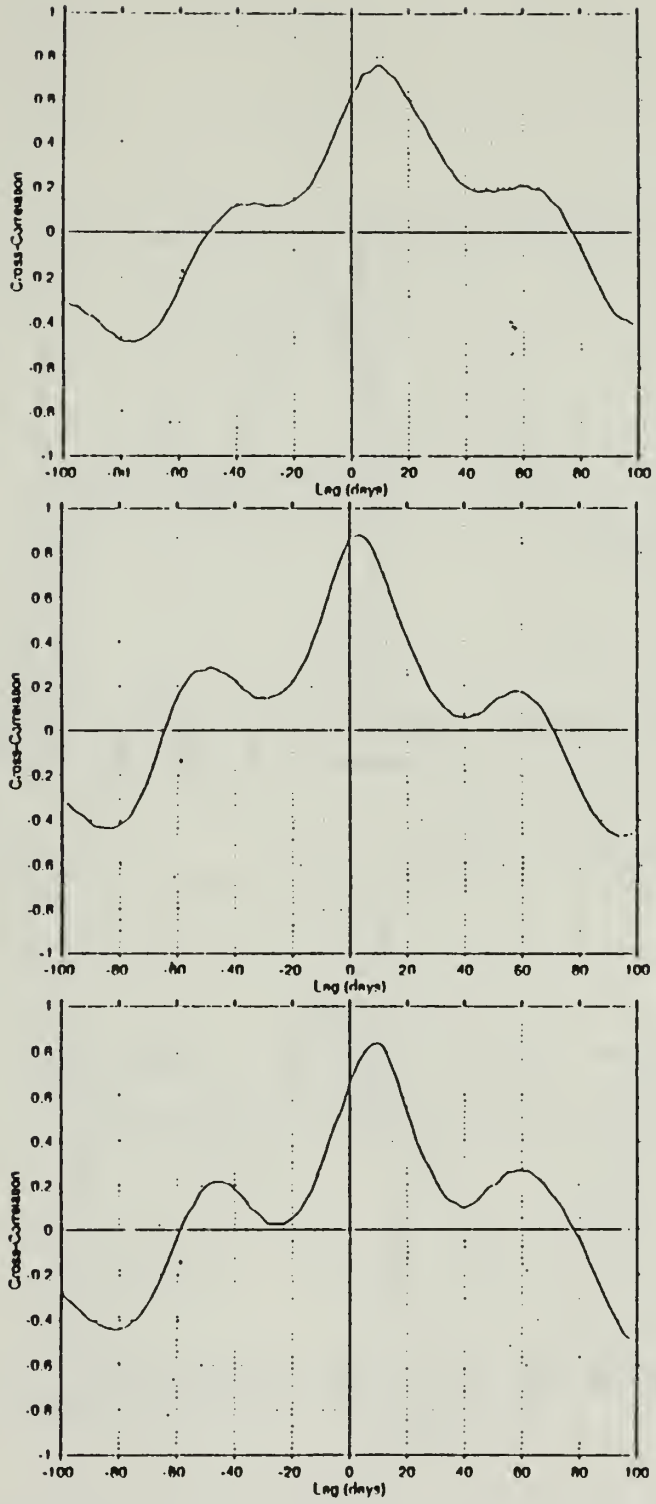

Fig. 23. Same as for Fig. 22 but for cross-correlations between different longitudes. Panels a-d are for temperatures at: a) 125m, 0° 170°W/125m, 0° 140°W, b) 125m, 0° 155°W/125m, 0° 140°W,

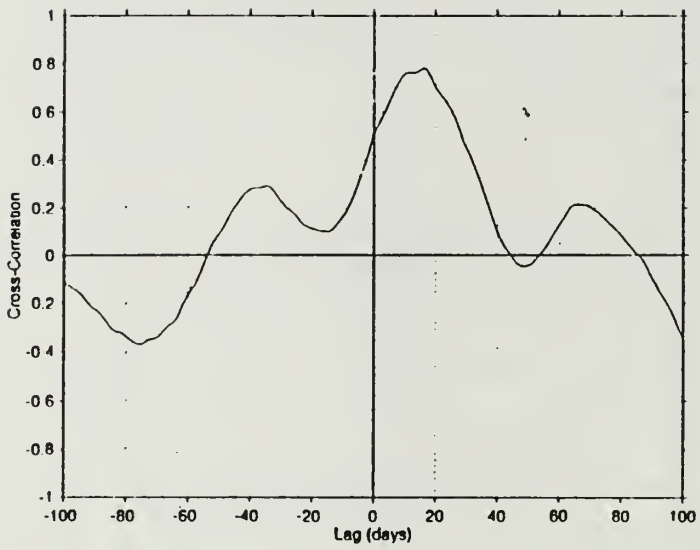

d

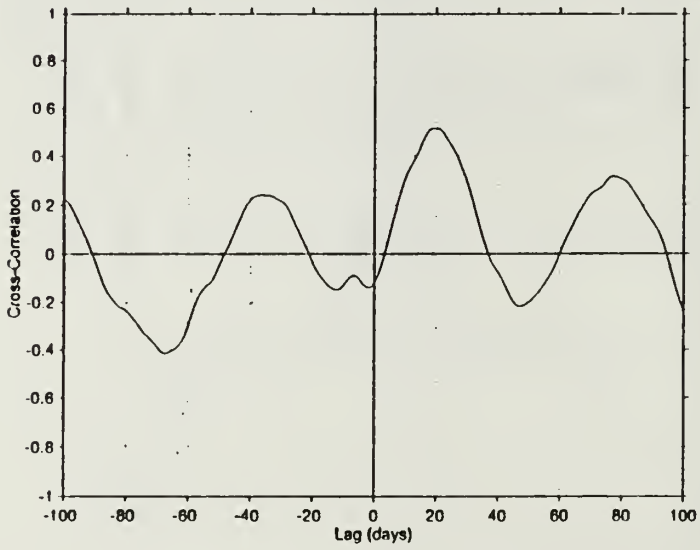

e

Fig. 23. (Continued) c) 125m, 0° 140°W/125m, 0° 125°W, d) 125m, 0° 140°W/100m, 0° 110°W. Panel e is for zonal current: e) 3m, 0° 140°W/10m, 0° 110°W.

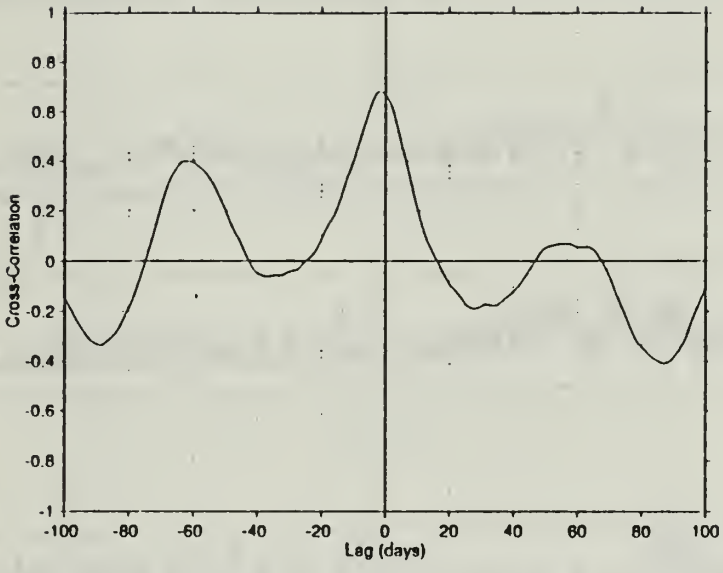

Fig. 24. Same as Fig. 22 but for cross-correlations at 0° 140°W between temperature at 125m/zonal current at 3m.

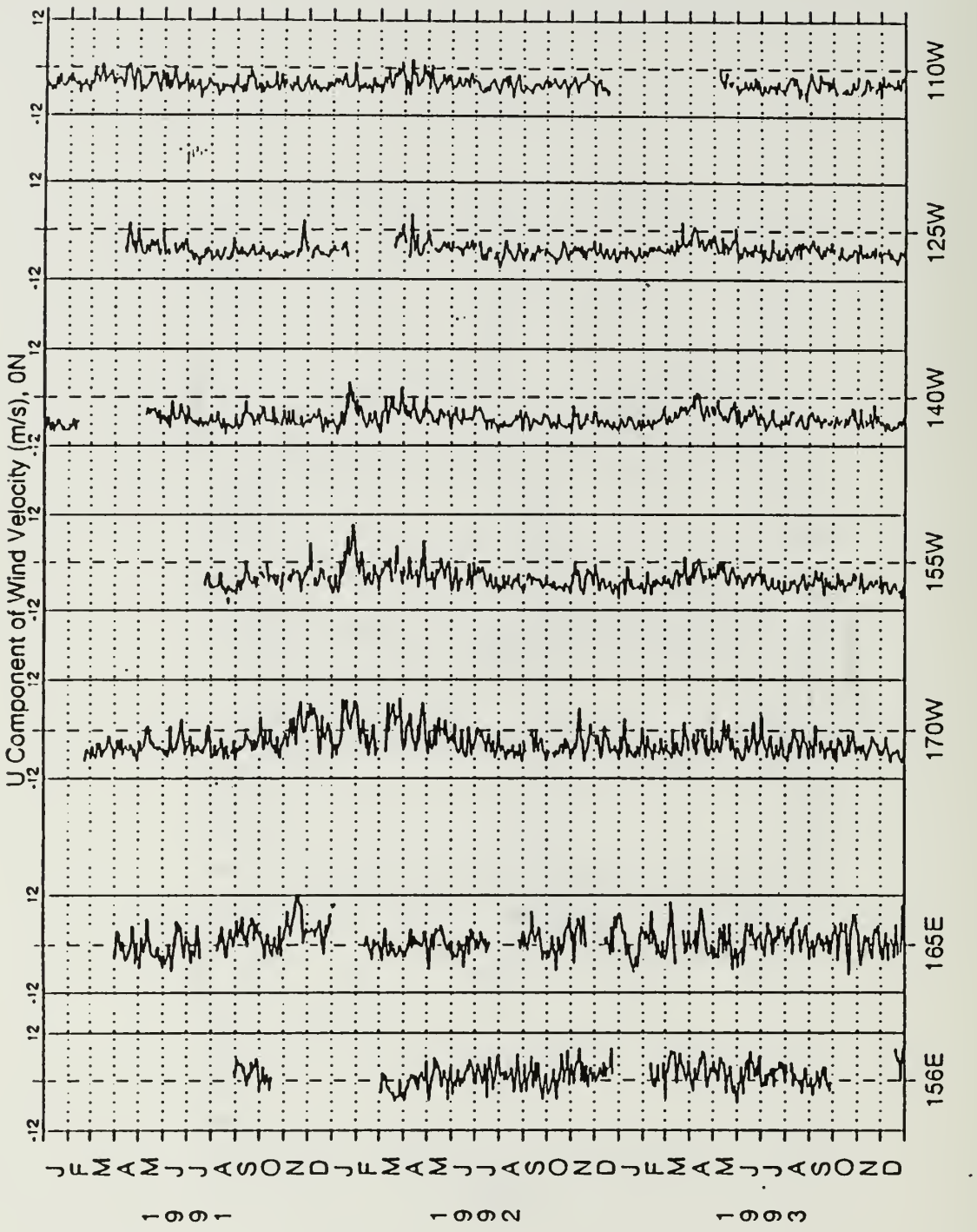

Fig. 25. Time-longitude display of zonal wind at the equator. Wind speed scale range is -12 to 12 m/s. Positive (negative) speeds indicate westerly (easterly) winds.

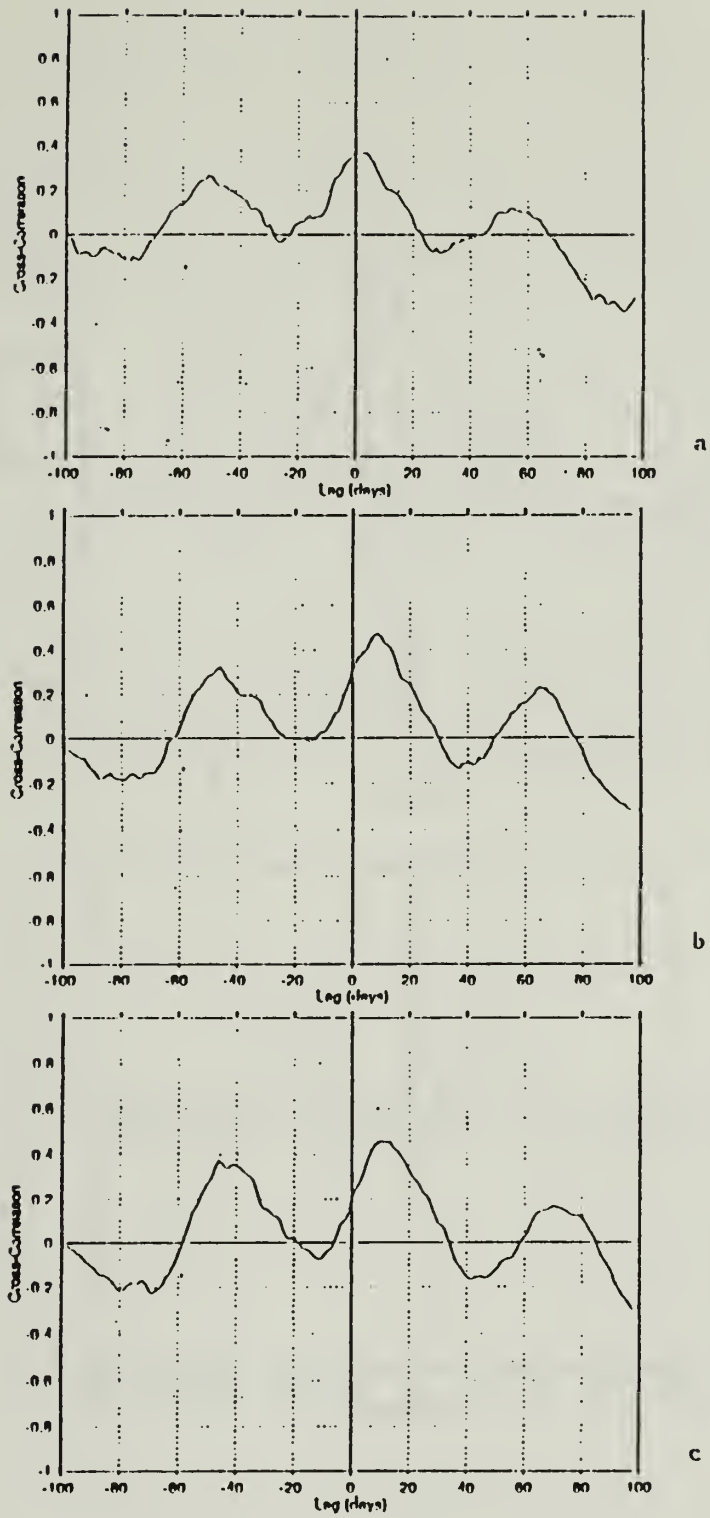

Fig. 26. Cross-correlations between zonal wind at 0° 170°W during 31 Aug 91-31 May 92 and temperature at: a) 125m, 0° 170°W, b) 125m, 0° 155°W, c) 125m, 0° 140°W, d) 125m, 0° 125°W,

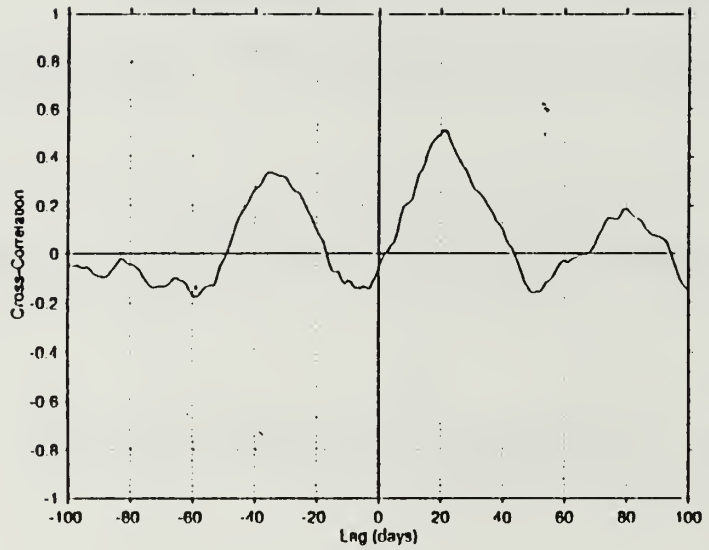

d

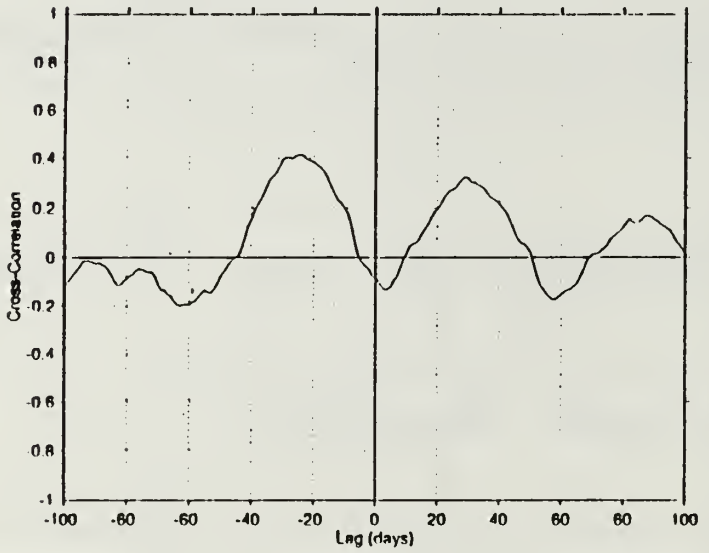

e

Fig. 26. (Continued) e) 100m, 0° 110°W. Positive (negative) lag means that the second time series lags (leads) the first.

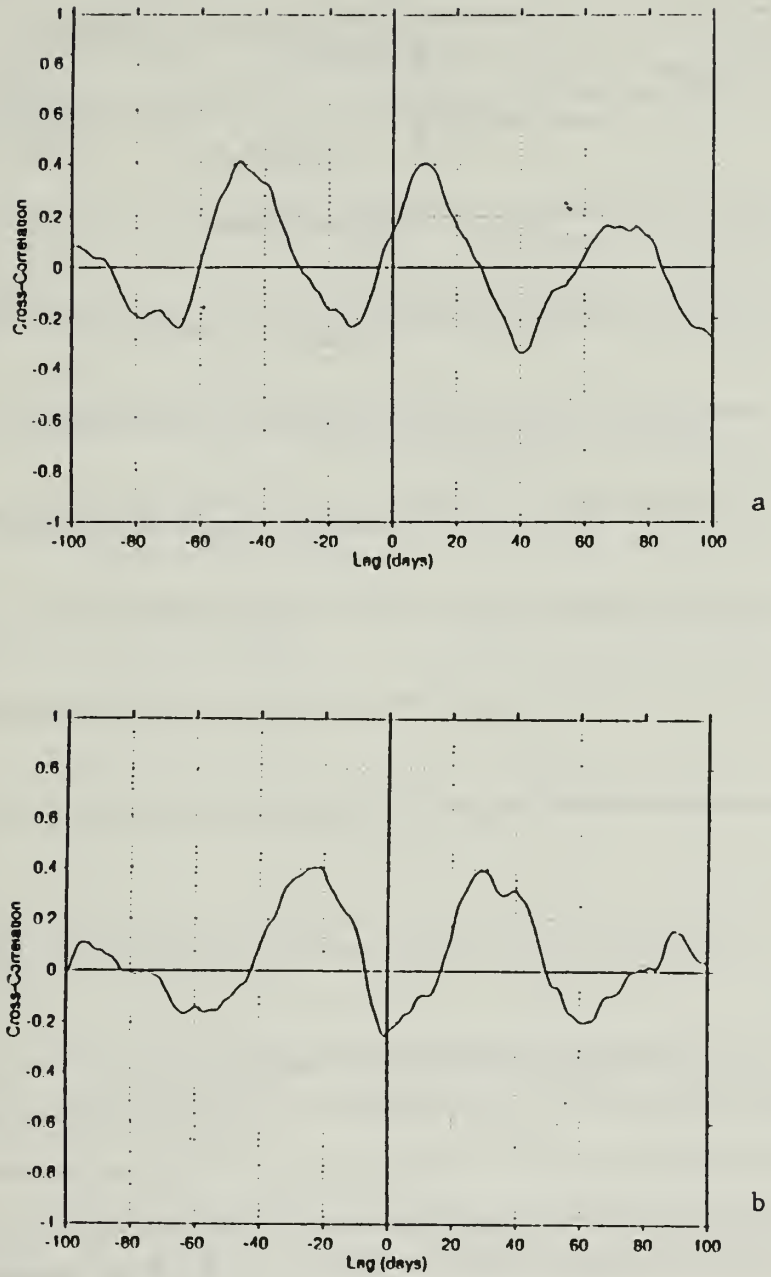

Fig. 27. Same as Fig. 26, except between zonal wind at 0° 170°W and zonal current at: a) 3m, 0° 140°W, b) 10m, 0° 110°W.

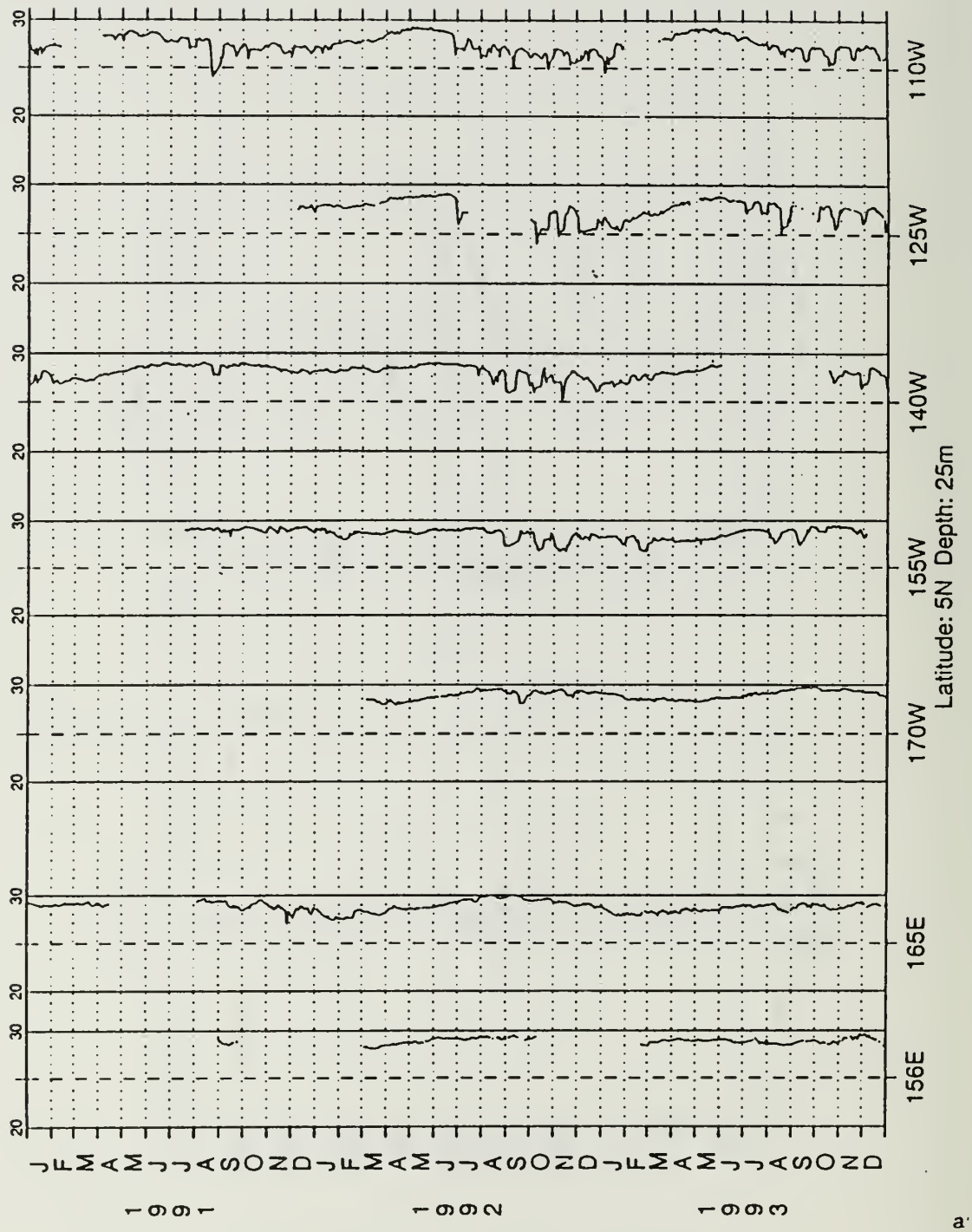

Fig. 28. Time-longitude display of temperature time series for 5°N at: a) 25m, b) 75m, c) 125m. Temperature scale range is 12 to 30°C.

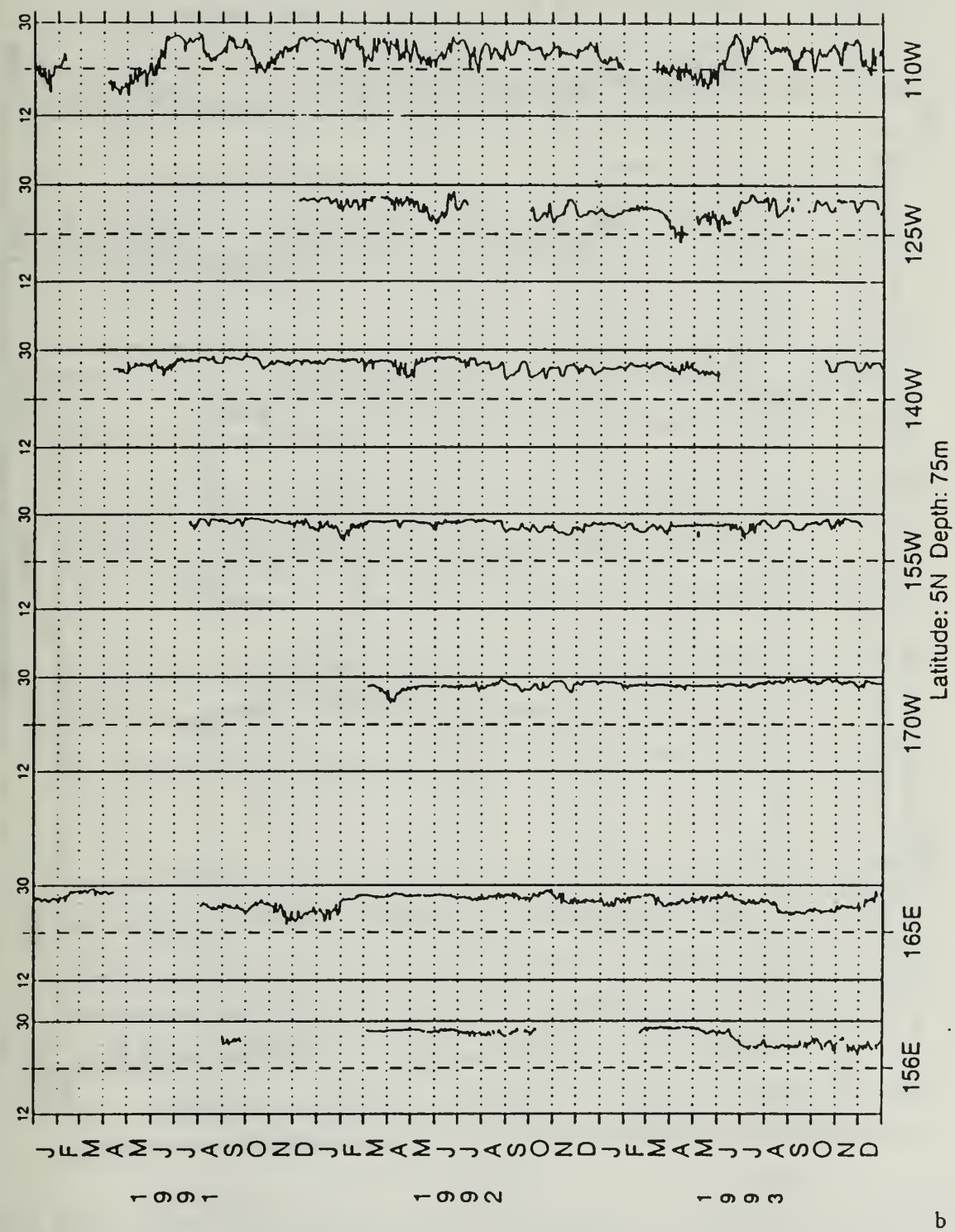

Fig. 28. (Continued).

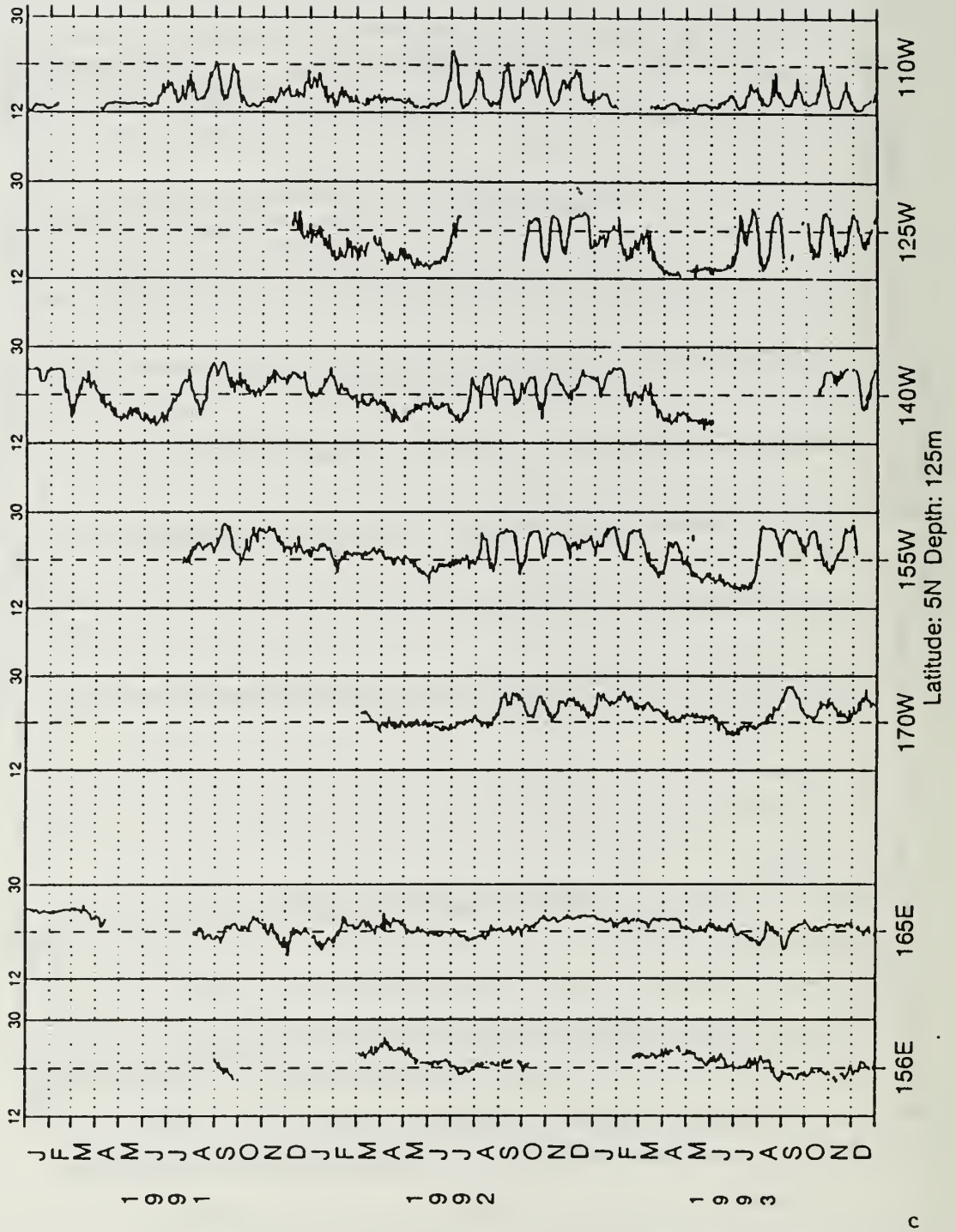

Fig. 28. (Continued).

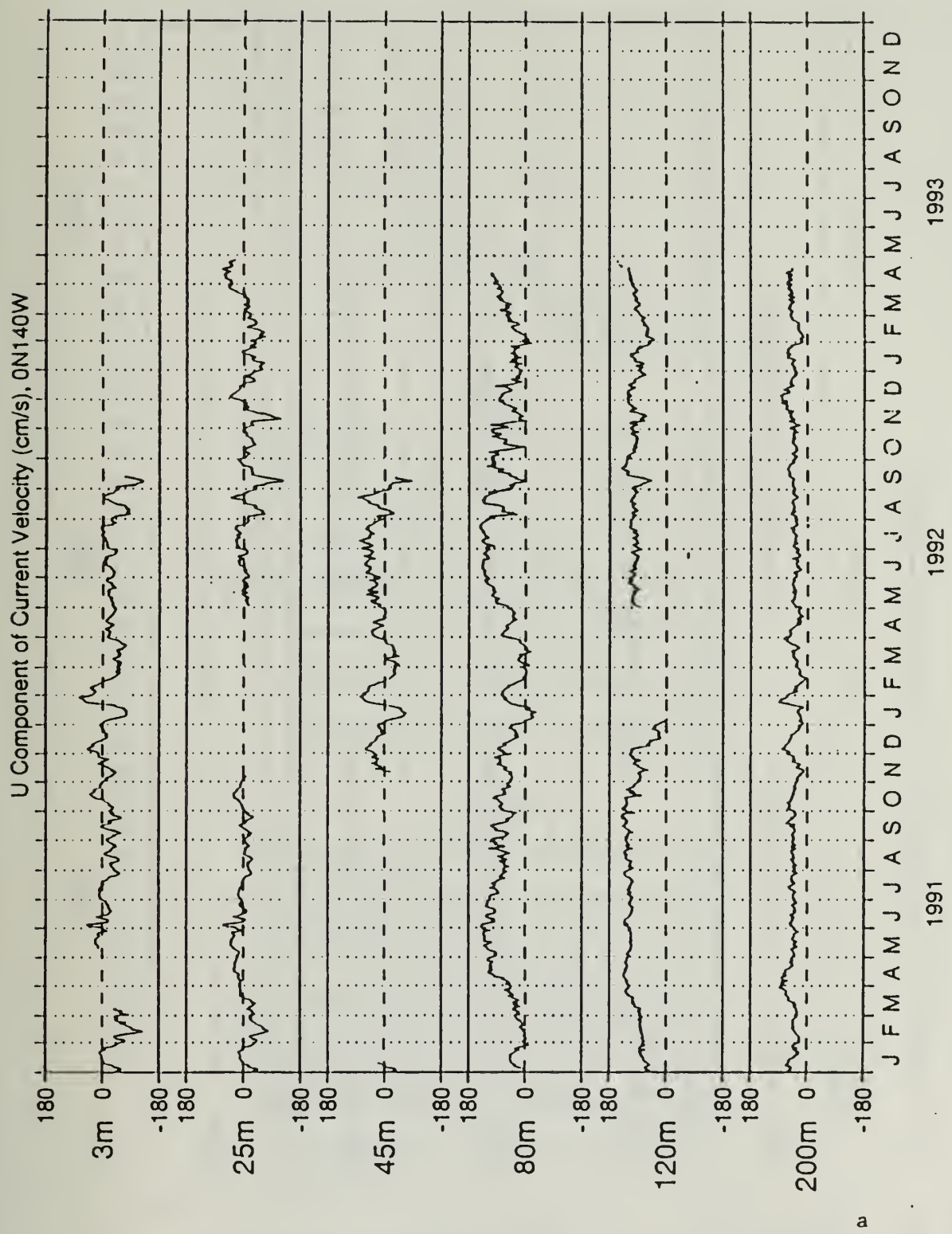

Fig. 29. Time series of current speed at 0° 140°W for a) zonal component, b) meridional component. Speed scale range is -180 to 180 cm/s.

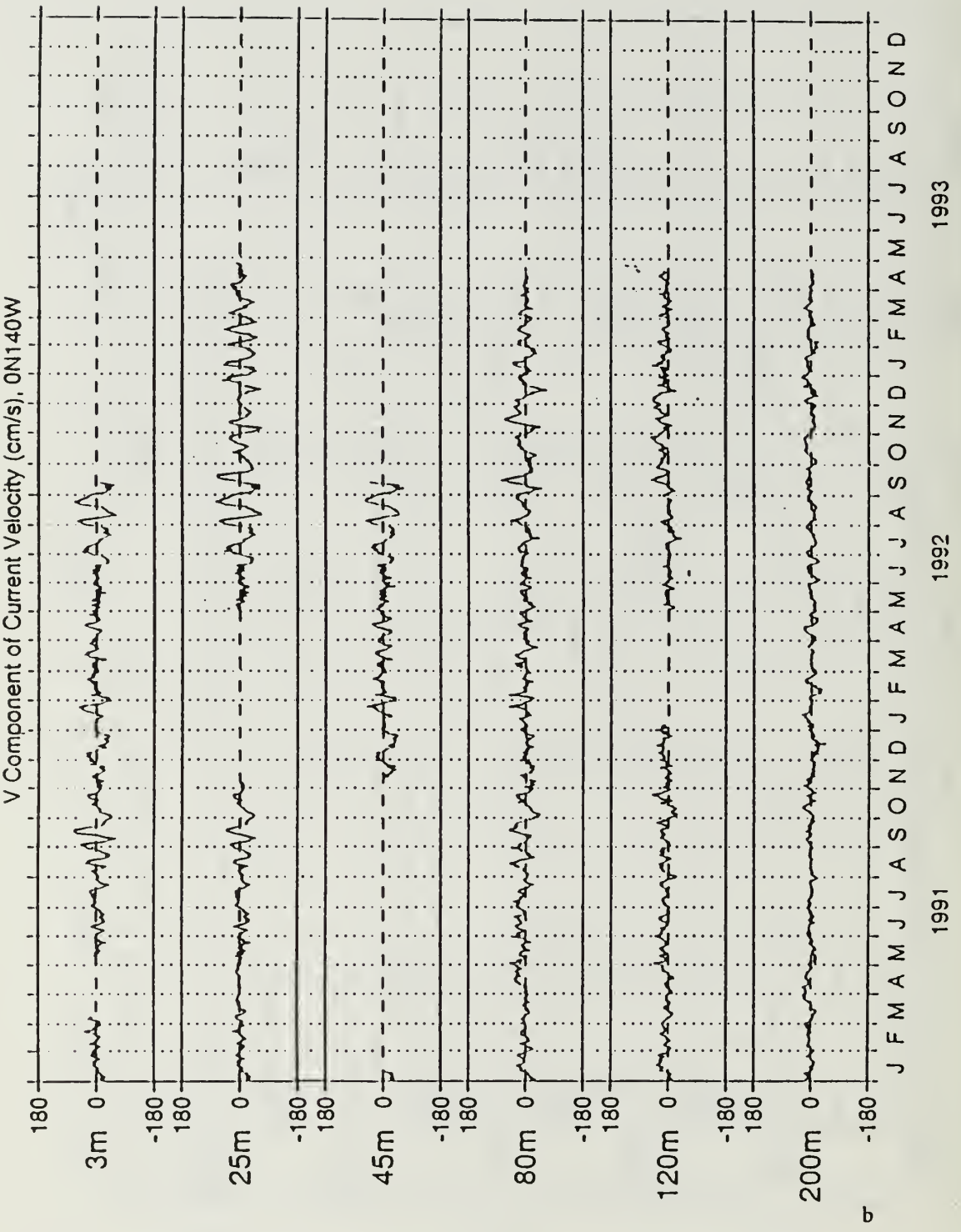

Fig. 29. (Continued) For zonal currents, positive (negative) speeds indicate eastward (westward) currents. For meridional currents, positive (negative) speeds indicate northward (southward) currents.

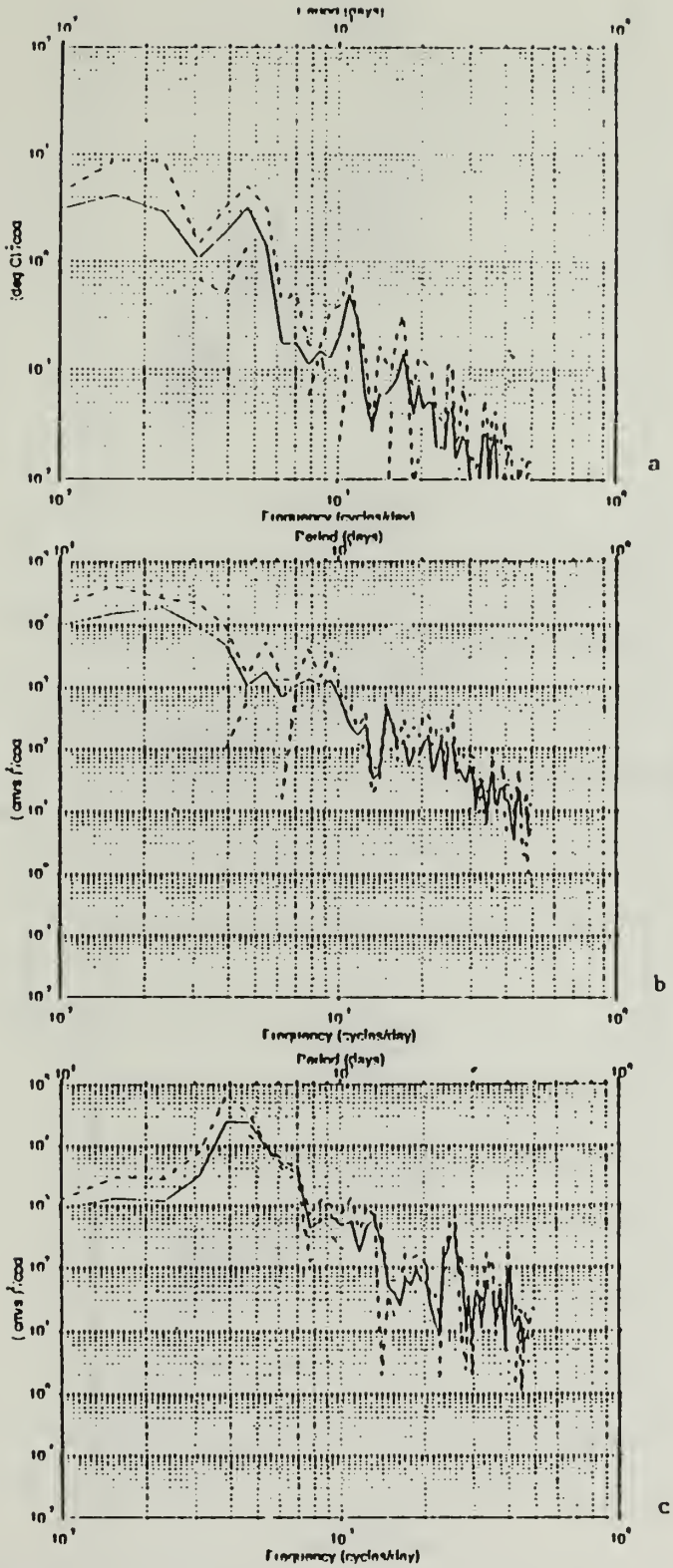

Fig. 30. Frequency spectrum at 5°N 140°W during 31 May 92-30 Apr 93 for linearly detrended: a) temperature at 25m, b) zonal current at 25m, c) meridional current at 25m,

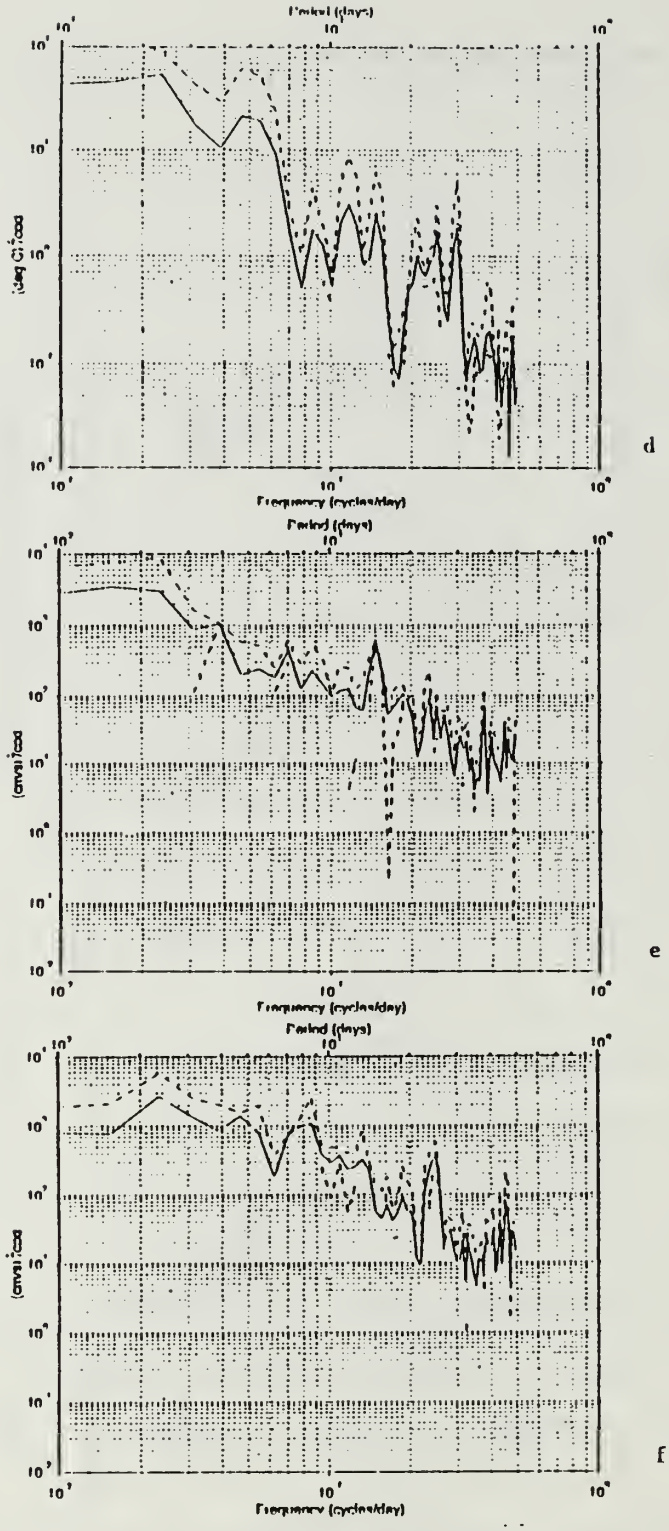

Fig. 30. (Continued) d) temperature at 125m, e) zonal current at 120m, f) meridional current at 120m. Dashed curves show the 95% confidence interval.

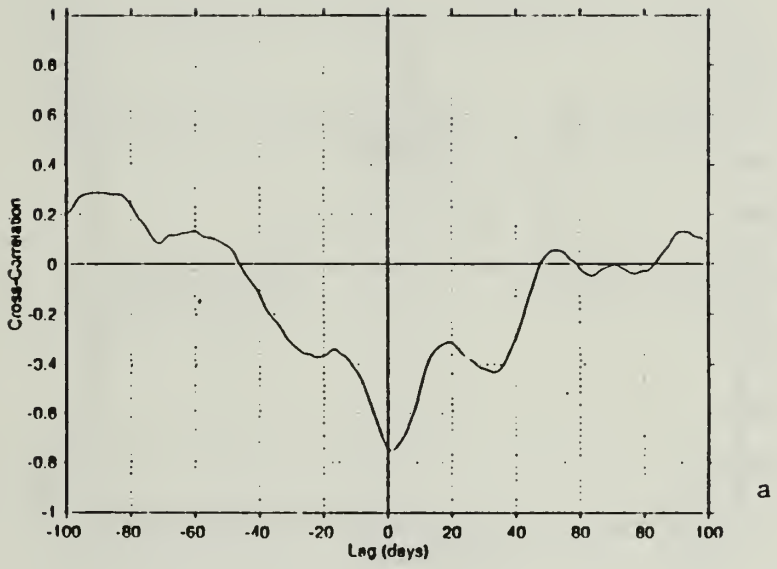

Fig. 31. Cross-correlations between different depths of linearly detrended temperatures at 5°N 140°W during 31 May 92-30 Apr 93. a) 25m/125m, b) 125m/250m.

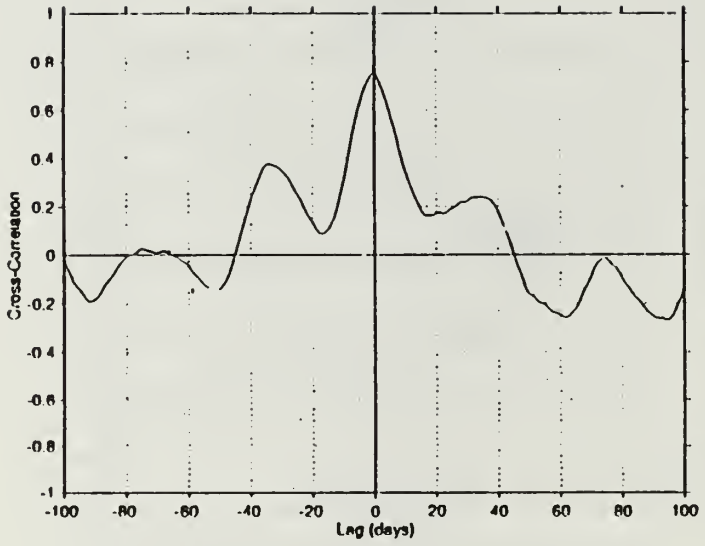

b

Fig. 31. (Continued) Positive (negative) lag means that the second time series lags (leads) the first.

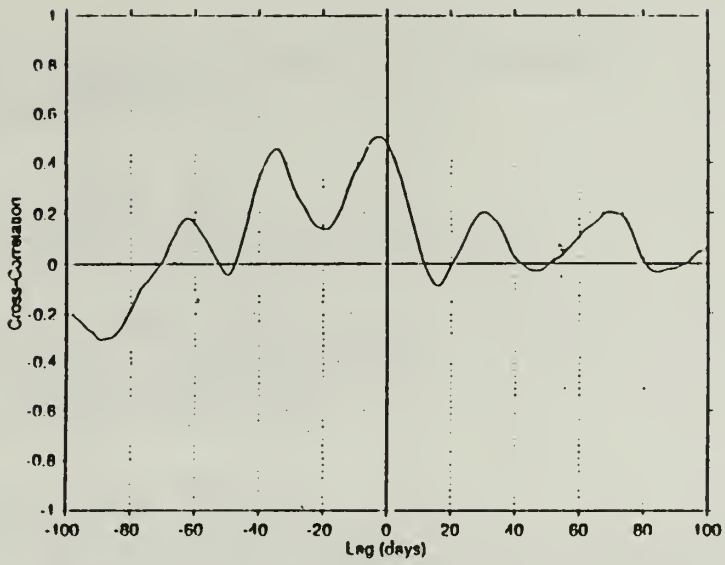

a

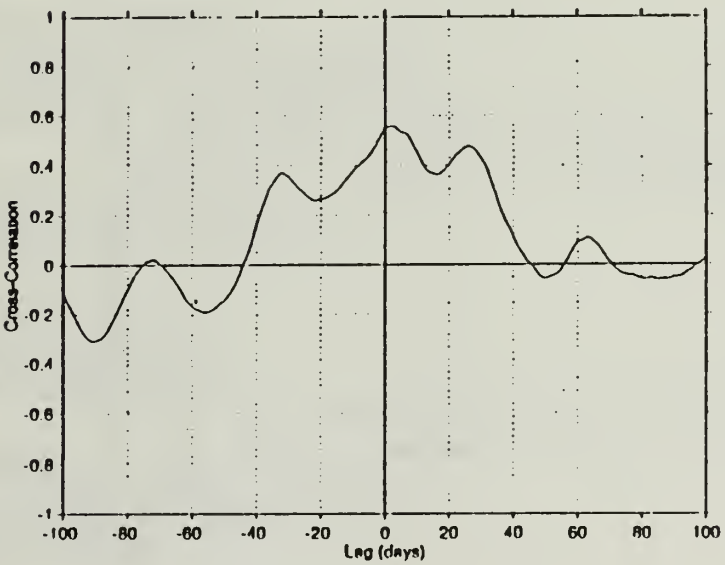

b

Fig. 32. Same as Fig. 31 but for cross-correlations between temperatures at different longitudes. a) 25m, 5°N 155°W/25m, 5°N 140°W, b) 125m, 5°N 155°W/125m, 5°N 140°W.

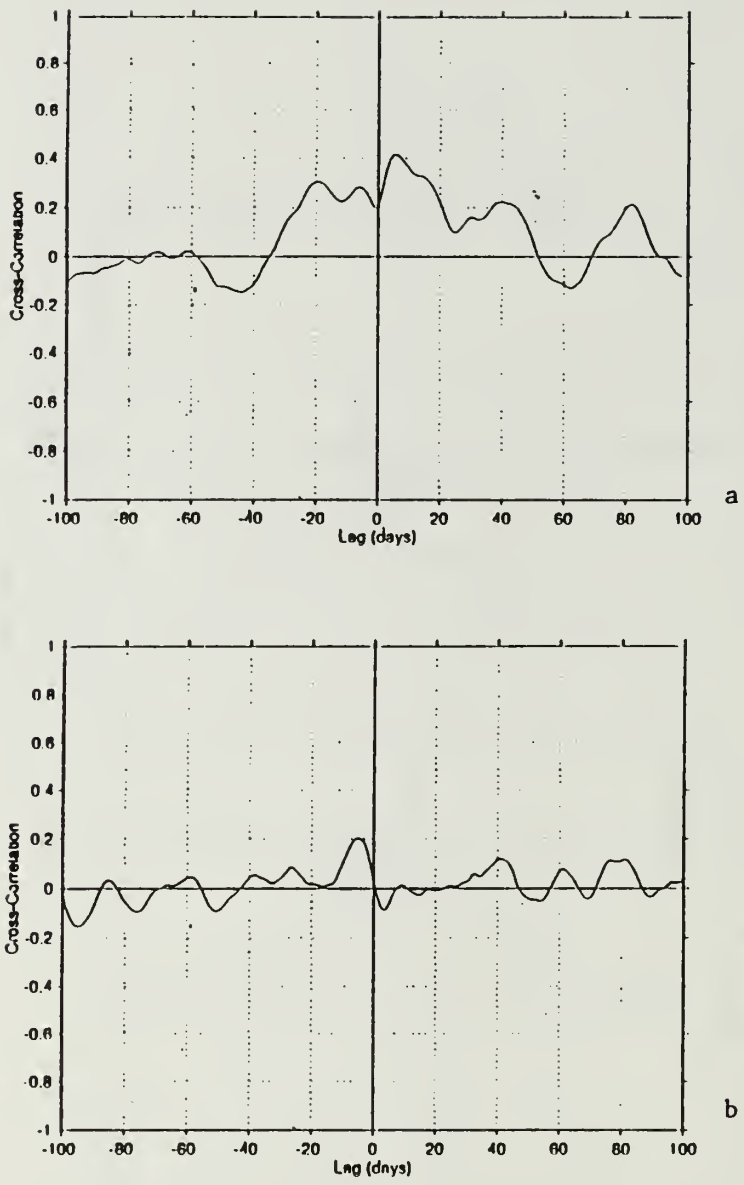

Fig. 33. Same as Fig. 31 but for cross-correlations at 0° 140°W between: a) temperature at 25m/zonal current at 25m, b) temperature at 25m/meridional current at 25m.

INITIAL DISTRIBUTION LIST

		No. Copies
1.	Defence Technical Information Center Cameron Station Alexandria VA 22304-6145	2
2.	Library, Code 052 Naval Postgraduate School Monterey CA 93943-5101	2
3.	Chairman (Code OC/Co) Department of Oceanography Naval Postgraduate School Monterey CA 93943-5000	1
4.	Chairman (Code MR/Hy) Department of Meteorology Naval Postgraduate School Monterey CA 93943-5000	1
5.	James T. Murphree Department of Meteorology Naval Postgraduate School Monterey CA 93943-5000	6
6.	Roland W. Garwood Department of Oceanography Naval Postgraduate School Monterey CA 93943-5000	2
7.	LT Todd W. Sitler 216 North Washington St Montoursville PA 17754	2
8.	William P. Sitler 233 Cottswald Dr Delaware OH 43015	1
9.	Commander Naval Oceanography Command Stennis Space Center MS 39529-5000	1
10.	Commander Naval Oceanographic Office Stennis Space Center MS 39529-5001	1

11. Associate Director of Research 1
for Ocean and Atmospheric
Science and Technology
Naval Research Laboratory
4555 Overlook Avenue, S.W.,
Washington DC 20375-5320

12. Director 1
Naval Research Laboratory
7 Grace Hopper Ave. STOP 2
Monterey CA 93943-5502

13. Ron Gelaro 1
Naval Research Laboratory
7 Grace Hopper Ave. STOP 2
Monterey CA 93943-5502

14. Pat Phoebus 1
Naval Research Laboratory
7 Grace Hopper Ave. STOP 2
Monterey CA 93943-5502

15. John Kindle 1
Naval Research Laboratory
Code 7331
Stennis Space Center
MS 39529

16. Library 1
Scripps Institution of Oceanography
University of California, San Diego
La Jolla, CA 92093